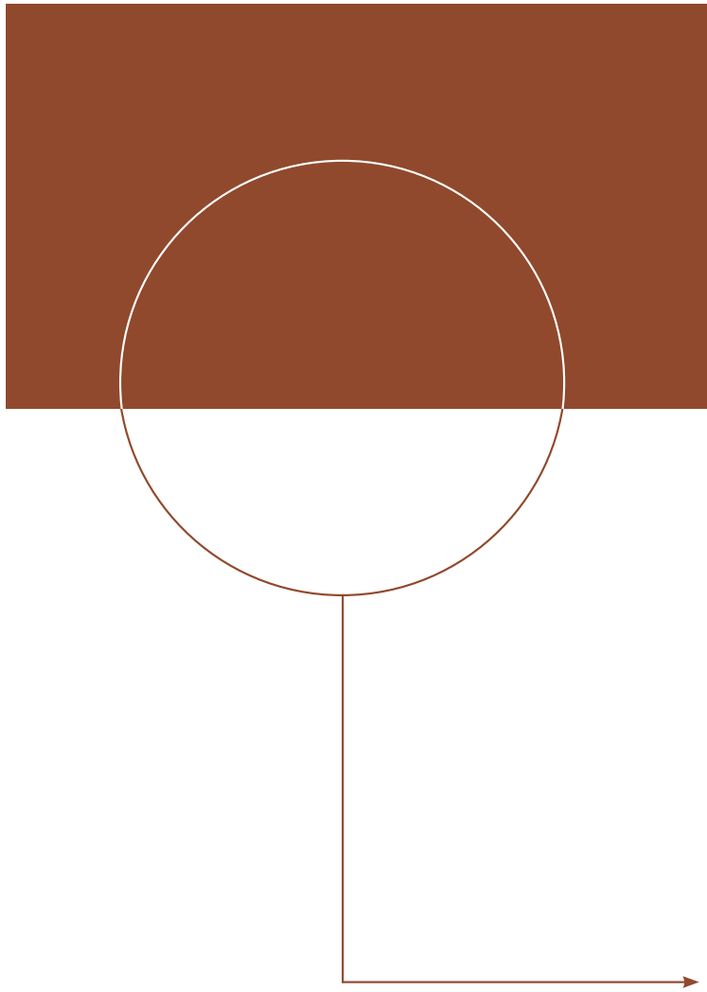

Master's thesis

2019

Simon Ross Stenger

NTNU
Norwegian University of
Science and Technology
Faculty of Engineering
Department of Geoscience and Petroleum

Simon Ross Stenger

The Influence of Sediment Composition on Trace Element Mobility in a CO_2 Leakage Scenario

May 2019

NTNU
Norwegian University of
Science and Technology

NTNU
Norwegian University of
Science and Technology

NTNU

Norwegian University of
Science and Technology

The Influence of Sediment Composition on Trace Element Mobility in a CO_2 Leakage Scenario

Simon Ross Stenger

Geology
Submission date: May 2019
Supervisor: Bjørn Frengstad
Co-supervisor: Murat Van Ardelan

Norwegian University of Science and Technology
Department of Geoscience and Petroleum

Acknowledgements

First of all, I would like to thank my supervisors, Bjørn Frengstad and Murat Van Ardelan, for their insightful feedback and willingness to engage in discussions during the writing of this thesis.

A thanks goes out to Ana Borrero-Santiago, Daniel Krause and Estefanía Miguel for their contribution to the realization of the CO_2 exposure experiments. The crew of RV Harry Bothern, the SINTEF SeaLab engineers, Laurentius Tijhuis and Syverin Lierhagen all deserve recognition for their valuable assistance.

Lastly, I am eternally grateful to Silje Mala Sætherø. This would not have been possible without you.

Table of contents

List of figures

List of Tables

List of Abbreviations

TF	Trondheimsfjord
BS	Barents Sea
CCS	Carbon Capture and Storage
BCR	Bureau Communautaire de Référence (in English: Community Bureau of Reference)
AS	Acid soluble fraction
RED	Easily reducible fraction
OX	Oxidizable fraction
RES	Residual fraction

1 Introduction

In 1896, Arrhenius became the first person to quantify the climatic forcing of atmospheric gases (Arrhenius, 1896). He suggested that the most important atmospheric components in regulating our climate are water vapor and the gaseous form of carbonic acid now commonly referred to as CO_2. From Arrhenius' time up until today, atmospheric CO_2 concentrations have increased from 290 ppm to more than 410 ppm (Keeling et al., 2001). This marked increase and the associated global warming since the mid-20th century can now, with a high degree of certainty, be attributed to anthropogenic greenhouse gas emissions (IPCC, 2013). The consequences of climate change have already been observed e.g. in the form of extreme weather, changes in precipitation patterns and ocean acidification (IPCC, 2014). Despite efforts to transition from fossil fuels to alternative energy sources, the International Energy Agency predicts that a majority of the world's countries will still be reliant on fossil fuels well into the second half of this century (IEA, 2017). Consequently, there is a high demand for solutions that can reduce greenhouse-gas emissions in a fossil-fuel dependent world. One of the proposed options is Carbon Capture and Storage.

1.1 Carbon Capture and Storage

The term Carbon Capture and Storage (CCS) refers to the storage of CO_2 in subsurface geological formations. It is considered a bridging technology that can be implemented to reduce our net greenhouse gas emissions until long-term alternative solutions are able to stabilize atmospheric greenhouse gas concentrations (IPCC, 2005; Cooper et al., 2009). CCS-technologies have been developed to capture CO_2 directly at point sources like power plants and industrial complexes, transport it by boat or pipeline to an on- or offshore location and store it securely in a subsurface geological reservoir. By doing so, large quantities of CO_2 can potentially be prevented from entering the atmosphere (IPCC, 2005).

Public approval is central to CCS implementation and concerns have repeatedly been directed towards the long-term integrity of CO_2 storage (e.g. Monastersky, 2013; Haszeldine et al., 2014). Although large-scale leakage is highly unlikely (Alcalde et al., 2018), complete retention of CO_2 within the subsurface on geological time scales is impossible to guarantee. For this reason, it is important to address two types of leakage scenarios: 1) abrupt and substantial leakage e.g. in the case of engineering failures and 2) slow, continuous seepage through geological pathways in the cap rock or along abandoned wells. While geophysical surveys are able to detect and monitor the gas leakage in the first case (e.g. Langseth and Landrø, 2012), it has been questioned whether a continuous low-flux leakage can be detected using the same methodology (Blackford et al., 2015). Hypothetically, minor amounts of CO_2 could therefore leak from the reservoir into the ambient environment undetected.

In the case of leakage into a marine environment, the introduction of high concentrations of CO_2 has the potential to induce geochemical changes and be of harm to residing marine biota (Ardelan et al., 2009). Primary effects of high concentrations of CO_2 like acidification and increased levels of dissolved inorganic carbon (DIC) have been demonstrated to have lethal effects on invertebrates (Basallote et al., 2015). However, possible secondary effects like changes in the mobility, solubility and bioavailability of trace elements and nutrients

are still poorly understood and their consequences for the marine environment even less so (Ardelan et al., 2009).

A number of studies have previously attempted to determine the geochemical changes associated with small-scale CO_2 leakage (Ardelan et al., 2009; Ardelan and Steinnes, 2010; Blackford et al., 2014; de Orte et al., 2014; Kirsch et al., 2014; Wunsch et al., 2014; Lichtschlag et al., 2015). Blackford et al. (2014) performed a controlled subsurface release of CO_2 into a shallow marine environment. They observed a pH decrease from 7.7 to 7.5 and a marked increase in the concentration of dissolved inorganic carbon (DIC) and [Ca^{2+}] within the sediment pore-water. Biological impacts were detectable but not significant nor chronic. The CO_2 exposure caused increased mobilization of Ca, B, Sr and Li from the marine sediments (Lichtschlag et al., 2015). The authors attributed this to dissolution of carbonate minerals in line with the findings of Wunsch et al. (2014). Ardelan et al. (2009), Ardelan and Steinnes (2010) and de Orte et al. (2014) performed batch-type laboratory-scale experiments in which marine and estuarine sediments were exposed to elevated CO_2 concentrations in a non-pressurized chamber. de Orte et al. (2014) found increased mobility of Co, Fe, Zn, Cu and Pb, while As mobility was reduced, possibly because of adsorption onto Fe-oxides (Sarmiento et al., 2009). Ardelan et al. (2009) observed increased pore-water concentrations of Al, Cr, Ni, Cu, Zn, Cd and Pb, while Ardelan and Steinnes (2010) demonstrated how CO_2 exposure can potentially disrupt the Fe- and Mn-shuttle by the development of sub- or anoxic conditions within the sediment pore-space.

The environmental risk associated CO_2 leakage from onshore storage sites has also been addressed in the literature (e.g. Harvey et al., 2013). However, onshore storage represents a separate geological setting characterized by properties distinct from those discussed in this study and will therefore not be treated further.

Common for all previous investigations on the environmental risk related to CO_2 storage is that they have been conducted at circum-atmospheric pressure. However, the sediment-water interface at the currently active offshore CO_2 storage sites in Norway are situated 100-300 meters below sea level and hence experience much higher pressures (Bickle et al., 2007; Hansen et al., 2013). The transferability of the previously mentioned studies could therefore be questionable. This study presents the findings from two mesocosm experiments conducted at a pressure of 30 bar in a flow-through chamber, effectively simulating the conditions present at the sediment-water interface at known CO_2 storage sites like the Snøhvit Project in the Barents Sea. During the experiments, surface sediment from two distinct geological settings (continental shelf and estuarine) are exposed to elevated CO_2 concentrations for a 50-day period followed by a two-week recovery phase. The CO_2 dosing is adjusted to simulate a gradual, low-flux CO_2 seepage. Sediment samples are collected throughout both of the experiments. These are subsequently extracted using a standardized four-step sequential extraction procedure and analyzed by ICP-MS. Through this, four operationally defined element fractions will be obtained: an acid soluble (easily exchangeable), an easily reducible, an oxidizable and a residual fraction. In combination with a mineral characterization based on x-ray diffraction (XRD) analyses, the geochemical data will be used to demonstrate the relationship between sediment composition and element mobility in a CO_2 leakage scenario at realistic pressure conditions.

The hypotheses of this study are:

- The effect of CO_2 exposure will primarily influence the elements within the acid soluble fraction by causing dissolution of primary $CaCO_3$-phases and mobilization of adsorbed species.
- The CO_2 exposure leads to a change in redox-conditions, which results in a disruption of the iron and manganese redox cycle and mobilization of elements from the reducible fraction.
- Key mineralogical differences, especially within the clay mineral fraction, will be reflected in different element mobilization patterns for the two types of surface sediment.

1.2 Geological setting

1.2.1 The Trondheimsfjord

The Trondheimsfjord is a deep, glacially carved fjord situated in central Norway. It was formed during the Pleistocene glaciations and was inundated following the retreat of the Scandinavian ice sheet (Ottesen et al., 1995). The Trondheimsfjord exhibits estuarine circulation with some tidal influence, the average tidal range being 1.8 meter (Bakken et al., 2000). Exchange of deep-water occurs biannually inhibiting the development of sub- or anoxic conditions at depth (Faust et al., 2014). A bedrock threshold separates the outer fjord from the coast, but because of its position at 330 mbsl it does not restrict the introduction of coastal water (Bøe et al., 2003). Multiple rivers feed into the fjord including Orkla, Gaula, Nidelva, Stjørdalselva, Verdalselva and Steinkjerelva. They carry with them suspended sediment and dissolved chemical species and are the main sources of the sediment that is deposited within the fjord (Faust et al., 2014). The composition of these sediments reflect the regional geology with a general trend towards higher marine input in the outer fjord (Faust et al., 2014). Bøe et al. (2003) report sedimentation rates of 2.5 mm/year for the central basin, however, higher rates can be expected close to river outlets. Mining of sulphide-deposits has taken place in the drainage areas of the rivers feeding into the Trondheimsfjord since the 16th century and several industrial complexes are still situated along the fjord margin. Both types of human activities can potentially have introduced organic and inorganic pollutants to the fjord system.

1.2.2 The South-Western Barents Sea

The Barents Sea is a shallow, marginal sea bound by Svalbard and the Polar Ocean to the north, Novaja Zemlya to the east, Eurasia (Norway and Russia) to the south and the Norwegian Sea to the west. The Norwegian Current feeds relatively warm, high salinity Atlantic Water into the southern part of the Barents Sea, an area also influenced by the less saline, relatively warm Norwegian coastal water (Steinsund and Hald, 1994). Seasonal sea-ice formation forms a cold, saline brine that sinks and produces dense bottom-water. Measurements of dissolved oxygen reveal well-oxygenated conditions within the sediments (Steinsund and Hald, 1994).

Settling from suspension is the primary mode of deposition in the south-western Barents Sea. The clay fraction is dominated by illite and chlorite, which are the common weathering products in areas dominated by physical weathering of crystalline bedrock (Sellwood et al., 1993; Vogt and Knies, 2009). This suggests that the clastic fraction of the surface sediments is sourced from northern Scandinavia. Sedimentation rates in the area are generally below 0.1mm/year (Steinsund and Hald, 1994).

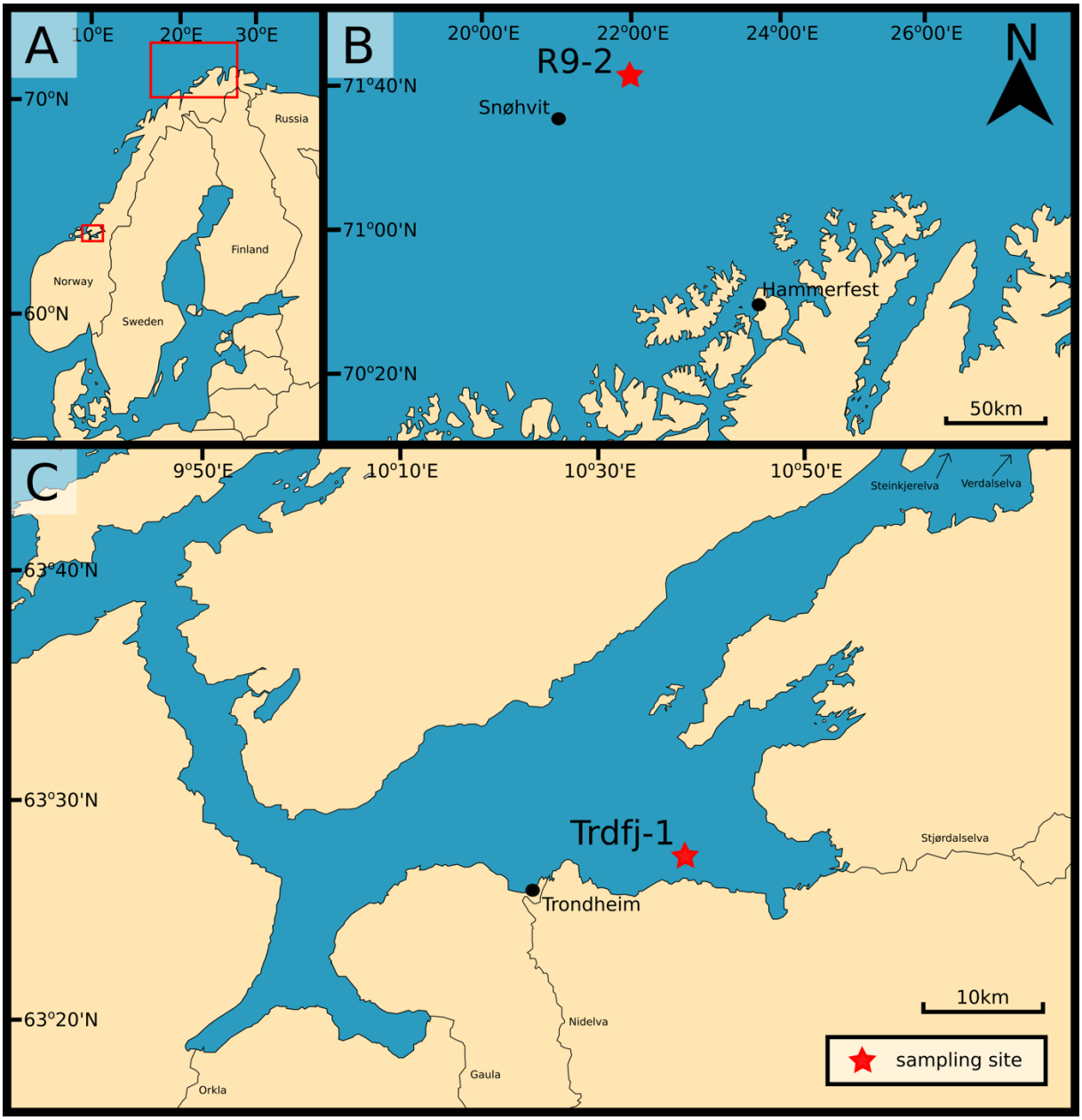

Fig. 1. Overview map with location of sampling sites. A. Northern Europe. B. Barents Sea. Shows location of the Snøhvit project and the regional station 9-2. C. The Trondheimsfjord. Shows the major rivers that drain into the fjord and the location of sampling site Trdfj-1.

1.2.3 CCS in the Barents Sea: The Snøhvit Project

Snøhvit is a gas field located in the south-western corner of the Barents Sea, 150 km off the Norwegian coast. The recovered gas has a 5-8% CO_2 content. The CO_2 is separated from the hydrocarbon gas at an onshore processing facility and re-injected into a saline aquifer in the subsurface (Hansen et al., 2013). CO_2 injection into the Tubåen Formation was commenced in 2008 with an initial goal to inject a total of 23 Mt CO_2 during a 30-year period. In 2011, the bottom-hole pressure approached the cap rock fracture pressure jeopardizing reservoir contingency. A well intervention was therefore performed and the injection shifted to the shallower Stø Formation (Hansen et al., 2013). Operations have since been working without further complications and no surface leakage has been detected.

2 Theory

To explain the chemical composition of a sediment and its properties with respect to element mobility, a general understanding of how sediments are produced, transported and deposited is necessary. The chemical properties of the aquatic phase also play a crucial role in the distribution of elements. As the sediment grains pass through the water column and following deposition during early diagenesis variations in pH, redox-conditions and solution composition might induce changes in element speciation and the solubility of these species. Finally, a large proportion of the potentially mobile elements are bound to sediments because of reactions taking place at the solid-solution interface. In the following, the abovementioned concepts will be introduced in order to facilitate a discussion of element mobilization from marine sediments upon exposure to increased concentrations of CO_2 and how these results may vary with sediment composition.

2.1 Sediment formation, transport and deposition

2.1.1 Sediment classification

According to Nichols (2009), sediments can be categorized as either clastic, chemical or biogenic based on their origin and composition. Clastic sediments consist of rock fragments or secondary minerals formed by the weathering of bed rock, while chemical sediments originate from the either spontaneous or biologically mediated precipitation of solids from a solution. The formation of biogenic sediments is carried out by living organisms and includes both calcareous and siliceous shells and tests, and organic matter. What controls the distribution of these major sediment types is first and foremost the geology and weathering conditions in the source area, the hydrodynamic sorting during transport and the physical and chemical characteristics of the depositional environment (Nichols, 2009).

The type of rocks exposed at the surface in an area is determined by its geological history. For instance, a sandstone dominated bed rock geology will produce a silica or quartz-rich sediment, while basaltic bed rock is prone to produce a more Fe- and Mg-rich sediment because of its high content of mafic minerals. Another source of chemical components is hydrothermal vent systems at oceanic spreading ridges. Hot fluids circulating within the oceanic crust dissolves chemical components from freshly solidified basaltic rocks and transport them into the marine environment (Emerson and Hedges, 2008, p. 47-49).

Clastic sediments can be transported by either aeolian, fluvial or glacial processes (Nichols, 2009). During transport, the sediment grains will be subject to hydrodynamic sorting according to grain size, density and/or shape. Grain size is considered the dominant parameter in depositional environments with a relatively homogeneous sediment composition (Allen, 1985, p. 57). The grains will eventually settle along a gradient from a high energy environment towards a low energy environment when the capacity and/or competence of the transporting fluid falls below a certain threshold limit (Leeder, 2011). These concepts can be applied to explain the accumulation of coarse grained clastic sediments in e.g. river beds and their fine-grained counterparts on the distal part of the continental shelf.

2.1.2 Weathering

Weathering can be generalized into two types: chemical and physical weathering (Nesbitt et al., 1996). Even though they describe two separate mechanisms they take place simultaneously in the process of breaking down rocks. Chemical weathering describes the chemical breakdown of rocks by hydrolysis, dissolution or redox (reduction and oxidation) reactions in the presence of a fluid. Hydrolysis is the process by which water reacts with the ion of a weak acid or base (Krauskopf and Bird, 1995, p. 36). The reaction consumes either H^+ or OH^--ions and may therefore leave the solution either slightly basic or acidic, respectively. Hydrolysis is important for the weathering of multiple mineral phases, including silicate minerals like K-feldspar (Krauskopf and Bird, 1995, p. 338):

$$\underset{K\text{-}feldspar}{2KAlSi_3O_8} + 11H_2O \implies 2OH^- + \underset{kaolinite}{Al_2Si_2O_5(OH)_4} + 4H_4SiO_4$$

This reaction is an incongruent reaction, meaning that the mineral is not completely dissolved. Instead, ions are leached to the solution and a secondary clay mineral is formed as a residual product of the reaction. Dissolution and precipitation reactions describe situations where a solid is dissolved or precipitated if the adjacent solution is undersaturated or supersaturated with respect to that solid. This process is congruent (complete dissolution of components) and is significant in the weathering of salts. Chemical weathering by redox reactions describes the process by which one or more electrons are transferred from one element (the oxidant) to another (the reductant), causing a change in the oxidation state of both elements. Redox processes are important weathering pathways for minerals composed of elements with two or more oxidation states and stability fields within the conditions encountered in the natural environment. An example of such an element is iron which has two oxidation states, Fe(II) and Fe(III). Fe(II)-minerals like pyrite (FeS_2) breaks down if their central cation, Fe(II), gets oxidized to Fe(III) e.g. through exposure to oxygen for prolonged periods of time (Krauskopf and Bird, 1995, p. 334). Some general trends can be seen in the efficiency of chemical weathering and which reactions that become dominant within a geographical area. Among other things, the efficiency of chemical weathering is enhanced by increased annual rainfall, annual mean temperature and vegetation density (Sellwood et al., 1993). Physical weathering describes the physical break down of rocks mediated by plants, frost shattering, changes in temperature or by exfoliation as a result of an uplift imposed pressure relief (Nichols, 2009). It follows that physical weathering dominates in primarily cold regions with large seasonal temperature variations like temperate and artic regions at mid to high latitudes. The strong dependency of weathering on both local and regional conditions is reflected in the extent of cation leaching and mineralogy of the sediment that is ultimately deposited (Nesbitt and Young, 1982; Sellwood et al., 1993).

Group	Layer type	Typical chemical formula
Chlorite	2:1	$(Mg,Al,Fe)_6((Al,Si)_4O_{10})(OH)_8$
Muscovite	*Not applicable*	$KAl_2(AlSi_3O_{10})(OH)_2$
Illite	2:1	$K_{0.5\text{-}0.75}Al_2(Al_{0.5\text{-}7.5}Si_{3.25\text{-}3.5}O_{10})(OH)_2$
Kaolinite	1:1	$Al_2Si_2O_5(OH)_4$
Smectite	2:1	$Na_{0.35}(Al_{1.65}Mg_{0.35})Si_4O_{10}(OH)_2 \bullet 4H_2O$

Table 1. Mineral groups. Reproduced from Krauskopf and Bird (1995)

2.1.3 Clay minerals

Clay minerals are a type of phyllosilicates relevant in a geochemical perspective because of their high specific surface area and chemical reactivity. They consist of interlayered octahedral aluminol sheets and tetrahedral siloxane sheets (Krauskopf and Bird, 1995, p. 338). Their categorization is based on the pattern of the interlayering, which is also what determines their physical and geochemical properties (Table 1). Kaolinite is a common example of a 1:1-type clay which consists of repeating layers of an octahedral and a tetrahedral sheet. The layers are held together by forming relatively strong hydrogen bonds. 2:1-type clays, on the other hand, consist of an octahedral sheet sandwiched by two tetrahedral sheets. Their repeating layers are held together by electrostatic interactions, the strength of which is governed partly by their surface properties and partly by the ionic strength of the solution (Hiemenz and Rajagopalan, 1997). 2:1-type clay minerals acquire a surface charge by isomorphic substitution of Al^{3+} and Si^{4+} for cations of lower charge, a phenomenon which is less common for 1:1-type clays. The excess charge may be balanced by binding cations onto the edges and faces of the particle or in their interlayering space. Some of these will form strong covalent bonds while others will be easily exchangeable. Examples of 2:1 type clays are illite and smectite. Illite is characterized by having K^+-ions as its primary interlayering cation and a crystallographic structure that closely resembles that of muscovite. The layers of minerals within the smectite group are weakly held together and may accommodate large ions and water in their interlayer space. This gives the mineral its characteristic swelling property, which may reduce the permeability of the bulk sediment even at low smectite contents (Krauskopf and Bird, 1995, p. 342). The variable layer spacing observed between different clay minerals is what enables their identification by a range of analytical methods including x-ray diffraction spectroscopy (XRD).

2.2 Ocean chemistry

2.2.1 Acid-base equilibria

An important factor of ocean chemistry is the concept of pH. It is linked to the self-ionization property of water and defined as the negative logarithm of the hydrogen ion activity in an aqueous solution (Krauskopf and Bird, 1995, p. 29-30). pH is the master variable of acid-base equilibria. In the Lewis definition, these are equilibrium reactions that involve exchange of electron pairs between weak acids and bases (Emerson and Hedges, 2008, p. 103). A generic example is the equilibrium between an acid (HA) and its conjugate base (A^-):

$$HA \rightleftharpoons H^+ + A^-$$

Thermodynamics predict that the ratio of the products to the reactants will always be the same for a given set of temperature and pressure conditions. The numeric value of this constant is also known as the equilibrium constant, K:

$$K = \frac{[H^+] + [A^-]}{[HA]}$$

pK is defined as minus the logarithm of the K and corresponds to the pH at which the concentration of the acid and the conjugate base is equal. Below pK the acid dominates and above the base is dominant. A unique solution for this simple acid-base equilibrium can be found if two additional mass balance equations are defined. If the total concentration of A is known, A_{TOT} = [HA] + [A^-] can be used alongside a charge balance

equation, $[H^+] = [A^-]$. In solutions of high electrolyte concentrations like seawater, K deviates from its value in dilute solutions because of the non-ideal behavior of solutes (Stumm and Morgan, 1996, p. 101). The dissolved ions interfere with each other and cause a change in their chemical reactivity. To account for this deviation, the ion concentration must be corrected by a scaling factor called the activity coefficient. This varies for different ions but depends primarily on the ionic strength of the solution and the charge of the ion. When these factors are accounted for in the calculation of K, it is called the apparent equilibrium constant (K').

2.2.2 The carbonate system

The governing set of acid-base pairs controlling pH in the marine environment are those of the carbonate system. When natural waters are in contact with the atmosphere there exists an equilibrium between the inorganic carbon species. The involved species are gaseous and dissolved CO_2, H_2CO_3, HCO_3^- and CO_3^{2-}. CO_2 is ubiquitous in natural waters due to its production during degradation of organic matter and gas exchange with the atmosphere. Dissolution of atmospheric CO_2 occurs according to Henry's law, which states that at constant temperature the solubility of a gas in a solution is proportional to the partial pressure of the gas in contact with the solution (Stumm and Morgan, 1996, p. 212):

$$CO_2(g) \rightleftharpoons CO_2(aq)$$

The constant of proportionality that determines the distribution between the gaseous and aqueous species is called Henry's constant. The dissolved CO_2 can then react with water to form carbonic acid, H_2CO_3:

$$CO_2(aq) + H_2O \rightleftharpoons H_2CO_3$$

The equilibrium constant of the above reaction is $2.5*10^{-3}$ at standard state (25°C, 1 bar), which means that the majority is present as $CO_2(aq)$. The relative concentration of the two species is difficult to determine analytically, which is why it is common to report the sum of their concentrations instead, denoted as $H_2CO_3^*$:

$$H_2CO_3^* = CO_2(aq) + H_2CO_3$$

H_2CO_3 is a weak acid which forms bicarbonate (HCO_3^-) when it deprotonates:

$$H_2CO_3^* \rightleftharpoons H^+ + HCO_3^-$$

Which again can deprotonate and form carbonate, CO_3^{2-}:

$$HCO_3^- \rightleftharpoons H^+ + CO_3^{2-}$$

Two additional parameters are commonly used to describe the carbonate system: total alkalinity (TA) and total dissolved inorganic carbon (DIC). TA is a charge balance equation that provides a measure for the excess of bases over acids in a solution (Stumm and Morgan, 1996). It is sometimes described as the acid neutralization capacity of an aqueous solution. DIC is the sum of the concentration of the dissolved inorganic carbon species. The speciation of the carbon species is governed by the pH as demonstrated by the Bjerrum diagram (Fig. 2). It shows that close to 98% of the DIC is present as HCO_3^- at the average pH of the oceans (pH ≈ 8.2), while at neutral pH, about 20% is present as $H_2CO_3^*$.

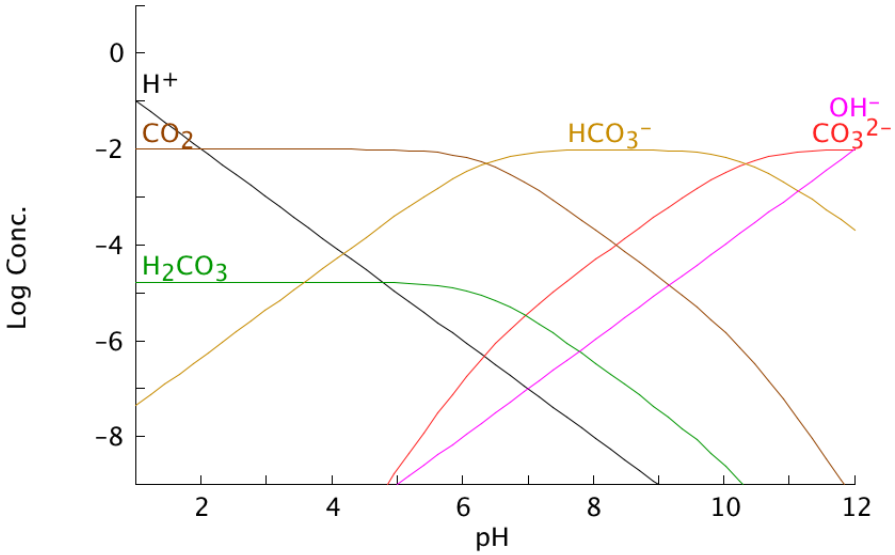

Fig. 2. Bjerrum diagram. DIC = 10nM. The diagram shows how the concentration of the different inorganic carbon species vary as a function of pH.

When an aqueous solution is in contact with sediments, it establishes an equilibrium with the solid phase. This is encountered in all natural waters and is critical to consider in the study of pore-waters. The salt of the dissolved CO_2 species can form when CO_3^{2-} reacts with a divalent metal cation (M^{2+}) to form MCO_3 of which $CaCO_3$ is the most important example in ocean geochemistry. Its two most common mineral polymorphs are aragonite and calcite. The solubility of either calcite or aragonite can be described by the following equilibrium reaction (Emerson and Hedges, 2008, p. 420):

$$CaCO_3 \rightleftharpoons Ca^{2+} + {CO_3}^{2-}$$

The pK' of this reaction is:

$$pK' = \frac{(Ca^{2+})({CO_3}^{2-})}{(CaCO_3)} = (Ca^{2+})({CO_3}^{2-})$$

The last simplification follows from the convention that solids have unit activity. Here, pK' is also known as the apparent solubility product of $CaCO_3$ (K'_{sp}). The ratio of the activities of the two components in the solution to K'_{sp} is defined as the saturation index, Ω:

$$\Omega = \frac{(Ca^{2+})({CO_3}^{2-})}{K'_{sp}}$$

From a thermodynamic viewpoint, if $\Omega > 1$, the solution is said to be supersaturated with respect to the solid phase and precipitation will occur. If $\Omega < 1$, the solution is said to be undersaturated and leads to dissolution of the solid. If $\Omega = 1$, the solid and the solution is said to be at equilibrium. K'_{sp} is pressure and therefore depth dependent. In the ocean, it attains twice the numerical value at four kilometers depth compared to at the surface (Emerson and Hedges, 2008, p. 421). In combination with a lower pH in the deep ocean due to oxidation of organic matter, this explains the low preservation potential of $CaCO_3$ in deep ocean sediments. The numerical value of K'_{sp} for aragonite is slightly higher than that of calcite, meaning that it is more susceptible to dissolution (Mucci, 1983).

2.3 Metal speciation and solid-solution reactions

2.3.1 Metal speciation in aqueous solutions

The importance of speciation in aqueous solutions cannot be underestimated as it determines the solubility, reactivity, bioavailability and toxicity of many key elements in the oceans. Metal ions do not exist as "free" ions in aqueous solutions but balance their charge by coordinating water molecules or forming metal complexes with inorganic or organic entities of opposite charge also known as ligands (Stumm and Morgan, 1996, p. 253). The number of coordinated water molecules or the type of complex depends on the electron configuration, size and charge of the metal ion and the pH of the solution. Metal ions with coordinated water molecules are Lewis acids and may therefore protolyze (expel protons) to form hydroxo- or oxo-complexes with OH^- or O^{2-} as the ligand, respectively. As a general trend, the tendency of the central metal ion to deprotonate coordinated water molecules increases with pH and oxidation state of the central metal ion (Fig. 3). Stumm and Morgan (1996, p. 668), free metal-ion species are more bioavailable than hydroxo- and oxo-complexes. A decrease in pH (e.g. as a result of CO2 leakage) may therefore increase the concentration of the free metal-ion species and hence bioavailability and toxicity of the metal.

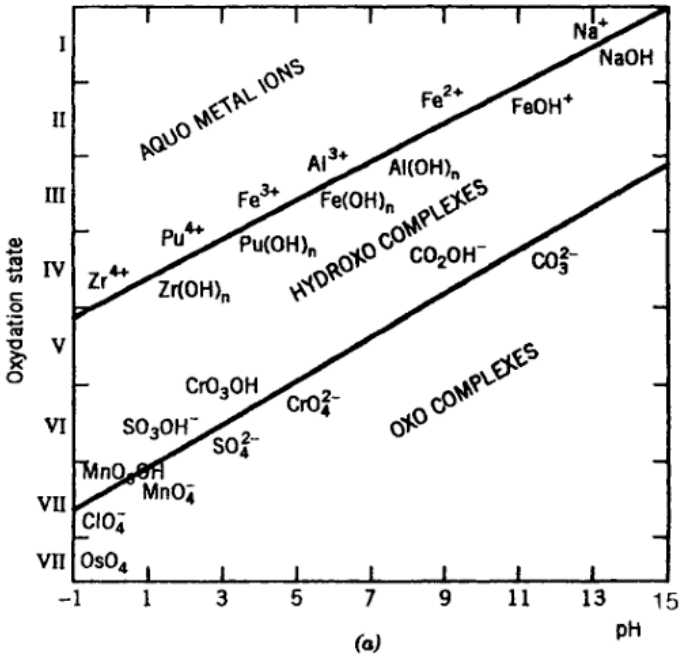

Fig. 3. Metal complexation and hydrolysis. The diagram shows a generalized scheme for the predominant pH-range for aquo metal ions, hydroxo complexes and oxo complexes. Reproduced from Stumm and Morgan (1996).

Complexes can be categorized as either inner-sphere complexes, where the ions interact directly and forms ionic or covalent bonds, or outer-sphere complexes, where the central ions are separated by one or more water molecules and bind primarily through electrostatic interactions (Stumm and Morgan, 1996, p. 541).

2.3.2 Adsorption

The formation of inner-sphere and outer-sphere complexes on solid surfaces is also known as adsorption. The large surface area to volume ratio of fine-grained particles like clay minerals, organic matter, metal carbonates and metal-(hydr)oxides settling through the water column provide an ample number of sites for adsorption reactions to occur. This makes adsorption a primary sink for trace metals in the oceans. The general model for metal complexation in aqueous solutions can also be applied to describe metal complexation on solid surfaces (Dzombak and Morel, 1990). Metal ions situated at the surfaces of solids have a reduced coordination number, i.e. their charge is incompletely balanced by the adjacent atoms in the crystal lattice. In the presence of water, this leads to the formation of surface functional groups, hydroxyls being the most common in the case of metal oxide and hydroxide particles at marine conditions (Stumm and Morgan, 1996, p. 533). Dissolved metal species can form inner-sphere complexes through metal binding, ligand exchange (if the metal is present in the solution as an anionic species) or ternary surface complex formation (Fig. 4). Complexation is competitive, which means that ligand or metal exchange will occur if it is thermodynamically favorable. An important consequence of this is that at low pH, H^+-ions compete effectively with metals for the ligands, while at high pH, OH^--ions compete effectively with ligands for the metals (Stumm and Morgan, 1996, p. 277). Good estimates of the concentration of complex species in natural waters are difficult to obtain because of competitive complexation and the rapid exchange of ligands between solution and complex (Manahan, 2017).

Acid-Base Equilibria		
$S{-}OH + H^+$	$\rightleftharpoons$	$S{-}OH_2^+$
$S{-}OH\ (+\ OH^-)$	$\rightleftharpoons$	$S{-}O^- + (H_2O)$
Metal Binding		
$S{-}OH + M^{z+}$	$\rightleftharpoons$	$S{-}OM^{(z-1)+} + H^+$
$2\ S{-}OH + M^{z+}$	$\rightleftharpoons$	$(S{-}O)_2M^{(z-2)+} + 2\ H^+$
$S{-}OH + M^{z+} + H_2O$	$\rightleftharpoons$	$S{-}OMOH^{(z-2)+} + 2\ H^+$
Ligand Exchange (L^- = ligand)		
$S{-}OH + L^-$	$\rightleftharpoons$	$S{-}L + OH^-$
$2\ S{-}OH + L^-$	$\rightleftharpoons$	$S_2{-}L^+ + 2\ OH^-$
Ternary Surface Complex Formation		
$S{-}OH + L^- + M^{z+}$	$\rightleftharpoons$	$S{-}L{-}M^{z+} + OH^-$
$S{-}OH + L^- + M^{z+}$	$\rightleftharpoons$	$S{-}OM{-}L^{(z-2)+} + H^+$

Fig. 4. Inner-sphere complexation models. Different potential surface complexation equilibria between a hydroxylated surface functional group (S-OH) and ions in the solution. Both monodentate (involving one surface site) or bidentate (involving two surface sites) ligands are considered. Reproduced from Stumm and Morgan (1996) who adapted it from Schindler and Stumm (1987).

2.3.3 Surface charge distribution

Due to the involvement of OH^- and H^+, surface complexation reactions are pH dependent and may result in the development of surface charge. The total net charge of a solid (σ_{solid}) is the sum of the permanent structural charge acquired by isomorphic substitution (σ_{psc})

and the charge that results from surface reactions (σ_{surf}), e.g. inner-sphere and outer-sphere complexation (Krauskopf and Bird, 1995):

$$\sigma_{solid} = \sigma_{psc} + \sigma_{surf}$$

σ_{psc} is typically small relative to σ_{surf} for Fe-(hydr)oxides, while σ_{psc} makes a bigger contribution to σ_{solid} in the case of clay minerals like smectite (Krauskopf and Bird, 1995). The pH at which σ_{solid} = 0 is called the point of zero charge (pH_{pzc}). This has important consequences for the adsorption of ions onto solid surfaces and varies between minerals (Fig. 5). Below pH_{pzc}, the surface will have a net positive charge and therefore a higher affinity to bind anions, while above pH_{pzc} the surface will have a net negative charge and preferably bind cations. The net surface charge is compensated by an increased concentration of counter-ions (ions with opposite charge of the surface) in the vicinity of the surface. This can be described as the diffuse layer ($\sigma_{diffuse}$) and fulfills the condition that:

$$\sigma_{solid} + \sigma_{diffuse} = 0$$

The arrangement of ions at the surface that cause the development of σ_{surf} and $\sigma_{diffuse}$ is known as the electrical double-layer. The two layers can be thought of as an inner-layer where the ions are bound to the surface, while the ions responsible for $\sigma_{diffuse}$ move "freely" in the solution. The distribution of charge in the diffuse layer with respect to distance from the surface is described in the Gouy-Chapman theory. It states that the charge decay rate is proportional to the square rote of the ionic strength of the solution. The suppression of the diffuse layer that results from an increase in ionic strength is what causes flocculation of colloidal particles to occur at the interface between fresh river-water and saline seawater in estuaries (Leeder, 2011).

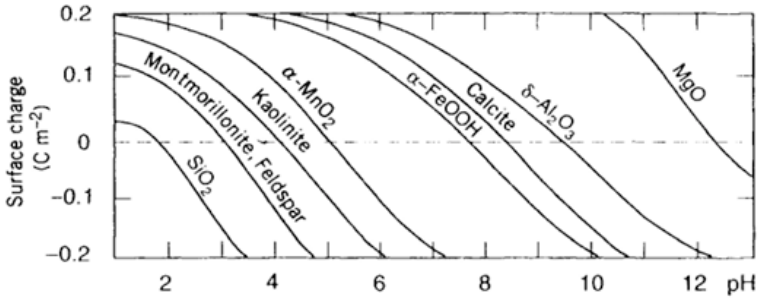

Fig. 5. The effect of pH on surface charge of a selection of solid phases. Reproduced from Stumm and Morgan (1996)

2.4 Ion exchange capacity

Stumm and Morgan (1996) describe ion exchange reactions as the exchange of one adsorbed, readily exchangeable ion for another. The process plays a significant role in the distribution of metals in natural waters. When more than one type of ion is present in a solution in contact with the surface they will be competing for the available surface sites. The ion exchange capacity of solid materials is operationally defined as the amount of ions that can desorbed from the surface per gram of solid (Stumm and Morgan, 1996, p. 586). The anion exchange capacity of a surface increase with decreasing pH, while the opposite is true for cation exchange. A general rule of thumb is that at constant temperature, pressure, pH and ionic strength, ions with higher valence and smaller hydrated radius will preferentially replace those with lower valence and larger hydrated radius on solid surfaces

(Krauskopf and Bird, 1995, p. 152). Selectivity sequences are commonly used to describe the relative affinity of different ions for a given surface.

2.5 Oxidation and reduction

Oxidation and reduction reactions, also known as redox-reactions, involve the transfer of one or more electrons from one element (the oxidant) to another (the reductant). Redox-reactions can be described as two half-reactions (a reduction and an oxidation reaction) that occur simultaneously. An example is the oxidation half-reaction of Fe^{2+}:

$$4Fe^{2+} + 4e^{-} \rightleftharpoons 4Fe^{3+}$$

and the reduction half-reaction of O_2:

$$O_2 + 4H^{+} \rightleftharpoons 2H_2O + 4e^{-}$$

When the two half-reactions are combined, the hypothetically "free" electrons cancel out. The full redox-reaction can then be noted as:

$$O_2 + 4Fe^{2+} + 4H^{+} \rightleftharpoons 4Fe^{3+} + 2H_2O$$

The loss or gain of an electron affects the oxidation state of the element, which again changes its chemical reactivity and speciation (Calvert and Pedersen, 1993). Using the same example as before, Fe^{2+} will form iron-sulfides in the presence of dissolved HS^{-}, but is soluble in the absence of sulfide. On the contrary, Fe^{3+} readily reacts with water to form insoluble Fe-hydroxides under oxic conditions (Canfield et al., 1993). It is relevant to point out that the kinetics of redox-reactions are slow and thermodynamic equilibrium is seldom reached (Stumm and Morgan, 1996, p. 425). Microbiota take advantage of these slow kinetics and harvest energy for their metabolic needs by using redox-reaction to catalyze oxidation of organic matter. This is a primary component in the concept of diagenesis.

2.6 Diagenesis

The physical and chemical processes that take place within sediment post-deposition can collectively be described by the term diagenesis. It encompasses sediment compaction, bioturbation, oxidation of organic matter and the dissolution and precipitation of solid phases.

Primary production of organic matter takes place in surface waters and is mediated by phytoplankton. As organic matter settles through the water column about 90% gets oxidized before it reaches the basin floor and is able to get incorporated into the sediment (Hensen et al., 2006). The oxidation of organic matter within marine sediments is one of the main drivers of early diagenesis and can take place either purely chemically or catalyzed by microorganisms (Rullkötter, 2006). The process consumes oxidants in an ordered sequence where the oxidant which result in the highest Gibbs free energy yield is preferentially used. The first conceptual model for degradation of organic matter of Redfield ratio composition was proposed by Froelich et al. (1979). They suggested that the sequence of oxidants is oxygen (O_2), Mn(IV), nitrate (NO_3^{-}), Fe(III), sulfate (SO_4^{2-}) and ultimately CO_2. The chemical reactions and their corresponding Gibb's free energy yield are shown in Fig. 6.

The permeability of fine-grained sediments is generally low, which restricts pore-water circulation and causes pronounced chemical gradients and microenvironments to develop. The influx of new oxidants is therefore limited and results in a depth zonation of the

dominant redox-reaction taking place in surface sediments (Canfield et al., 1993). The zonation may be disrupted by sediment-burrowing animals through bioturbation and bioirrigation. It is important to note that redox-reactions may induce profound changes in pore-water composition. An example is the reduction of Mn(IV)- and Fe(III)-(hydr)oxides which dissolve upon reduction and simultaneously release the chemical species adsorbed to their mineral surfaces (Tribovillard et al., 2006). Similarly, diagenesis generally increases the pore-water concentration of dissolved CO_2 and lowers pH, not unlike the experimental conditions tested in this current study. From a quantitative perspective, Mn(IV)- and Fe(III)-reduction play only minor roles in organic matter oxidation (Jørgensen, 2006), but might be the main anaerobic pathways for the oxidation of organic matter in areas where their solid species are abundant in the sediments (Canfield et al., 1993). In the modern marine environment, concentrations of oxygen and sulfate is generally high why these two oxidants are responsible for the vast majority of oxidation of organic matter on a global scale (Jørgensen, 2006).

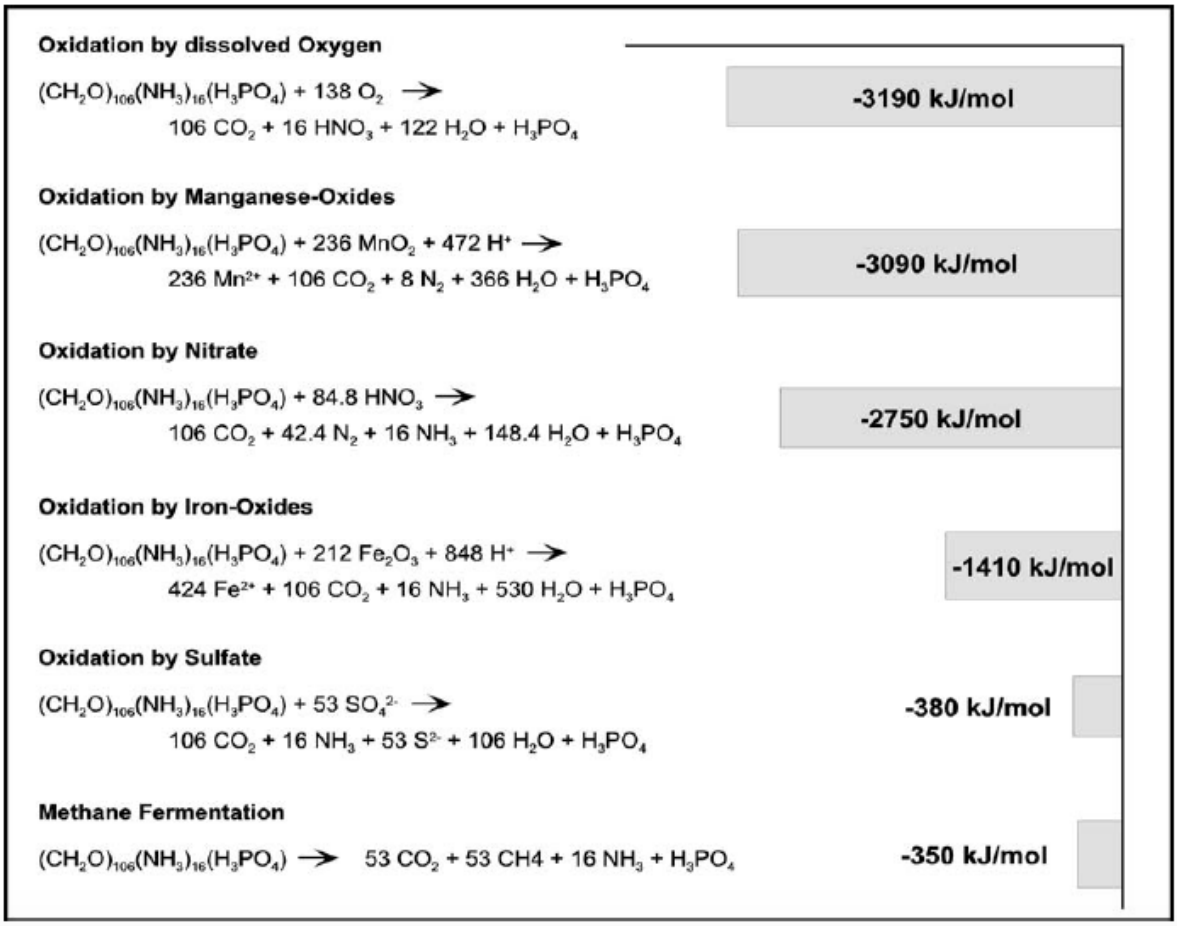

Fig. 6. Oxidation reactions of organic matter in marine sediments. Sequence proposed based on the magnitude of the Gibbs free energy yield of the reactions by Froelich et al. (1979). Reproduced from Schulz (2006b).

3 Materials and Methods

3.1 Sediment collection and preparation

3.1.1 The Trondheimsfjord

The Trondheimsfjord sediment was collected in August, 2017 at sampling station Trdfj-1 (Fig. 1). The GPS coordinates of the sampling site are: 63°27'31''N and 10°39'11''E. A box corer mounted onboard the research vessel Harry Bothern was used to retrieve the sediment from a depth of 160-180 meters below sea level (mbsl). Sediment which had been in direct contact with the box corer was separated and discarded using a square plastic tube. The remaining uncontaminated sediment was subdivided into two fractions: a surface (top 2 cm) and a subsurface fraction. The two fractions were homogenized separately and stored in closely lid plastic containers immediately after retrieval. Bivalve specimens for the Trondheimsfjord experiment was collected from the same area at similar depths by trawling a transect of the seafloor.

Upon return to Trondheim, the sediment was distributed into 41 plastic trays, surface sediment on top of subsurface sediment. The trays were then placed in plastic boxes and Four specimens of *Astarte sp.* (bivalves) placed in 15 preselected trays. The trays were then submerged in seawater and left to acclimatize for ten days at 6-8°C. On the first day of both experiments, the sediment trays were loaded into a titanium tank (TiTank), after which the TiTank was filled with water and the pressure increased to 30 bar using an external pump.

3.1.2 The South-Western Barents Sea

Sediment from the Barents Sea was collected in June, 2016 by DNV GL at sampling station R9-2 located approximately 40 kilometers north-east of the Snøhvit project (Fig. 1). A modified Van Veen grab was used to retrieve the sediment from 358 mbsl. Surface and subsurface sediment was separated, homogenized and stored in rilsan bags at -18°C until the experiment was commenced.

3.2 Experimental setup

The results presented in this thesis were obtained from two experiments conducted using the Karl Erik TiTank located at the SINTEF SEALAB, Trondheim. The TiTank is a 1.4 m^3 titanium-oxide pressure tank that has been custom built by SINTEF in collaboration with Equinor and NTNU for environmental research related to CO_2 storage (Fig. 7). The use of titanium oxide as the bulk material for the tank inhibits corrosion by seawater and CO_2, and reduces the risk of trace metal contamination. The TiTank is equipped with a decompression chamber, a fixed video camera, a tray carousel and a robotic arm which is used in the process of retrieving sediment samples while the experiment is ongoing (Fig. 7).

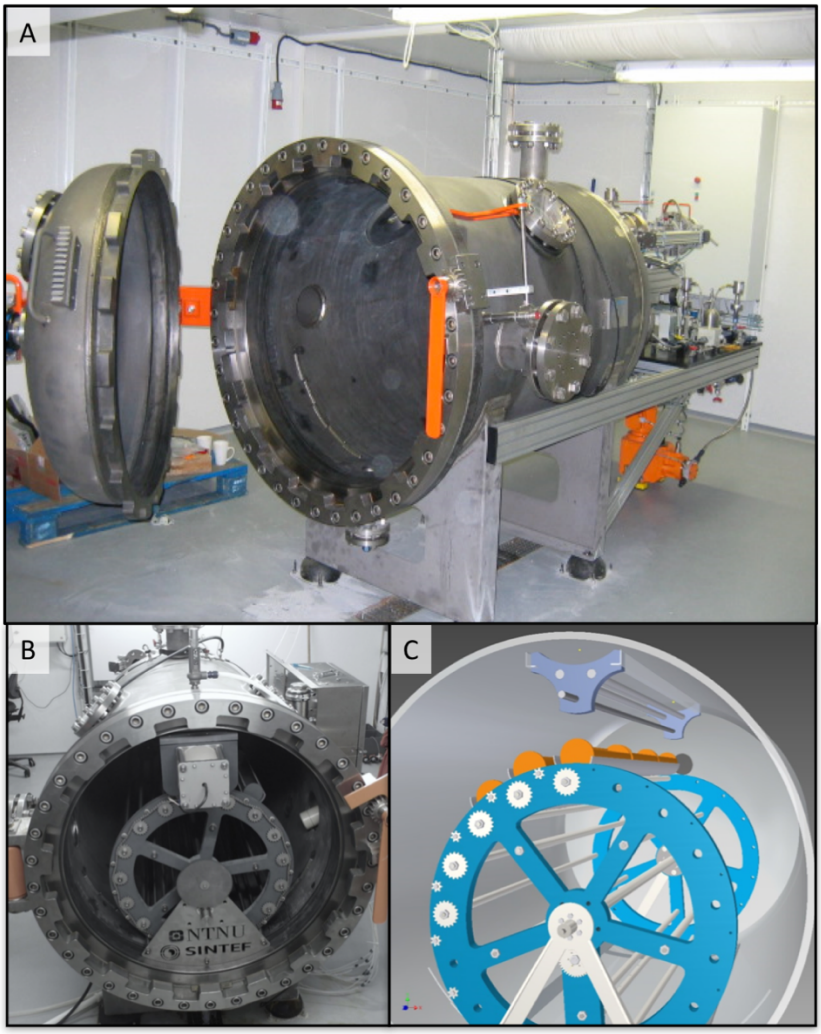

Fig. 7. The Karl Erik TiTank. A. Main chamber in the foreground, decompression chamber in the background. B. Main chamber of the TiTank showing the tray carousel. C. sketch of the TiTank interior including the water inlet at the top (Photos by Ida B. Overjordet).

3.2.1 Trondheimsfjord water inlet

The water used in the experiments was pumped from the Trondheim Bay at a depth of 75 meters. An external pump is used to regulate the inflow of sea-water and attain the desired pressure inside the TiTank, while a water outlet is positioned at the opposite end. During the CO_2 exposure period, the seawater is mixed with gaseous CO_2 before it enters the main chamber of the TiTank.

3.2.2 Sediment sampling and measurement of solution master variables

The first experiment used the Trondheimsfjord sediment, collected at sampling station trdfj-1 (Fig. 1). The experiment commenced the 11th of September 2017 and consisted of a 14-day control phase, a 50-day CO_2 exposure phase and a 14-day recovery phase (Appendix 1). The second experiment used the Barents Sea sediment, collected at sampling station R9-2 (Fig. 1). It was commenced the 26th of February 2018 and consisted of a 21-day control phase, a 50-day CO_2 exposure phase and a 14-day recovery phase (Appendix 2).

Sediment sampling took place on predetermined dates selected in order to attain the desired data resolution. To retrieve a sample, the externally operated robotic arm was used to push the selected tray into the decompression chamber. Pressure-communication between the two chambers was then halted and decompression initiated by draining the water from inside the decompression chamber. The decompression process lasted 30 minutes equivalent to a pressure decrease of 1 bar per minute.

Immediately upon opening the decompression chamber, the tray was transferred to a shielded, metal-free environment to avoid contamination by airborne particles. Triplicates of surface and subsurface sediment were then sampled from each tray and transferred to 15 mL metal-free vials using a plastic spatula. The vials were stored in a freezer at -18°C.

Temperature, salinity, pH, redox potential and oxygen saturation were measured at 1.5 hour intervals during the experiments. For the inlet water, a Thermo Scientific Orion 5 Star pH, Cond, and DO meter with an Orion 013025MD Conductivity Cell and a Mettler Toledo HA405-DXK-S8/120 combination pH probe was used for measuring temperature, pH, and salinity. A Thermo Scientific Orion 3 Star pH meter with a Mettler Toledo Pt4805-DXK-S8/120 combination redox probe was used for measuring the redox potential. For the outlet water, a Thermo Scientific Orion Star A211 pH Meter with a Mettler Toledo HA405-DXK-S8/120 combination pH probe and an Orion 927005MD Epoxy ATC Probe was used for measuring temperature and pH. A Thermo Electron Corp. Orion 4 Star pH and Conductivity meter with a Mettler Toledo Pt4805-DXK-S8/120 combination redox probe was used for measuring the redox potential. Additionally, a Hach HQ20 O2 pH meter with a Hach LDO probe was used for measuring dissolved oxygen, temperature, and ambient barometric pressure.

Total alkalinity (TA) was determined by titration of water samples with HCl until an abrupt change in pH indicates that the buffer capacity of the solution had been surpassed. Sample triplets from both input and output water were collected twice during the control phase, eight times during the exposure phase and three times during the recovery phase. TA is reported in meq/L.

Bivalves were sampled on the same days as the sediment, while outlet water samples were collected on separate days during the experiments. The results from the bivalve study and the outlet water analysis are currently being analyzed but are not the subject of this thesis.

3.3 X-Ray powder diffraction (XRD)

X-ray powder diffraction (XRD) is a powerful tool for mineral identification and quantification. The method exploits that all minerals have a unique atomic spacing within their crystal lattice. When an incipient x-ray hits a crystalline surface at an angle, it gets diffracted and creates an interference pattern which can be measured by a detector. Constructive interference occurs when Bragg's Law ($n\lambda = 2dsin\theta$) is satisfied. By knowing the wavelength of the x-ray (λ) and the integer (n), the atomic spacing (d) can be related to the incipient angle (θ). It is then possible to deduce the atomic spacing in the minerals present within a sample by systematically changing the incipient angle in small increments and recording the diffraction signal.

The raw data from an XRD analysis is a diffractogram (intensity vs. 2θ), from which mineralogical information can be extracted. Minerals are identified by comparing the measured peak positions with a database of known mineral phases. Mineral quantification

is done by fitting a modeled phase distribution to the observed spectrum solving a least square problem using the Rietveld-method (Young, 1993).

The most common issues recognized for XRD analyses emerge from the sample preparation process. The method assumes that the powder is homogeneous and that all mineral grains are randomly oriented. The first condition can be compromised if the powder is not homogenized after the milling and drying process. The second condition is particularly important to consider when non-spherical grains, e.g. mica, are expected to be present in the sample. If pressure is applied during the preparation, the mica grains will align perpendicular to the pressure and inhibit the x-rays from hitting the grains from all directions with equal frequency and thereby produce a false distribution. Furthermore, insufficient milling can result in a poor fit between the observed and modeled data, while excessive milling may destroy the crystal structure of weak minerals and compromise their identification.

The XRD method has some important key limitations. First off, with a detection limit close to 1 Wt%, only the major mineral phases can be identified. In the perspective of this study, geochemically important phases might pass by undetected because of their low volumetric contribution. Secondly, the output does not provide a unique solution but depends on the chosen input parameters and the quality of the database.

Two fractions were analyzed by XRD: a bulk and a fine fraction. The fine fraction (defined as grains smaller than 6μm) was separated by suspending a few grams of the sediment in a graduated cylinder and allowing the sediment resettle. The time required for all grains larger than 6μm to have settled was calculated to be 1 hour and 46 minutes using Stoke's law (Allen, 1985). When the time had passes, the fine fraction was vacuum-filtered from the suspension and transferred to a glass plate. Duplicate samples of both the Trondheimsfjord and the Barents Sea sediment were obtained. One from each sediment type was placed in an airtight container containing glycol and placed in an oven overnight at 60°C. Glycol enters between the layers of expanding clay minerals and makes them swell. The effect on the diffractogram retrieved by the XRD analysis is a shift of the mineral's primary peak. The following day, both the glycol treated and the untreated duplicate were analyzed by XRD. An identification of the expanding clay minerals can be made by comparing the diffractogram of the treated and untreated sample.

For the bulk analysis, sample powders were prepared by wet milling approximately one gram of each sediment sample with 10mL of ethanol for 180 seconds using a McCrone micronizing mill. The powders were then oven-dried at 110°C for 2 hours, homogenized and subsequently transferred to specimen holders where the surfaces were smoothed using a glass plate.

The sample preparation and XRD analysis was done at the chemical/mineralogical laboratory at the department of Geoscience and Petroleum, NTNU. The XRD analysis was carried out by Laurentius Tijhuis, NTNU, using a Bruker D8 ADVANCE X-ray Powder Diffractometer. Mineral identification was done in DIFFRAC.EVA using the PDF-4+ database and quantification in TOPAS.

3.4 Sequential extraction procedure

The total concentration of an element provides limited information about how the element is bound to the sediment and the likelihood of it being mobilized to the water column. Kersten (2002) argue that the reason for this is that a majority may be situated within

detrital mineral grains where it is inaccessible under the conditions encountered in the natural environmental. To obtain a better understanding of how various elements are bound to the sediments and their potential mobility, a four step sequential extraction was conducted in this study.

A sequential extraction is an analytical procedure which enables the determination of element concentrations in a sample based on their partitioning into a set of operationally defined species. Several protocols for the sequential extraction of sediments have been proposed (Tessier et al., 1979; Kersten and Förstner, 1986; Ure et al., 1993). However, many of these protocols have received criticism due to poor methods comparability and unsatisfactory interlaboratory reproducibility (Usero et al., 1998). The Standards, Methods and Testing Program of the European Commission undertook the task of resolving these issues and their work led to the development of the harmonized and improved BCR sequential extraction procedure (Rauret et al., 1999). The same study led to the certification of a reference material (BCR-701) in which the determination of Cd, Cr, Cu, Ni, Pb and Zn could be proven to have good interlaboratory reproducibility (Pueyo et al., 2001). The BCR sequential extraction procedure provides four operationally defined element fractions: an acid soluble (easily exchangeable), an easily reducible, an oxidizable and a residual fraction. It has been applied successfully to sediments from a large range of settings including marine deposits (Morillo et al., 2004; Cuong and Obbard, 2006; Sutherland, 2010). The BCR sequential extraction procedure was therefore chosen for this study.

Three subsamples from eleven sampling days were selected from each of the two experiments. The samples were split into three batches consisting of 22 samples and six blanks. The extraction was carried out at the Department of Chemistry, NTNU, during the fall of 2018. In February 2019, the sequential extraction was carried out on five replicas of the certified reference material BCR-701. Ideally, this should have been carried out alongside the sample extractions, but was not possible due to logistics.

3.4.1 Apparatus

Polypropylene or Teflon containers were used for handling samples and solutions. All materials were cleaned prior to the extraction by submerging them in 1M ultrapure nitric acid for a minimum of 24 hours and subsequently rinsing them with Milli-Q water a minimum of three times. An IEC Centra GP8 centrifuge and a GRANT OSL Aqua Pro water bath was used. A Kika LABORTECHNIK KS501 orbital shaker was used in this study instead of an end-over-end shaker as suggested in the protocol (Rauret et al., 1999). The shaker speed was adjusted such that the sediment remained in suspension throughout the shaking period as specified to account for this discrepancy.

3.4.2 Reagents

Four solutions are necessary to perform the sequential extraction procedure (Table 2). The hydrogen peroxide solution (solution B) was ready to use from the distributor, while the glacial acetic acid (solution A), the hydroxylamine hydrochloride (solution B) and the ammonium acetate solutions (solution D) were prepared in the clean lab of the Department of Chemistry at NTNU. Trace select or ultratrace select glacial acetic acid, hydroxylamine hydrochloride and hydrogen peroxide were used alongside analytical grade ammonium acetate. To eliminate the risk of trace metal contamination from the ammonium acetate solution, a Chelex-100 slurry was used to clean it as part of the solution preparation.

Solution	Primary reagent	Chemical formula	Concentration [M]	Used in
A	Acetic acid	CH_3COOH	0.5	Step 1
B	Hydroxylamine hydrochloride	$HONH_2 \cdot HCl$	0.5	Step 2
C	Hydrogen peroxide	H_2O_2	8.8	Step 3
D	Ammonium acetate	$C_2H_7NO_2$	1	Step 4

Table 2. Reagents. Overview of the composition and final concentration of the four solutions used in the sequential extraction procedure.

3.4.2.1 Water

Filtered and doubly deionized i.e. Milli-Q water was used in all steps of the sequential extraction procedure.

3.4.2.2 0.5M Acetic Acid (Solution A)

To prepare solution A, 500mL of Milli-Q water was added to a 1000mL graduated cylinder followed by 29.06 ± 0.2mL glacial acetic acid (Fluka TraceSelect Ultra, ≥ 99.0%). The graduated cylinder was then filled to 1000mL with Milli-Q water, after which the solution was transferred to a polypropylene flask.

3.4.2.3 0.5M Hydroxylamine Hydrochloride (Solution B)

A fresh batch of solution B was prepared on the day of the extraction by adding 540mL Milli-Q water to a 1000mL graduated cylinder and dissolving 20.85g of hydroxylamine hydrochloride (Sigma-Aldrich trace metal basis) in it. 3.45mL ultrapure nitric acid was then added to acidify the solution. Milli-Q water was subsequently poured into the graduated cylinder until the solution volume was 600mL. Thereafter, the solution was transferred to a polypropylene flask.

3.4.2.4 8.8M Hydrogen Peroxide (Solution C)

Fluka TraceSelect hydrogen peroxide 300mg/g was used. The solution is stabilized at pH = 2 by the manufacturer.

3.4.2.5 1M Ammonium Acetate (Solution D)

Solution D was prepared by adding 800mL Milli-Q water to a 1000mL graduated cylinder and dissolving 77.08g ammonium acetate in it. The pH of the solution was then adjusted to 5.9 using ultrapure nitric acid. 2-3 mL of Chelex-100 slurry was added to the solution, which was then transferred to a polypropylene flask and placed on a shaker. After two days, the solution could be filtered through a chromatographic column into a polypropylene flask. Finally, the solution was acidified to pH = 2.0 ± 0.1 using ultrapure nitric acid and made up to 1000mL with Milli-Q water.

3.4.3 Sequential Extraction Procedure

3.4.3.1 Sample preparation

The dry mass content was determined by drying approximately one gram of sample at 70°C to a constant weight. The sample mass before and after drying was used to calculate the solid mass content in the wet sample. Based on the above calculations, the approximate mass equivalent to 0.5 grams of dry material was transferred from each sample to a 50 mL centrifuge vial using a plastic spatula and the weight recorded.

3.4.3.2 Extraction step 1

The first step extracts the acid soluble fraction, sometimes also referred to as the easily exchangeable fraction. First, 15.6 mL of Milli-Q water was added to each sample followed by 4.4 mL of solution A to attain a 0.11 M concentration of acetic acid in the solution. Shortly after, the samples were placed on a shaker and shaken for 16 hours at 250 rpm. After turning off the shaker, the sediment was left to settle for 10-15 min and then centrifuged at 3000g for 20 minutes. The following procedure was used to collect the supernatant succeeding the first three extraction steps. 14-15 mL of supernatant was transferred to a 15 mL trace metal free vial and preserved by adding 5 drops of ultrapure nitric acid. The excess supernatant was discarded. To rinse the residue, 10 mL of Milli-Q water was added after which the samples were shaken at 250 rpm for 15 minutes and then centrifuged at 3000g for 20 minutes, as before. A minimum volume of water is used to rinse the sample to minimize solubilizing the solid fraction (Tessier et al., 1979). The liquid residue was then carefully decanted and discarded.

3.4.3.3 Extraction step 2

In the second step, the residue from step 1 was treated to extract the easily reducible fraction. First, 20mL of solution B was added to the vials, which were afterwards shaken for 16 hours at 250 rpm. Thereafter, the vials were centrifuged and the supernatant collected. This was done following the same procedure as described for extraction step 1.

3.4.3.4 Extraction step 3

In the third step, the residue from step 2 was treated to extract the oxidizable fraction. Firstly, 5mL of solution C was added to each vial and the lids loosely placed on top to allow the produced gas phase to escape. Secondly, the solution was left to react with the sediment for one hour, with occasional shaking during the first half hour. When the hour had passed, the vials were transferred to a water bath heated to 70°C. The temperature was then gradually increased to 85°C and the content of the vials was left to react for another hour. Afterwards, the lids were removed and the temperature increased again, this time to 90°C. When the volume had been reduced to 1-2mL, another 5mL of solution C was added and the lids loosely placed on top of the vials. After an additional hour in the water bath at 85°C, the lids were removed and the temperature increased to 90°C. When the liquid volume had been reduced to approximately 1mL, the vials were removed from the water bath and left to cool to room temperature with the lids on. 25mL of solution D was then added to the vials, which were subsequently shaken for 16 hours as during the previous steps. The ammonium acetate is added to avoid adsorption of extracted elements onto the particulate surfaces (Tessier et al., 1979). Finally, the supernatant was collected using the procedure described for step 1.

3.4.3.5 Extraction step 4

The final step extracts the residual fraction. The rinsed residue from step 3 was stored at -20°C until step 1-3 had been carried out for all three batches in order to allow step 4 to be carried out for all samples simultaneously. An UltraClave was used to extract the residual fraction instead of *agua regia* (which is recommended in the standard protocol) for HSE reasons (Rauret et al., 1999). The first step in the UltraClave digestion process was to quantitatively transfer the samples from the centrifuge vials to acid-washed Teflon tubes. This was done by adding a total of 10mL 50% ultrapure nitric acid in three split doses, shaking the container to suspend the sediment and pouring the suspension into the Teflon tubes. The samples were digested in an UltraClave for two hours at a temperature and pressure of up to 240°C and 120 bar, respectively. The exact temperature and

pressure profile can be seen in Appendix 3. Thereafter, each of the extracts were diluted by the addition of 110mL of Milli-Q water. 14-15mL of the diluted extracts were collected in 15mL trace metal free vials.

3.5 High Resolution Inductive Coupled Plasma Mass Spectrometry (HR-ICP-MS)

ICP-MS is a preferred choice for element analysis because of its reliability, low quantification limits and ability to measure the targeted elements time-efficiently (Skoog et al., 2013). In an ICP-MS analysis, a plasma ion source produces a high-temperature argon plasma capable of ionizing the elements of the sample. The ionized elements are then transferred to the mass spectrometer where they are separated based on their mass-to-charge ratio (m/z). The concentrations are determined from the strength of the specific m/z signal. Argon is chosen because of its high ionization potential which enables it to ionize all elements of the periodic table except He, F and Ne.

An issue related to the use of ICP-MS for element analysis is the interference between ions of similar mass from either the sample matrix or the plasma. This affect the determination of certain important elements including As, Cr, Fe and Ca. The issue can be solved for the first three elements (but not Ca) by increasing the resolving power to distinguish the signal peaks. A consequence of doing so is reduced sensitivity, which may complicate the quantification, but only if the analyte concentration is low. No issues of this type were identified during the sample analysis.

Element concentrations were determined by Syverin Lierhagen at the Department of Chemistry at NTNU, using a Thermo Finnigan Element 2 High-Resolution Inductive Coupled Plasma Mass Spectrometer (HR-ICP-MS). Three repeated measurements were completed for each element of each extract. The reported analytical results correspond to the mean of these three measurements, together with two times the analytical standard deviation.

3.6 Data analysis

3.6.1 Preprocessing

ICP-MS results were first subtracted the average blank value and then back-calculated from μg/L to solid sample (μg/g or parts per million - ppm) using the dry mass of each sample and the volume of supernatant retrieved from each extraction step.

3.6.2 Method detection limit

The method detection limit (MDL) for ICP-MS is here defined as the lowest concentration that can be determined above the level of a blank sample with a 99% probability. Practically, the MDL is found by comparing the instrument detection limit (IDL) with the blank detection limit (BDL) and setting the highest as the MDL. The BDL is defined as 3.3 times the standard deviation of the mean of the blank samples. The IDL provided by the instrument manufacturer represents the IDL that can be attained under ideal conditions with a clean instrument. This is commonly not representative for routine analyses. A laboratory-specific IDL was therefore used in this study. The laboratory-specific IDL was defined as the concentration above which the relative standard deviation of repeated measurements was less than 25%. This value was subsequently corrected for matrix effects. Elements with more than half of the samples below the MDL was excluded from further analysis.

3.6.3 Quality assurance

To ensure reproducibility, the certified reference material (CRM) for the four-step sequential extraction procedure (BCR-701) was extracted and analyzed using the same procedure as for the samples. Certified values of the CRM are provided for Cd, Ni, Cu, Cr, Pb and Zn (Pueyo et al., 2001). The results were compared to the certified values by means of calculating the percentage recovery and Z-scores for each of the six elements within the four fractions. Z-scores is a common method for assessing interlaboratory reproducibility (Sutherland, 2010). They are computed by:

$$Z\text{-}score = \frac{X_{det} - X_{cert}}{h(a)}$$

where X_{det} is the determined concentration, X_{cert} is the certified value and $h(a)$ is the target value which must be calculated for each fraction and element using:

$$h(a) = 0.02 * \left(\frac{X_{cert}}{10^6}\right)^{0.8495} * 10^6$$

The generally accepted interpretation of Z-scores is that $Z \leq 2$ represents a satisfactory reproducibility, $2 \leq Z \leq 3$ is questionable and $Z \geq 3$ is unsatisfactory (Sutherland, 2010).

3.7 Statistical analysis

A statistical analysis can be used to determine trends in datasets and verify their statistical significance. The two main methods used in this study are linear regression models and two-sample hypothesis test for difference in mean responses. Box plots are used to present summary statistics. These three methods will be introduced in the following sections. All data processing and statistical analyses were carried out in Matlab R2018b (version 9.5).

3.7.1 Linear regression models

A linear regression model can be used to describe the relationship between variables where one is expected to respond to changes in the other at a constant rate. Mathematically, it can be noted as $Y = \alpha X + \beta$, where the two constants, α and β, describe the relationship between X and Y, known as the independent variable and the dependent variable, respectively. The ordinary least squares method (OLS) is thereafter used to calculate the values of α and β which ensure the smallest difference between the linear regression model and the observations (Gardiner, 1997). The residuals of the OLS can be used to calculate the R^2-value of a correlation. The R^2-value describes the proportion of the variance observed in Y that is explained by X in the model.

3.7.2 Two-sample hypothesis test for difference in mean responses

A CO_2 exposure experiment can be treated as a two-sample experiment: one sample subset is collected prior to the CO_2 exposure (the control phase) and one after the exposure (the recovery phase). This enables the performance of a two-sample hypothesis test, or t-test, for difference in mean responses (Gardiner, 1997). According to Gardiner (1997), a t-test determines whether a hypothesis can be accepted or rejected at a predetermined significance level. The output of the test is a p-value and represents the likelihood that a random process alone could have produced the observed response. A commonly applied hypothesis is the null-hypothesis. The null-hypothesis states, in the two-sample case, that there is no difference between the mean responses of the two samples. If the t-test returns a p-value below the chosen significance level, the hypothesis can be rejected and one can conclude that the two samples have a statistically significant difference in mean responses.

If the p-value is above the significance level, the null-hypothesis cannot be rejected. Importantly, failure to reject the hypothesis does not prove the hypothesis to be true. A significance level of 0.05 was used in this study.

A hypothesis test assumes that the samples are independent and normally distributed around their mean and can be performed both with and without assuming equal variance. Which version to be used was determined by calculating the ratio of largest sample variance to smallest sample variance, a so-called the F-test (Gardiner, 1997). If the ratio, F, was below 3, the samples were said to have equal variance and a pooled t-test was performed. If F was above 3, the samples were said to have unequal variance and a Welch's test was performed.

3.7.3 Box plots

A box plot is a convenient tool for presenting summary statistics. A red line in the box represents the median, while the edges of the box mark the extend of q_1 and q_3, the 25^{th} and 75^{th} percentiles, respectively. Potential outliers are defined as values greater than $q_3 + 1.5(q_3 - q_1)$ or less than $q_1 - 1.5(q_3 - q_1)$. These are marked by a "+". The range corresponds to 99.3% of the area under a normal distribution with the same mean and standard deviation as the data. The fences (or whiskers) are marked by broken lines and extend to the most extreme data points not determined as outliers. In this study, one box plot is made for the control phase samples and one for the recovery phase samples. This is done to facilitate a comparison between the two subsets.

3.8 Data presentation

3.8.1 Chemical equilibrium diagrams

The chemical systems have been defined using the thermodynamic database Hydra. Medusa have been used to create the chemical equilibrium diagrams. Both programs have been developed by Ignasi Puigdomenech at the Department of Chemistry at Kungliga Tekniska Högskolan, Sweden. The software is based on the SOLGASWATER (Eriksson, 1979) and HALTAFALL (Ingri et al., 1967) algorithms.

4 Results

4.1 Mineral phases and bulk composition

Mineral phases were identified based on their primary d-value peaks and verified through an identification of their secondary peaks. As examples, chlorite was identified by its primary 14.2Å and secondary 7.2Å peaks, and kaolinite by its primary 7Å and secondary 3.58Å peaks. Illite is a common product from the physical weathering of muscovite. They therefore have similar crystal structures and share a primary d-value peak at 10Å. Due to the similar d-values, it was not possible to distinguish illite and muscovite in the samples by XRD. Their contribution to the total sediment volume is therefore presented collectively. Additional mineral phases were identified during the quantification process by doing multiple iterations of the model run and testing whether the addition of another phase would significantly improve the model fit to the measured XRD-spectrum. 2-5% halite was identified in all samples. This is considered an artifact from the sample preparation process prior to the XRD-analysis. It is inferred that drying the samples caused precipitation of halite from the saline pore-water. To eliminate this artifact from the dataset, the mineral quantification is presented on a halite-free basis.

XRD spectrums of representative samples from the Trondheimsfjord dataset and the Barents Sea dataset are presented in Fig. 8 and Fig. 9, respectively. The amplitude of the fluctuations in the residual error plots (grey lines) are small compared to the peak height in the same interval indicating that the modeled XRD-spectrums (red lines) have a satisfactory fit to the measurements (blue lines). Furthermore, all peaks are matched by the model, which suggests that no quantitatively important mineral phases were omitted from the model.

The mineral phases which contribute to >1% of the total sediment mass were identified and quantified by XRD. The composition of four control phase samples and four recovery phase samples from the Trondheimsfjord sediment is depicted in Fig. 10a and Fig. 10b, respectively. No compositional differences can be identified between the control phase and the recovery phase samples. The average composition of the Trondheimsfjord sediment samples is 27% quartz, 25% feldspars, 21% muscovite/illite, 8% Mg-rich biotite, 12% chlorite and 6% other minerals (pyroxenes/amphiboles) (Fig. 11a). Calcite and dolomite were identified, but both contribute less than 1% to the total sediment mass.

The composition of four control phase samples and four recovery phase samples from the Barents Sea sediment is depicted in Fig. 10c and Fig. 10d. It is noteworthy that contrary to previous studies on CO_2 exposure (e.g. Blackford et al., 2014), the XRD results do not indicate that the calcite and dolomite content of the sediment is reduced during the exposure phase. The average composition of the control phase samples of the Barents Sea sediment is 34% quartz, 24% feldspars, 16% muscovite/illite, 6% Mg-rich biotite, 8% chlorite, 5% kaolinite, 3% calcite, 2% dolomite and 3% other minerals (pyroxenes/amphiboles) (Fig. 11b).

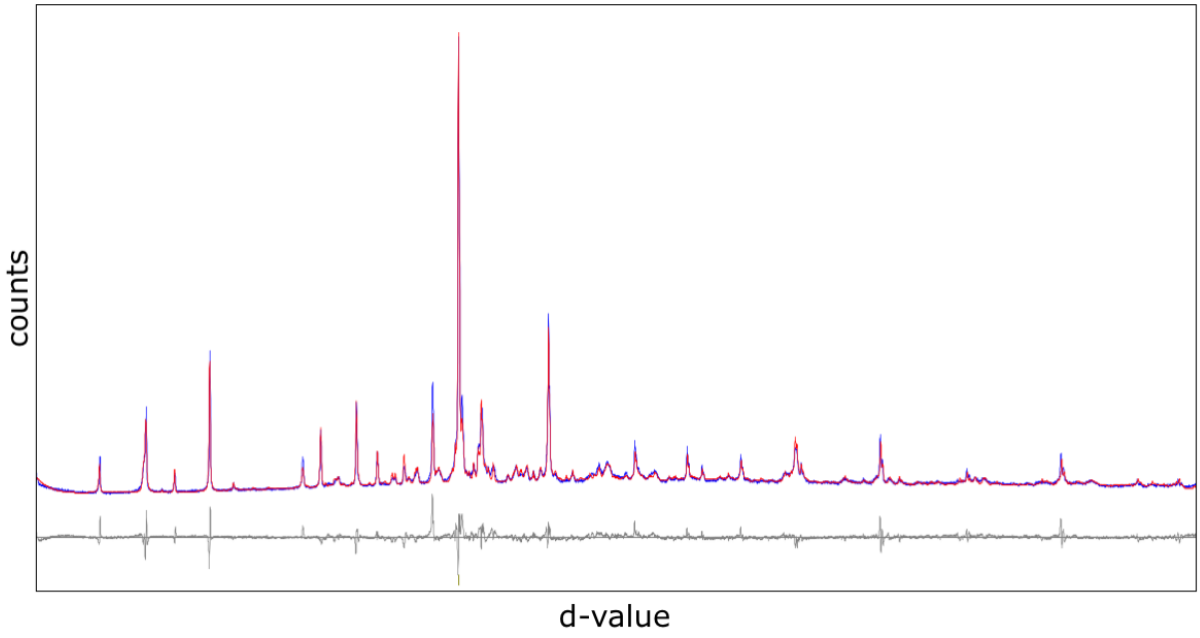

Fig. 8. XRD-spectrum of the Trondheimsfjord sediment. The modeled spectrum (red curve) shows a good fit to the measurements (blue curve), which is also indicated by the low amplitude of the residual error plot (grey curve).

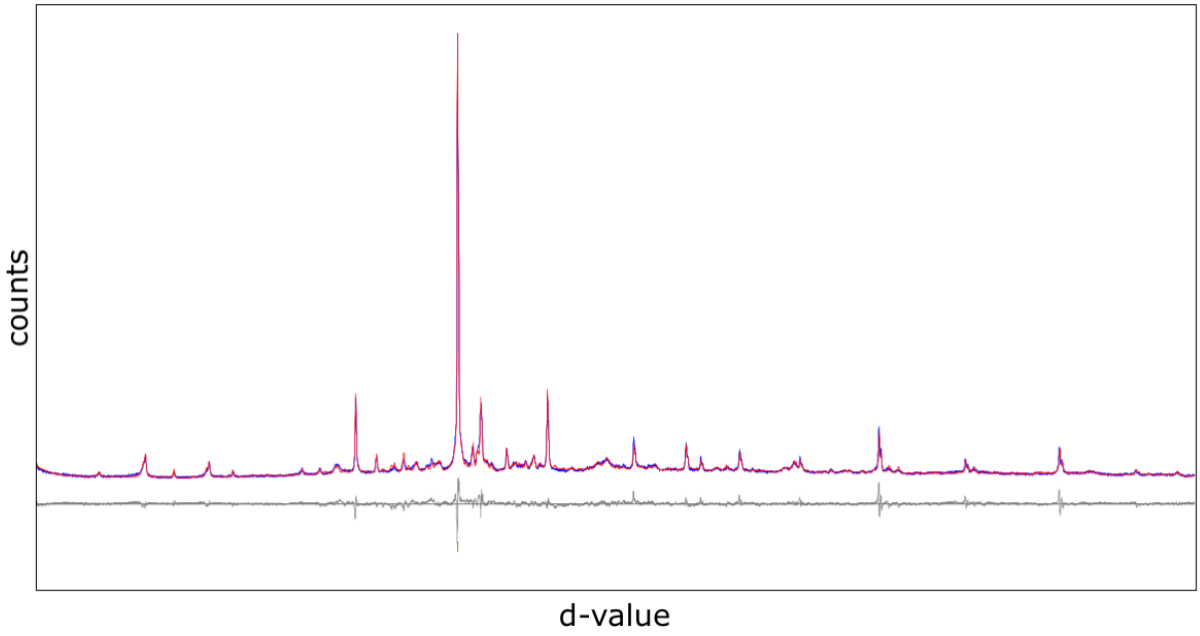

Fig. 9. XRD-spectrum of the Barents Sea sediment. The modeled spectrum (red curve) aligns well with the measured spectrum (blue curve), which is also indicated by the low amplitude of the residual error plot (grey curve).

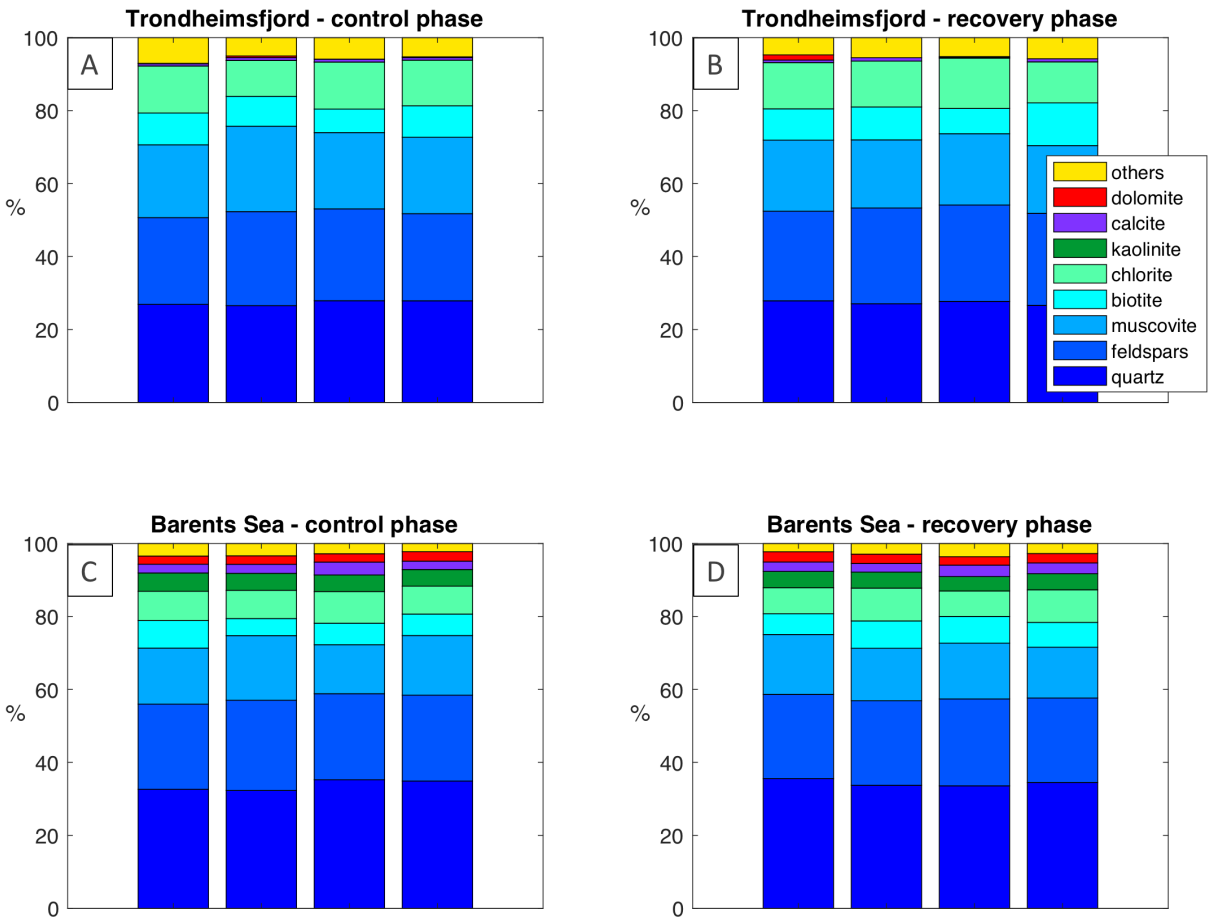

Fig. 10. Distribution of major mineral phases. A. Control phase of the Trondheimsfjord sediment. B. Recovery phase of the Trondheimsfjord sediment. C. Control phase of the Barents Sea sediment. D. Recovery phase of the Barents Sea sediment. Some variations in the relative abundance of the phyllosilicates muscovite, biotite and chlorite can be observed, but the samples display an overall homogeneous composition within the same phase. The control phase and recovery phase samples appear to have very similar composition in both experiments.

The Trondheimsfjord and Barents Sea sediments primarily consist of the felsic minerals quartz and feldspars alongside the phyllosilicates muscovite, biotite and chlorite. The major differences between the two sediments are found among the minor mineral phases. The Barents Sea sediment contains kaolinite, which is absent in the Trondheimsfjord sediment. The sediment from the Barents Sea also contains a larger proportion of calcite and dolomite. Furthermore, the Trondheimsfjord sediment contains twice the amount of pyroxene and amphibole present in the Barents Sea sediment. These observations are in agreement with previous studies of surface sediments from the same areas (Vogt and Knies, 2009; Faust et al., 2014).

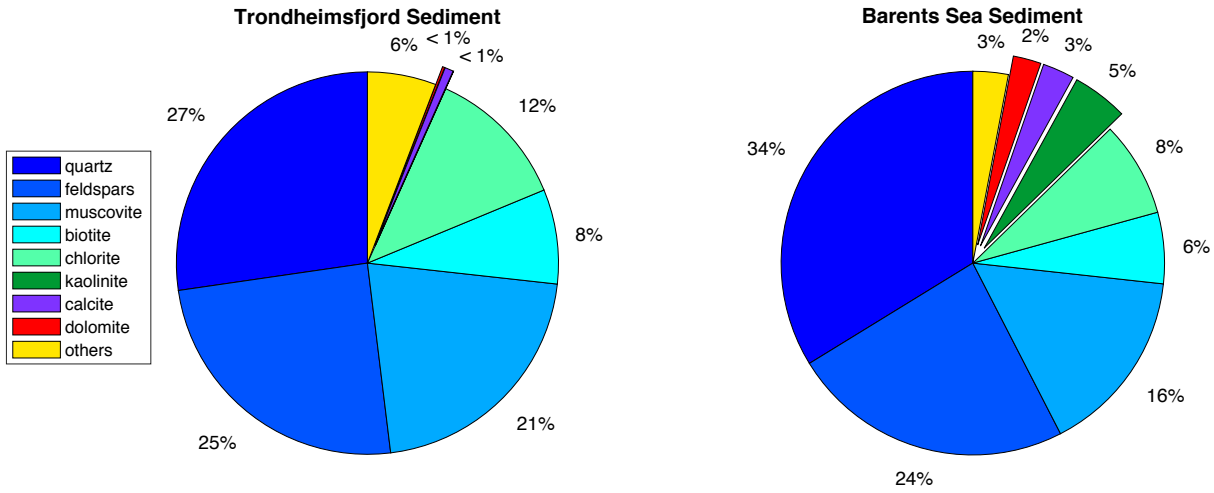

Fig. 11. Average mineral composition of the control phase samples. A. Trondheimsfjord sediment. B. Barents Sea sediment. Kaolinite, calcite and dolomite is more abundant in the Barents Sea sediment, while pyroxene and amphibole contribute more to the bulk composition of the Trondheimsfjord sediment.

The fine fraction (here defined as grains smaller than 6μm) of one sample from the control phase of both sediment types was split into two subsamples, resulting in four subsamples. A swell test was conducted on one subsample from each of the sediments. All of the four subsamples were then analyzed by XRD. For both the Trondheimsfjord and the Barents Sea sediment, the results revealed that all primary d-value peaks found in the bulk sample can be identified within the fine fraction with no appearance of additional primary peaks (Appendix 4 and 5). Upon treating the Barents Sea sample with glycol, the narrow 14Å peak shifted to a broad 16.5Å peak, indicative of expanding clay minerals. This signature is common for clay minerals within the smectite group. In this case, beidelite is considered the most likely mineral based on a good match of its secondary peaks. No shifting of the 14Å peak was observed in the glycol treated sample from the Trondheimsfjord. It was not possible to attain a quantification of the mineralogical composition of the fine fraction. The separation method did not allow a collection of the necessary 0.5-1 gram to guarantee a representative result from the XRD-analysis.

4.2 Solution master variables

The solution master variables are summarized in Table 3 and Table 4. A full disclosure of the data can be found in Appendix 6 and 7. Dissolved inorganic carbon (DIC), pCO_2 and CO_3^{2-} have been calculated in CO2SYS (van Heuven et al., 2011). $\Omega_{aragonite}$ and $\Omega_{calcite}$ were calculated by adopting a salinity-corrected marine $[Ca^{2+}]$ applying the rule of constant proportions (Millero, 2005) and pressure-corrected solubility products for aragonite and calcite from Sarmiento and Gruber (2006).

	Trondheimsfjord	Barents Sea
pH_{inlet}	8.0	7.9
Dissolved O_2 (%)	100	100
pE_{outlet} (mV)	355	333
T_{inlet} (°C)	8.2	8.0
T_{outlet} (°C)	8.6	8.9
Salinity (‰)	30	30
Ca (mmol/kg)	8.80	9.10

Table 3. Average values of solution master variables. All values represent measurements except [Ca^{2+}] which was calculated from the salinity assuming constant proportions between the major ions in seawater (Millero, 2005).

Experiment	Trondheimsfjord			Barents Sea		
phase	control	exposure	recovery	control	exposure	recovery
pH_{outlet}	8.01	6.89	7.9	7.96	6.97	7.8
TA_{in} (meq/L)	2279	2291	2303	2323	2357	2328
TA_{out} (meq/L)	2291	2243	2273	2346	2353	2335
DIC (µmol/kg)	2156	2537	2177	2229	2606	2270
pCO_2 (µatm)	454	6545	595	539	5792	800
[CO_3^{2-}] (µmol/kg)	104.7	8.7	82.7	96.3	10.9	68.5
$\Omega_{aragonite}$	1.27	0.11	1.01	1.21	0.14	0.86
$\Omega_{calcite}$	2.02	0.17	1.59	1.92	0.22	1.36

Table 4. Average values of the solution master variables. pH_{outlet}, TA_{in}, TA_{out} are averages of measurements, while DIC, pCO_2 and CO_3^{2-} have been calculated using CO2SYS (van Heuven et al., 2011). $\Omega_{aragonite}$ and $\Omega_{calcite}$ have been calculated from the ion activity product of [Ca^{2+}] and [CO_3^{2-}], and the equilibrium constants for the solubility products corrected to P = 30 bar following (Millero, 1983, cited in Sarmiento and Gruber, 2006).

4.2.1 pH

In the Trondheimsfjord experiment, the inlet water pH remains stable within the range of 7.96 to 8.1 throughout the course of the experiment. Two days after the onset of CO_2 injection (day 16), the pH of the outlet water drops from 7.9 to 7, and later stays between 6.8 and 7.1 until the CO_2 injection is terminated on day 50. Within the first three days of the recovery phase, the pH had recovered to above 7.8.

In the Barents Sea experiment, the pH of the inlet water stays within the range of 7.83 and 8.02 during the course of the experiment. In the outlet water, the pH is maintained above 7.9 during the control phase. By the onset of CO_2 injection, the pH starts to drop and does so at a gradually decreasing rate until it stabilizes at pH = 6.7 after six days. An intermission occurred four days later. The CO_2 gas container had been emptied and as a result, the pH started to increase. The incident was discovered after two days and the container was immediately replaced such that CO_2 injection could be resumed. After another four days, the pH had stabilized at pH = 7.1. During the first four days of the recovery phase, the pH increased to above 7.8.

4.2.2 Redox potential

In the Trondheimsfjord experiment, the redox potential (Eh) of the inlet water begins at 100mV and increases like a bounded exponential function until it reaches 340mV one week into the exposure phase. The redox potential of the outlet water starts at 150mV, but increases to 340mV within the first three days.

In the Barents Sea experiment, the redox potential of the inlet water remains stable within the range of pE = 260-360mV throughout the experiment. The redox potential of the outlet water starts at pE = 210mV and increases like a bounded exponential function to 340mV across the duration of the control phase. During the first week of the exposure phase the redox potential experiences a drop to a nadir of 240mV from which it gradually builds up to 350mV and maintains for the remainder of the experiment duration.

4.2.3 Total alkalinity

Total alkalinity (TA) of both the inlet and outlet water remains within 2170-2428 meq/L for the Trondheimsfjord experiment and 2250-2431 meq/L for the Barents Sea experiment. The mean TA-values for each experiment phase are listed in Table 4. The mean TA was slightly higher during the Barents Sea experiment compared to the Trondheimsfjord experiment.

4.2.4 Dissolved oxygen saturation

The dissolved oxygen saturation level (DO) remained above 90% throughout the course of both the Trondheimsfjord and the Barents Sea experiment.

4.2.5 Temperature & salinity

In the Trondheimsfjord experiment, the average salinity was 30 and the range of the inlet and outlet water temperatures were T_{inlet} = 7.3-9.3°C and T_{outlet} = 8.4-9.3°C. In the Barents Sea experiment, the average salinity was 31 and T_{inlet} = 7.5-8.6°C and T_{outlet} = 8.7-8.9°C.

4.2.6 Saturation index

The water is slightly supersaturated ($\Omega > 1$) with respect to aragonite and calcite during the control phase and undersaturated during the exposure phase (Ω = 0.1-0.2) of both experiments. During the recovery phase $\Omega_{aragonite} \approx 1$ in the Trondheimsfjord experiment and $\Omega_{aragonite} < 1$ in the Barents Sea experiment, while $\Omega_{calcite} > 1$ in both cases.

4.3 Element concentrations

4.3.1 Preprocessing

Preprocessing of the ICP-MS data from the sequential extraction was carried out to ensure that the results are reported in relevant units and to screen the data for outliers. The outliers may be a product of contamination during the experiments, the sequential extraction process or the ICP-MS analysis. Using the extract volume and the initial dry sediment mass, the results from the ICP-MS analysis were converted from microgram per liter of extract ($\frac{\mu g}{L}$) to microgram per gram of sediment ($\frac{\mu g}{g}$), or parts per million (ppm). The results are presented in ppm for concentrations above 1ppm and parts per billion (ppb) for concentrations below 1ppm. For certain elements, half of the samples or more fell below the method detection limit (MDL) and were therefore omitted from further analysis (Table 5).

	Elements with more than half of samples below MDL	
Fraction	Trondheimsfjord	Barents Sea
Acid soluble	Se, Nb, Mo, Sn, W	Se, Nb, Mo, Sn, Hf, W, Hg, Sc
Easily reducible	Se, Sn	Se, Sn
Oxidizable	Sn, Sb	Sn, Sb
Residual	Se, Sb	Se, W, Hg, Sb

Table 5. Elements with more than half of samples below the method detection limit (MDL). MDL was determined as the highest value of the instrument detection limit (IDL) and three times the standard deviation of the blank.

The concentration of certain elements cannot be determined reliably by ICP-MS and are therefore not included in the results. These include the noble gasses, light elements (H, O, N and C), and some common anions (Cl, I and F).

Repeating tests revealed that the first five samples from the acid soluble fraction of the Trondheimsfjord sediment had been contaminated with mercury (Hg), caused by leaching from the mass spectrometer. This is a commonly observed issue when analyzing samples containing acetic acid by ICP-MS analysis, but only affects the first few samples (Syverin Lierhagen, personal communication, 2019). To resolve the issue, the results for Hg from the first ten measurements were omitted from further analysis.

In the Trondheimsfjord experiment, bivalve specimens (*Astarte sp.*) were placed atop the sediment in a selected number of trays. A screening of the dataset revealed that the samples taken from trays containing bivalves have systematically higher concentrations of Fe, V, Co, Cu, Zn and As, and lower Mn in the acid soluble fraction than the trays without bivalves. Within the easily reducible fraction, Mn is higher, while the concentration of Fe, V, Co, Cu, Zn, As is lower. This is interpreted as a disruption of the vertical redox-zonation within the sediment by bioturbation (Thomson et al., 1993). The affected sample days are day 11 and 14 of the control phase, day 24 and 39 of the exposure phase and day 78 of the recovery phase. Because of this, the data for Fe, Mn, V, Co, Cu, Zn and As from the aforementioned sample days have been omitted from further analysis.

4.3.2 Quality assurance

The sequential extraction procedure was carried out on replicate samples of the certified reference material BCR-701 in order to assess the quality of the extraction. Certified values for Cd, Pb, Cr, Ni, Cu and Zn are provided by Pueyo et al. (2001). The certified values are

listed in Table 6, alongside median values of five replicate extractions. The percentage recovered and Z-scores are calculated following the methodology of Sutherland (2010). Z ≤ 2 represents a satisfactory reproducibility, 2 ≤ Z ≤ 3 is questionable and Z ≥ 3 is unsatisfactory.

Fraction	Value	Cd	Pb	Cr	Ni	Cu	Zn
AS	Determined	6.7	3.0	1.9	11.3	42.6	186.4
	Certified	7.3 ± 0.4	3.18 ± 0.21	2.26 ± 0.16	15.4 ± 0.9	49.3 ± 1.7	205 ± 6
	% recovery	92	96	83	73	86	91
	Z-score	-0.64	-0.33	-1.18	-2.52	-1.53	-1.27
RED	Determined	2.6	96.3	22.4	14.3	97.4	72.1
	Certified	3.77 ± 0.28	126 ± 3	45.7 ± 2.0	26.6 ± 1.3	124 ± 3	114 ± 5
	% recovery	68	76	49	54	79	63
	Z-score	-2.42	-3.05	-5.67	-4.72	-2.77	-4.68
OX	Determined	0.4	15.5	150.5	17.1	57.6	54.1
	Certified	0.27 ± 0.06	9.3 ± 2.0	143 ± 7	15.3 ± 0.9	55 ± 4	46 ± 4
	% recovery	165	167	105	112	105	118
	Z-score	3.33	5.87	0.69	1.09	0.54	1.96
RES	Determined	0.2	20.1	97.3	37.3	40.3	112.6
	Indicative	0.13 ± 0.08	11 ± 6	63 ± 8	41 ± 4	39 ± 12	95 ± 13
	% recovery	151	183	154	91	103	119
	Z-score	2.35	7.45	6.35	-0.99	0.36	2.30

Table 6. Quality assurance results from the extraction of the certified reference material BCR-701. The determined value is the median value obtained from extracting five replicas of the CRM. Certified and indicative values are provided by Pueyo et al. (2001). Z-scores have been calculated to evaluate the reproducibility of the certified values. Z < 2 is satisfactory, 2 < Z < 3 is questionable, Z > 3 is unsatisfactory. Unsatisfactory Z-scores are presented in bold.

The certified values are slightly underestimated for all six elements in the acid soluble fraction. Ni had the lowest recovery (73%) and is the only element that has a questionable Z-score. The results show an unacceptably low recovery in the easily reducible fraction

ranging from 49% for Cr to 79% for Cu. The poor recovery is also evident from questionable Z-scores for Cd and Cu and unsatisfactory Z-scores for Pb, Cr, Ni and Zn. The concentrations of Cr, Ni, Cu and Zn are slightly overestimated in the oxidizable fraction (105-118%), while a 165% and 167% recovery were obtained for Cd and Pb, respectively. The pattern is less systematic in the residual fraction. The concentration of some elements are overestimated (Cd, Pb, Cr and Zn), while the determined values for Ni and Cu are in good agreement with the indicative values.

In general, the element concentrations underestimated in the acid soluble fraction and the easily reducible fraction, and overestimated in the oxidizable and residual fraction. Cu is an exception as it has a 91% recovery in the residual fraction. A total of 11 elements have satisfactory Z-scores, 5 are questionable and 8 are unsatisfactory.

4.4 Distribution of major elements by fraction

The relative contribution of the major elements within each fraction has been determined. The results presented are average concentrations of these elements in the control phase samples. The contribution of minor and trace elements (here defined as <1% of the total mass within the fraction) is presented collectively.

In the acid soluble fraction of the Trondheimsfjord sediment samples, Na accounts for more than half of the mass, followed by Ca, Mg, S, K and Fe (Fig. 12). A part of this stems from dissolved Na, Ca, Mg, S and K in the pore water. In the easily reducible fraction, Fe is the most abundant element, succeeded by Al and Si, thereafter Ca and Mg, and finally P and K. In the oxidizable fraction, Mg, Al, Si and Fe occupy almost equal parts, followed by K, Na and Ca. In the residual fraction, Al and Fe together contribute to two-thirds of the total mass. The last third consist of Mg, K, Ca and Si. These are listed in order of decreasing concentration.

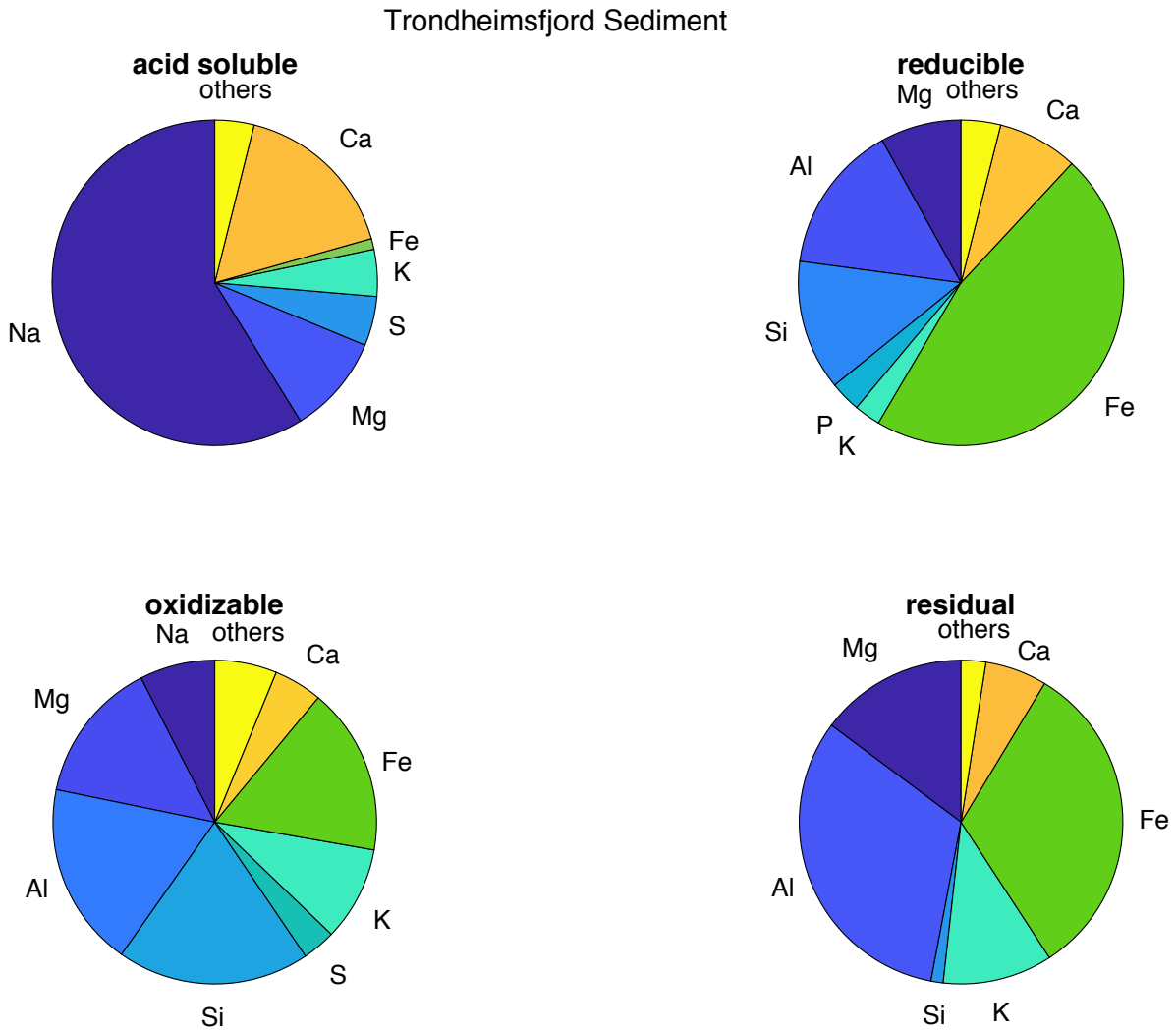

Fig. 12. Major elements in the four fraction of the Trondheimsfjord sediment. Calculated from the average concentration of the control phase samples.

Ca is the most abundant element in the acid soluble fraction of the Barents Sea sediment followed by Na and Mg, while K, S and Fe make minor contributions (Fig. 13). Some part of the Na, Mg, K and S stems from dissolved species in the pore water. In the easily reducible fraction, Fe and Ca together account for slightly more than half the mass. They are followed by Si, Al, Mg, K and P. The oxidizable fraction contains approximately equal parts of Fe, Al, Si and Mg but also significant amounts of Na, K and Ca. In the residual fraction, Al and Fe together represents to two-thirds of the total mass. The last third consist of Mg, K, Ca and Si, listed in order of contribution.

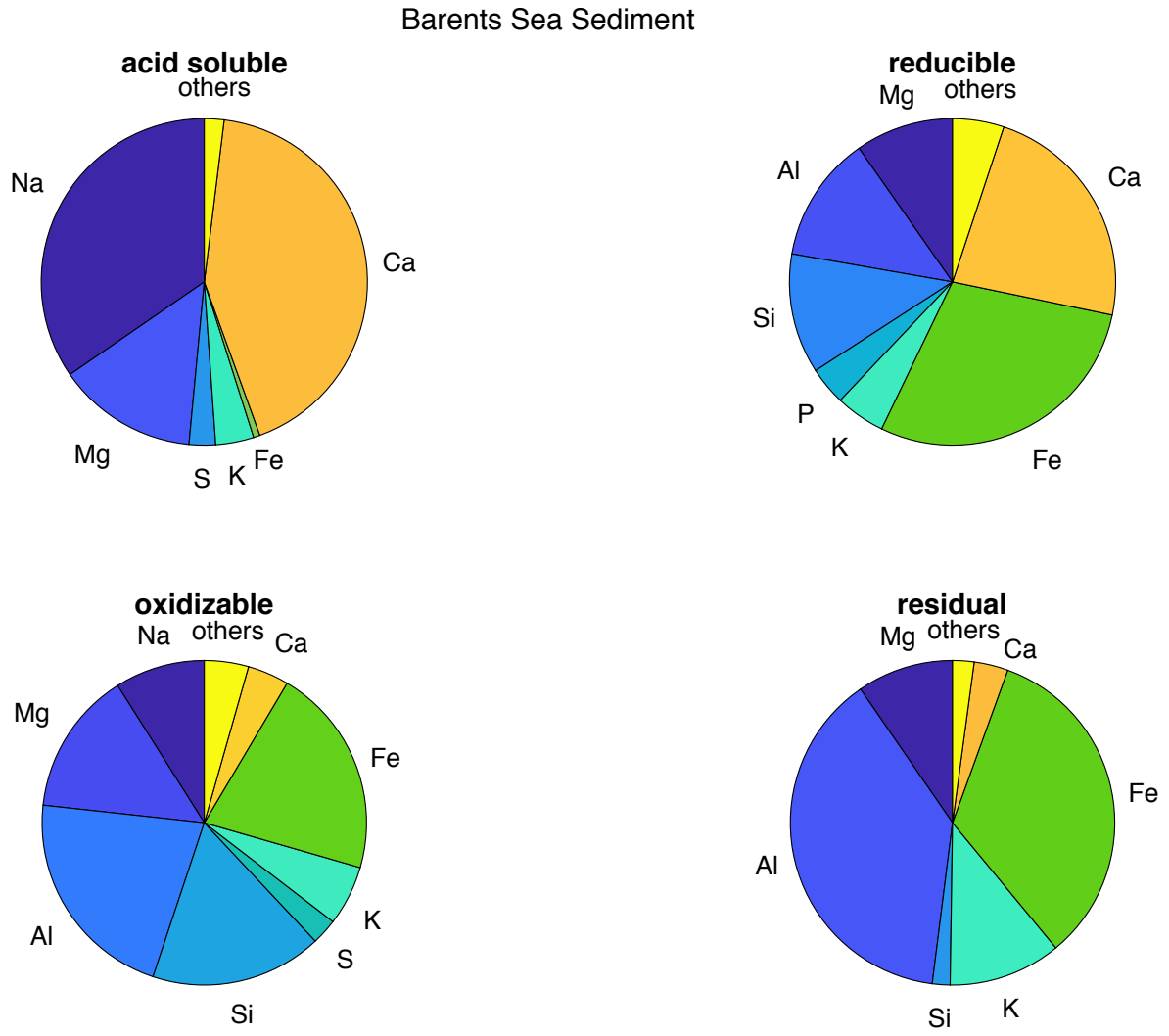

Fig. 13. Major elements in the four fraction of the Barents Sea sediment. Calculated from the average concentration of the control phase samples.

By assuming a relatively pure $CaCO_3$-phase (e.g. aragonite or low-Mg calcite), the Ca-concentration in the acid soluble fraction of the Trondheimsfjord sediment corresponds to a $CaCO_3$-content of 0.96%. Doing the same calculation for the Barents Sea sediment results in a $CaCO_3$-content of 2.4%. These estimates correlate well with the results from the XRD-analysis.

4.5 Distribution of selected minor and trace elements by fraction

The distribution of the minor and trace elements Cd, Hg, Pb, U, V, Cr, Mn, Co, Ni, Cu, Zn and As between the four analyzed fractions is presented in this section. The purpose of this approach is to determine where a given element is most abundant and, hence, under which conditions mobilization may occur. Emphasis is placed on the acid soluble, easily reducible and oxidizable fraction, as these fractions are the most vulnerable to mobilization (Rauret et al., 1999). They will from now on be referred to as the "environmentally accessible fractions". The selection of elements is made based on well-established knowledge about their roles within the marine biogeochemical cycles. They can be seen as participants in the Fe and Mn redox-shuttle across the sediment-water interface (Fe, Mn, Cd, Pb, As, Co, Ni, Cu, Zn and V), (micro-)nutrients for primary producers or cofactors in enzymes (P, Zn, Ni, Co, Cu, Fe and Cd) and toxicants (Cd, Hg, Pb, U, As and Cr) (Lane and Morel, 2000; Morel and Price, 2003; Tribovillard et al., 2006; Bendell, 2010). As is evident from this subcategorization, many of these elements occupy multiple roles in the marine environment. They will from now on be referred to as the "reactive elements".

	Cd	Hg	Pb	U	V	Cr	Mn	Co	Ni	Cu	Zn	As
TF	0.04	0.05	23	1.5	92	109	1000	17	53	28	130	6.9
BS	0.09	0.02	13	1.1	78	67	450	12	34	15	70	3.1
BAC	0.31	0.07	38	-	-	81	-	-	36	27	122	25

Table 7. Comparison of total element concentrations with the Background Assessment Criteria (BAC) as defined by OSPAR (2005). Concentrations are noted in ppm. TF = Trondheimsfjord, BS = Barents Sea. Cr, Ni, Cu and Zn exceed the BAC in the TF sediment and are therefore presented in bold.

The distribution of the reactive elements between the four fractions of the Trondheimsfjord sediment is depicted in Fig. 14a. Cd (30%) and Mn (50%) have a large component within the acid soluble fraction, while Pb (75%), As (60%), Cu (40%), Zn (30%), V (20%) and Co (15%) are abundant within the easily reducible fraction. In the oxidizable fraction only Hg (60%), Cu (20%) and U (15%) are particularly abundant. Elements that have more than 50% of their total mass hosted by detrital grains (the residual fraction) are Cr, Ni, V, U, Co and Zn.

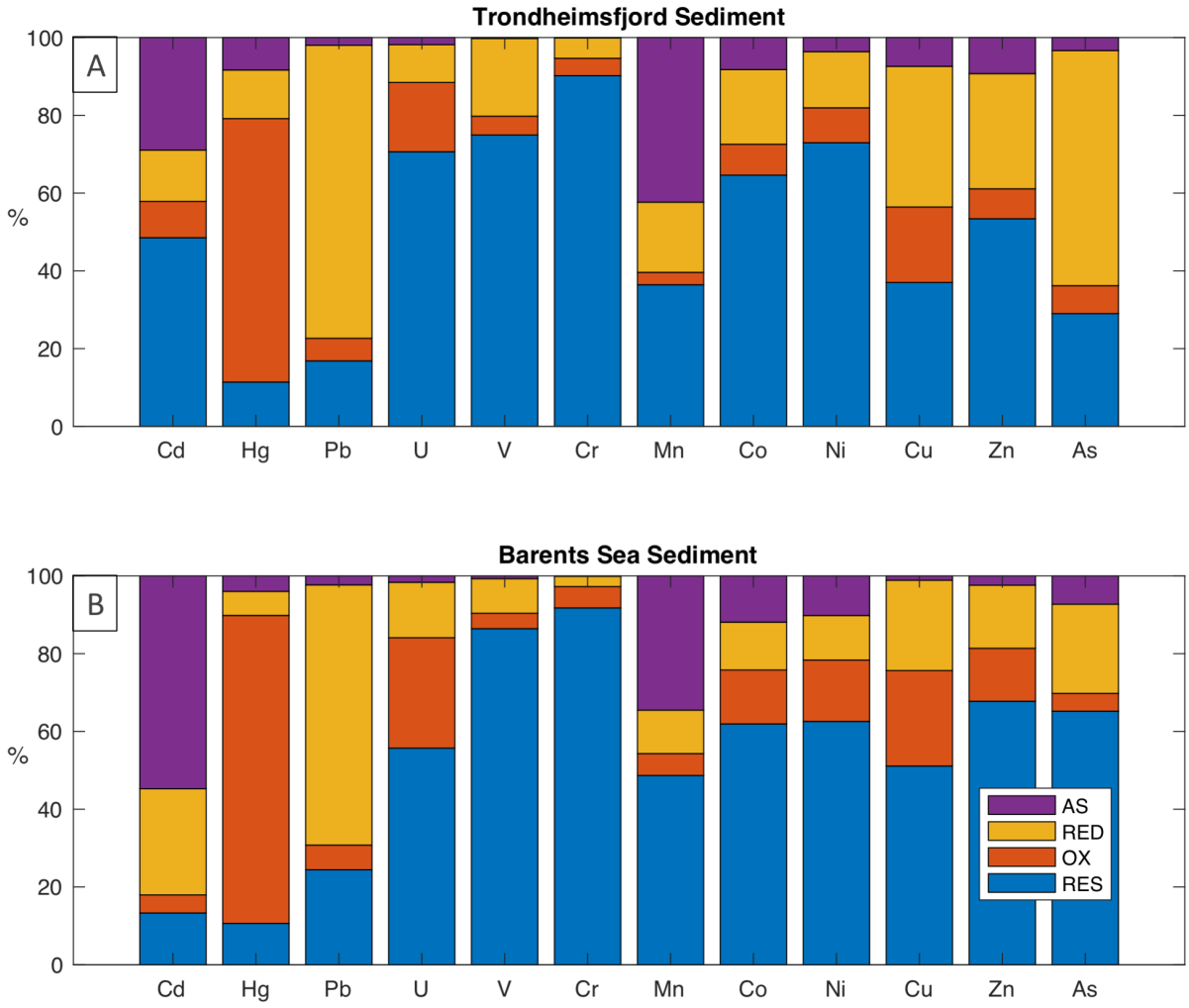

Fig. 14. Distribution of selected minor and trace elements between the four extracted fractions. A. Trondheimsfjord sediment. B. Barents Sea sediment. It can be seen that Cd and Mn are primarily abundant in the acid soluble fraction, Pb, Cu, Zn and As in the easily reducible fraction, Hg, U and Cu in the oxidizable fraction while several elements, including V, Cr and Ni, are dominated by a large detrital input.

The distribution of the reactive elements between the four fractions within the control phase samples of the Barents Sea sediment is depicted in Fig. 14b. Similar to the Trondheimsfjord sediment, Cd (55%) and Mn (35%) are primarily found within the acid soluble fraction, but in the Barents Sea sediment, 30% of the total Cd is hosted by the easily reducible fraction compared to 10% within the Trondheimsfjord sediment. While the portion of Pb (65%), As (20%), Cu (20%), Zn (15%), V (10%) and Co (10%) in the easily reducible fraction is lower, the share of Hg (90%), Cu (25%) and U (30%) hosted by the oxidizable fraction is slightly higher than in the Trondheimsfjord sediment. More than 50% of the total Cr, V, Zn, As, Ni, Co, U and Cu stems from detrital grains (the residual fraction).

The total concentrations of the reactive elements are generally higher in the Trondheimsfjord sediment than the Barents Sea sediment, except for Cd which is twice as abundant in the Barents Sea sediment (Table 7). The total concentrations of Cr, Ni, Cu and Zn are above the Background Assessment Criteria (BAC) as determined by OSPAR (2005). Of these, only Ni exceeds the "Predicted No Effect Concentration" as defined in the EU's risk assessment program (EC, 2003). However, the results from the sequential extraction

demonstrate that less than 30% of the total Ni is situated within the environmentally accessible fractions (Fig. 14).

4.6 Changes in element concentrations over time

Scatterplots are used to demonstrate the changes in element concentrations that occur during the experiments. Three subsamples were collected on each sample day. The individual data points presented in the following correspond to the mean of three ICP-MS measurements of each subsample. When relevant, a linear regression model is fitted to the scatterplots. Box plots are used to summarize the descriptive statistics of the control phase and the recovery phase samples.

4.6.1 The acid soluble fraction

4.6.1.1 Calcium

The concentration of calcium in the acid soluble fraction of the Trondheimsfjord and the Barents Sea sediments is presented in Fig. 15 and Fig. 16, respectively. In the Trondheimsfjord samples, the mean concentration of the control phase samples is 3797ppm, while that of the recovery phase is 3399ppm. The difference between the two is 398ppm, which corresponds to a 10.5% decrease. The difference is statistically significant (p = 0.028). The linear regression model with the best fit to the observations can be expressed as $[Ca] = -8.9059 \frac{ppm}{day} * t + 4041.1 ppm$ and has an R^2-value of 0.7217. The box plots of the control and recovery phase samples reveal that four potential outliers are present in the dataset, three from the control phase and one from the recovery phase. The two box plots have no overlap, further strengthening the argument that the two subsets are significantly different.

In the Barents Sea samples, no changes in the Ca-concentration can be observed during the experiment, and the box plots of the control and recovery phase overlap completely (Fig. 16).

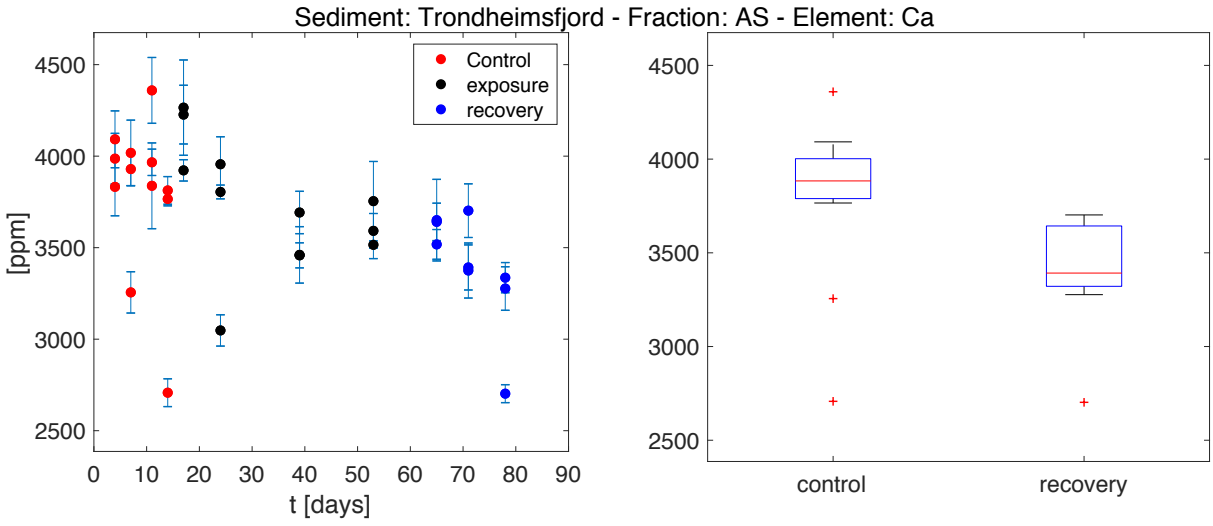

Fig. 15. Concentration of Ca in the acid soluble fraction of the Trondheimsfjord sediment. The data shows a statistically significant decrease in the concentration of Ca of 10.5% (p = 0.028) from the control phase to the recovery phase. The boxplots (right panel) show limited overlap between the control phase and recovery phase samples, except for two potential outliers in the control phase subset.

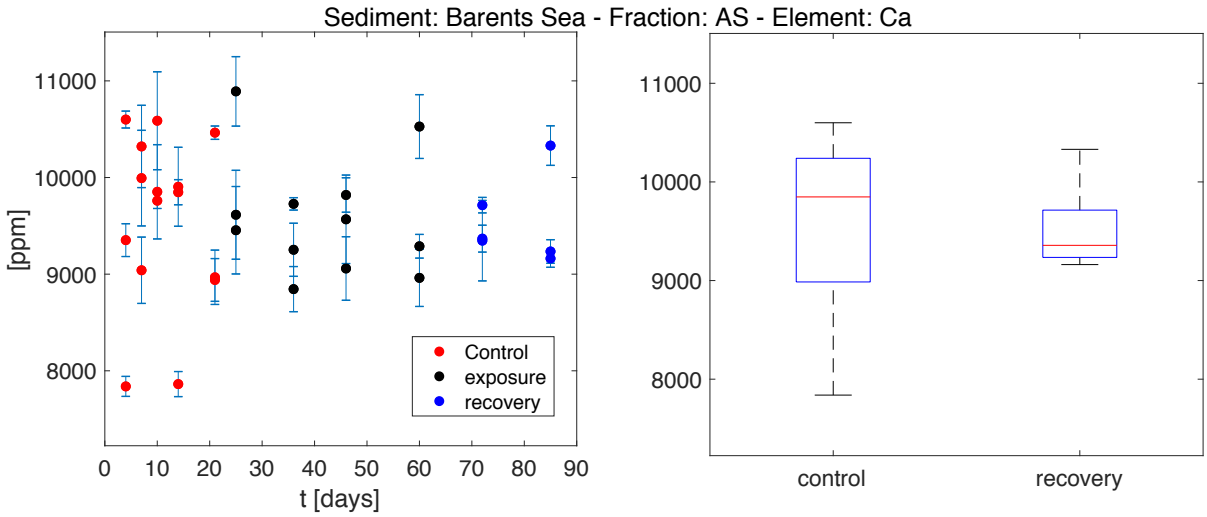

Fig. 16. Concentration of Ca in the acid soluble fraction of the Barents Sea sediment. The concentration of Ca does not change in response to the CO_2 exposure. This is evident from the complete overlap between the boxplots of the control phase and the recovery phase samples (right panel).

4.6.1.2 Uranium

In the Barents Sea sediment, the uranium (U) concentration of the control phase samples ranges from 14.6 to 22.8 ppb, with a mean value of 18.6 ppb (Fig. 17). The control phase samples therefore span almost the entire range of the U-data for the acid soluble fraction (14.6-23.6 ppb). Yet, the median values of each sample day show less variation and they all lie between 17.4 and 18.9 ppb. During the exposure phase, the median concentration of each sample day steadily climbs from 17.8 ppb on day 25 to 22.8 ppb on day 60, equivalent to a 28% increase. The box plots of the control phase and the recovery phase samples have a considerable overlap; hence the two subsets are not significantly different.

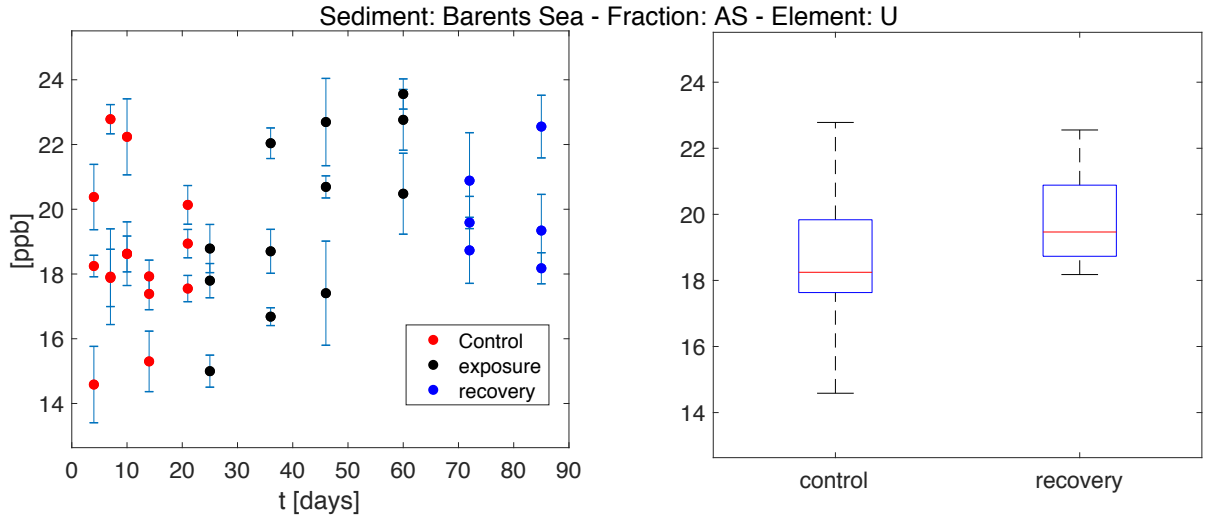

Fig. 17. Concentration of U in the acid soluble fraction of the Barents Sea sediment. The data show a large spread within the control phase and a linear increase during the exposure phase. The difference in concentration between the control phase and recovery phase samples is not statistically significant ($p > 0.05$).

4.6.1.3 Fe, P, V, Ni, Co and Zn

The concentrations of Fe, P, V, Ni, Co and Zn diminish during the control phase in the Barents Sea sediment (Fig. 18). Two different modes of decrease can be observed. Fe, P and V experience an abrupt drop between day 7 and 10, while the decrease in Ni, Co and Zn occurs gradually throughout the control phase. None of these elements experience a change in concentration as a result of the CO_2 exposure during the exposure phase.

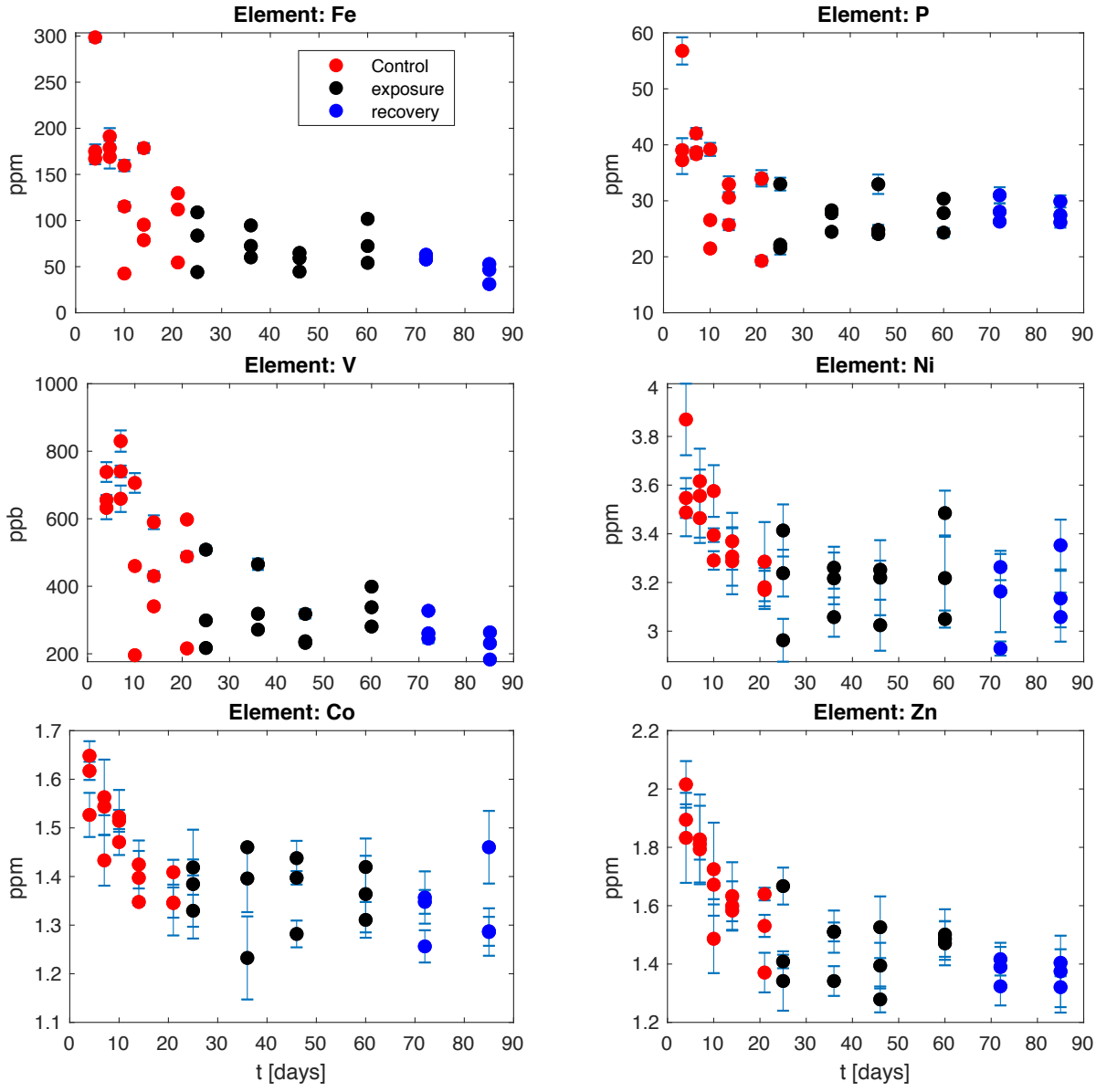

Fig. 18. Concentration of Fe, P, V, Ni, Co and Zn in the acid soluble fraction of the Barents Sea sediment. These elements show a marked decrease in concentration during the control phase indicating that some process have mobilized them from the acid soluble fraction prior to the CO_2 exposure.

4.6.1.4 Cadmium

Cadmium (Cd) in the Trondheimsfjord sediment experiences a 1.6 ppb decrease during the CO_2 exposure phase from a mean of 12.5 ppb in the control phase to 10.9 ppb in the recovery phase (Fig. 19). A t-test cannot confirm the statistical significance of this decrease ($p = 0.088$). However, if the first sample day of the exposure phase is included in the control phase subset and the last sample day of the exposure phase in the recovery phase subset, the t-test returns $p = 0.0076$. The box plots of the control and recovery phase samples does not overlap, but their whiskers do.

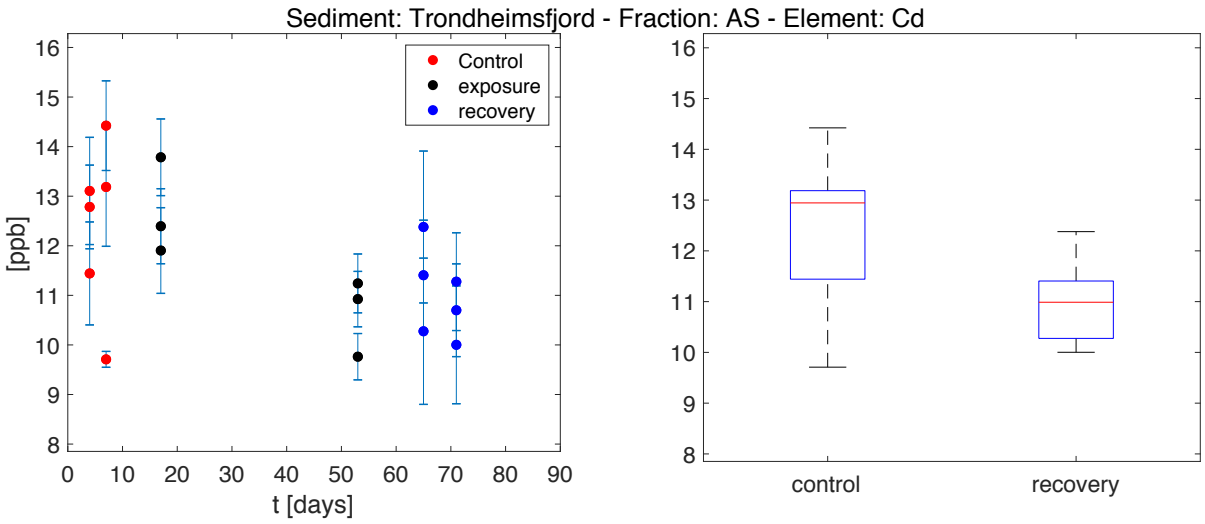

Fig. 19. Concentration of Cd in the acid soluble fraction of the Trondheimsfjord experiment. The mean concentration is 12.8% lower in the recovery phase compared to the control phase.

4.6.1.5 Arsenic

The mean arsenic (As) concentration of the Trondheimsfjord sediment decreases from 217ppb in the control phase to 155ppb in the recovery phase (Fig. 20). This 29% difference is statistically significant ($p = 0.0085$), which can also be deduced from the separation of the two box plots. The upper fence of the recovery phase box plot overlap with the control phase box because of one sample from the recovery phase with an As-concentration of 230ppb.

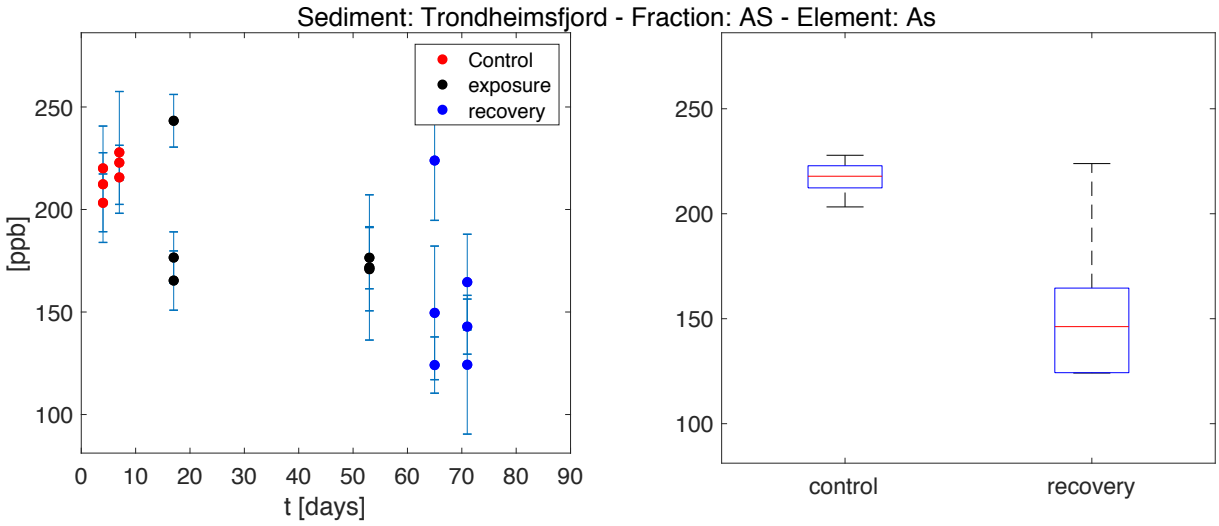

Fig. 20. Concentration of As in the acid soluble fraction of the Trondheimsfjord sediment. The 29% decrease in concentration from the control phase to the recovery phase is statistically significant (p = 0.0085). One sample from the recovery phase subset overlaps with the control phase samples.

4.6.2 The easily reducible fraction

4.6.2.1 Iron

In the Barents Sea sediment, the mean Fe-concentration of the easily reducible fraction increases by 153ppm, or 6%, from a mean of 2496ppm within the control phase to a mean of 2649ppm in the recovery phase (Fig. 21). A two-sample t-test for difference in mean response returns a p-value of 0.015 verifying that the increase in concentration has statistical significance.

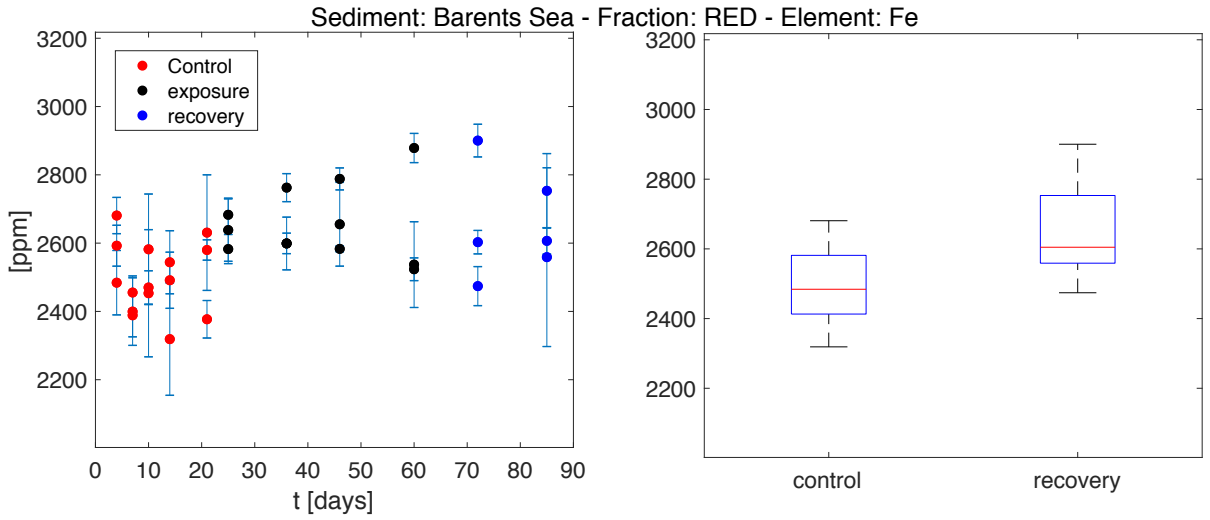

Fig. 21. Concentration of Fe in the easily reducible fraction of the Barents Sea sediment. The concentration increase by the onset of the exposure phase. The increase has statistical significance (p = 0.015), even though box plots of the control phase and recovery phase samples overlap.

4.6.2.2 Cadmium

From the control phase to the recovery phase, the mean Cd-concentration decreases from 24.4 to 16.7ppb, i.e. 7.7ppb or 31% (Fig. 22). A two-sample t-test for difference in mean response results in a p-value < 0.001, indicating that the decrease is statistically significant. The best fit linear regression model is $[Cd] = -0.11\ \frac{ppb}{day} * t\ + 25.8ppb$ and has an R^2-value of 0.85.

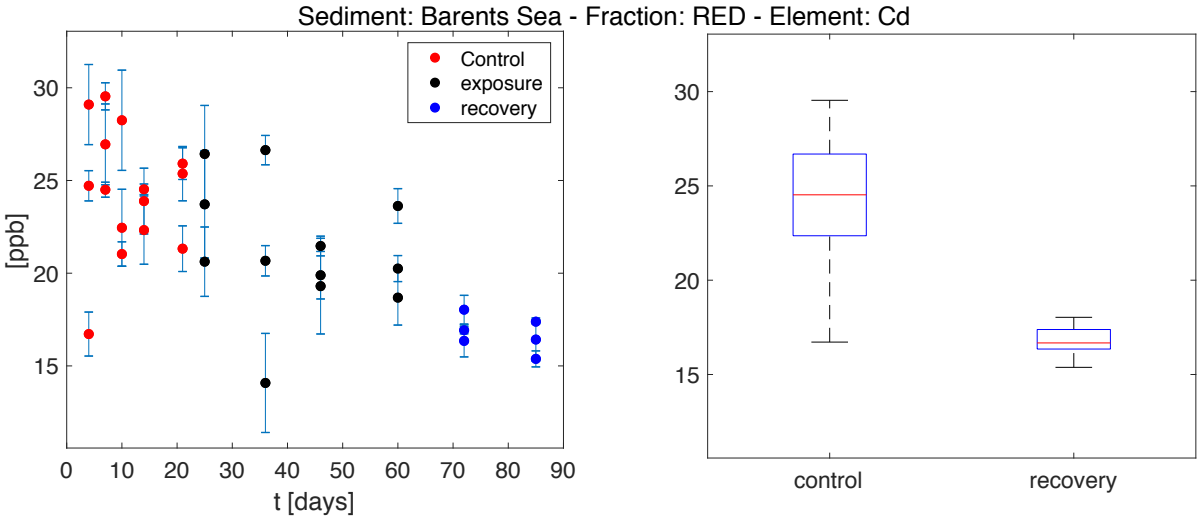

Fig. 22. Concentration of Cd in the easily reducible fraction of the Barents Sea sediment. The concentration decreases by 31% from the onset of the exposure phase to the recovery phase.

4.6.2.3 Uranium

Uranium in the easily reducible fraction of the Barents Sea sediment experiences a decrease during the control phase, from a median value of 173ppb on day 4 to 0.150ppb on day 14 (Fig. 23). Following the onset of the exposure phase, the median U-concentration of each sample day increases linearly from 148ppb on day 25 to 177ppb on day 60. The U-concentration decreases again to below 165ppb during the recovery phase.

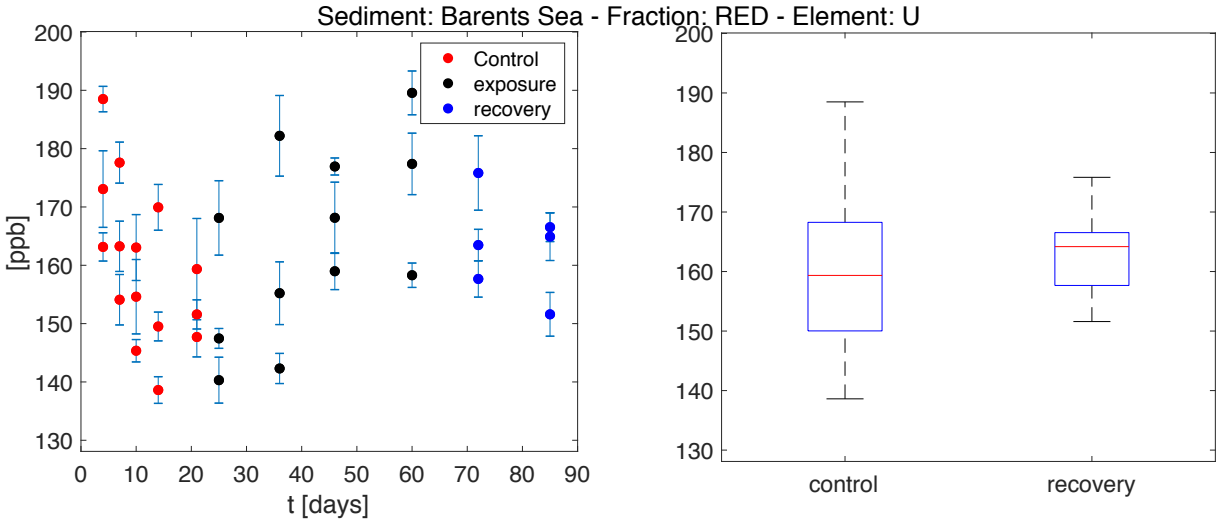

Fig. 23. Concentration of U in the easily reducible fraction of the Barents Sea sediment. It is evident that the U concentration decreases during the control phase but increases during the exposure phase.

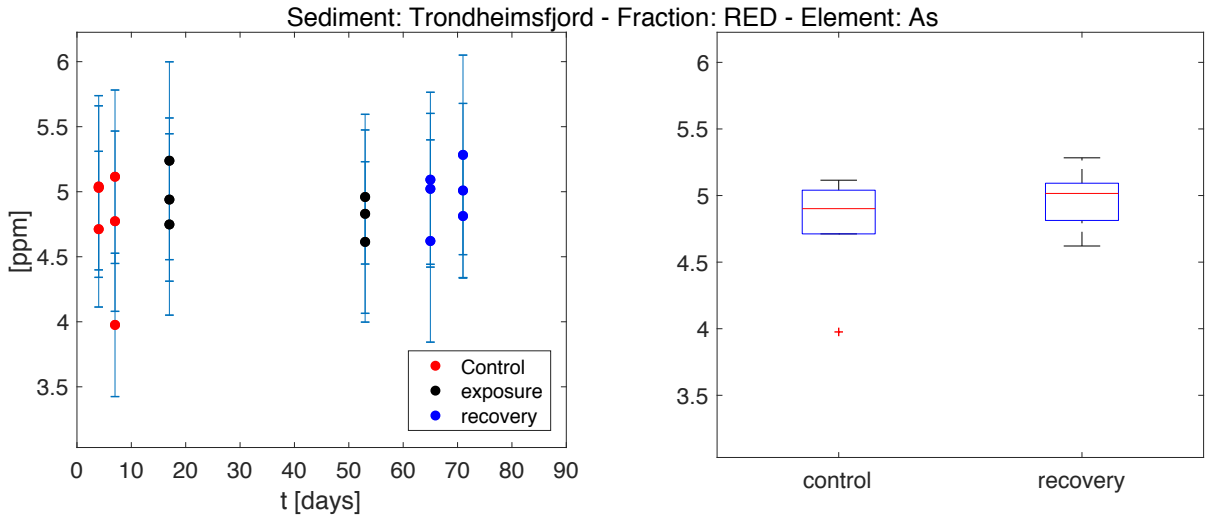

Fig. 24. Concentration of As in the easily reducible fraction of the Trondheimsfjord experiment. The concentration is unchanged throughout the experiment.

4.6.2.4 Arsenic

The arsenic concentration in the easily reducible fraction of the Trondheimsfjord experiment remains constant between 4-5.25 ppm throughout the experiment (Fig. 24). No difference can be observed between the control phase and the recovery phase samples.

4.6.3 The oxidizable fraction

4.6.3.1 Mercury

Similar to Fe, P, V, Ni, Co and Zn in the acid soluble phase, mercury (Hg) shows a gradual decrease during the control phase, from a median value of 16.71ppb on day 4 to 10.4ppb on day 21 in the Barents Sea sediment (Fig. 25).

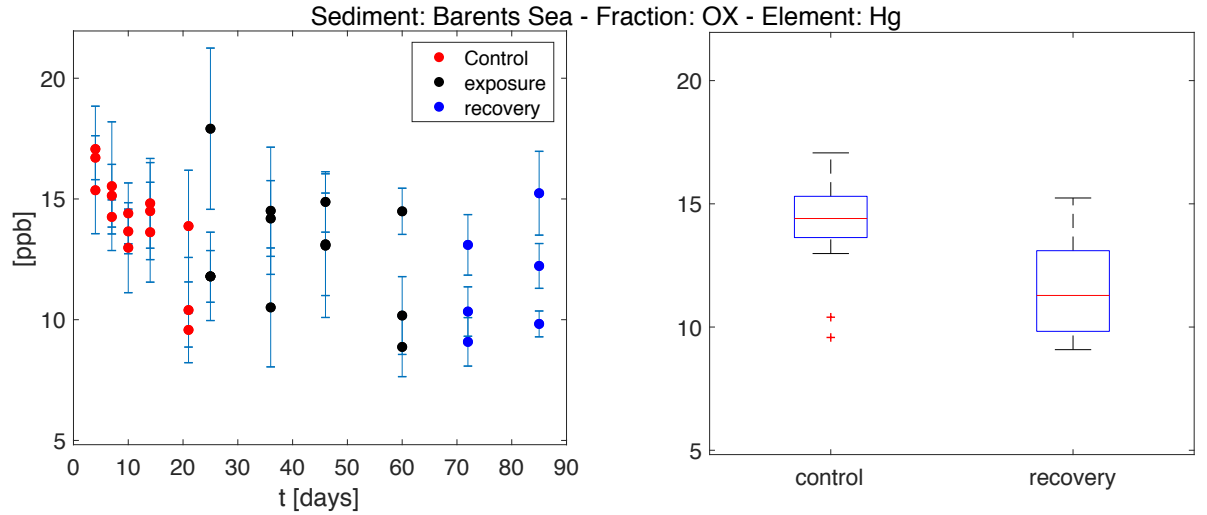

Fig. 25. Concentration of Hg in the oxidizable fraction. The concentration decreases within the control phase but stabilizes by the onset of the exposure phase.

5 Discussion

5.1 XRD – bulk sediment composition

Four bulk samples were analyzed by XRD from the control phase and the recovery phase of both the Trondheimsfjord and the Barents Sea sediment. The variability observed in the mineral distribution within each of the four-sample subsets is small and confined within the uncertainty of the XRD method. This implies that the homogenization done prior to the experiments was satisfactory with respect to the major mineral phases. Importantly, the XRD analysis does not reveal any changes in the mineral distribution between the control phase and the recovery phase. Therefore, the CO_2 exposure did induce dissolution or precipitation of quantitatively important mineral phases. The similarities between the results of the XRD analysis of the bulk fraction and the fine fraction indicate that the two fractions represent the weathering products of the same primary mineralogy.

The bulk mineralogical composition of both the Trondheimsfjord and the Barents Sea sediments is dominated by the igneous and metamorphic minerals quartz, feldspars, chlorite and biotite. Northern Norway is the most proximal sediment source for the South-western Barents Sea and is composed of a mixture of crystalline bedrock and metamorphosed Precambrian sediments (Nordgulen and Andresen, 2013). The sediment deposited within the Trondheimsfjord has been shown to be sourced locally from the adjacent ophiolite complex and metamorphic terrains (Faust et al., 2014). Higher concentrations of amphibole and pyroxene in the Trondheimsfjord samples compared to the Barents Sea samples is likely to reflect this difference in bedrock composition. A similar mechanism can be invoked to explain the higher concentration of quartz in the Barents Sea sediment, yet progressive sorting could also have led to an enrichment of quartz in sediments deposited distally on a continental shelf (the Barents Sea) relative to a proximal location in an estuary (the Trondheimsfjord).

The presence of muscovite and chlorite in fine-grained sediments and the formation of illite from weathering of muscovite is diagnostic of physical weathering in cold climates (Sellwood et al., 1993). The high concentrations of muscovite/illite and chlorite in both the Trondheimsfjord (33% combined) and Barents Sea sediments (24% combined) therefore suggest that the provenance of these areas are characterized by low degrees of chemical weathering compared to physical weathering. The high abundance of biotite relative to its common weathering products smectite and kaolinite, especially in the Trondheimsfjord sediment, support the idea that the sediment formed through physical weathering (Fordham, 1990).

5% kaolinite is identified in the bulk analysis of the Barents Sea sediment and smectite is positively identified within the glycol treated <6μm fraction. This implies that both mineral groups are present in the Barents Sea sediment. Unfortunately, a quantification of the relative abundance of kaolinite and smectite could not be obtained. Vogt and Knies (2009) also identified smectite and kaolinite in the clay mineral fraction of the surface sediment of the South-Western Barents Sea and found smectite to be slightly more abundant than kaolinite. The fact that both clay mineral groups are present within the same sample is to be expected, as kaolinite can form from the break-down of smectite (Krauskopf and Bird, 1995).

The formation of smectite in terrestrial soils is considered to reflect a warm and humid climate (Sellwood et al., 1993), but smectite can also form by hydrolysis and submarine weathering of volcanogenic rocks (Vogt and Knies, 2009). The current climatic conditions of Scandinavia are cold and hence unfavorable for smectite formation, which is why a recent smectite source is unlikely. Erosion of the smectite and kaolinite-rich early Mesozoic paleosoils of northern Norway, on the other hand, constitute a potential source (Lidmar-Bergström, 1995) as well as hydrolysis and submarine weathering of young basaltic rocks at the north Atlantic mid-ocean ridge (Vogt and Knies, 2009). Both proposed sources imply lateral transport of kaolinite/smectite across large distances by the Norwegian Atlantic current. On the contrary, transport of kaolinite and smectite from the north Atlantic into the Trondheimsfjord can be considered negligible. It would simply be diluted by the riverine input to the fjord (Bøe et al., 2003). Based on the preceding arguments, the absence of quantifiable amounts of smectite and/or kaolinite in the Trondheimsfjord sediment indicates that these clay minerals are not present in the provenance area of the Trondheimsfjord.

A noticeable difference between the Trondheimsfjord and Barents Sea sediments is the larger amount of calcite and dolomite in the Barents Sea samples. Previous studies have found marine carbonate productivity to be the main source of $CaCO_3$ in both areas (Steinsund and Hald, 1994; Faust et al., 2014). On the contrary, direct precipitation of dolomite from the water column is extremely uncommon and highly unlikely to have occurred in either of the study areas (Warren, 2000). The dolomite content of the samples is therefore more likely to be detrital dolomite grains eroded from sedimentary and metamorphic rocks. An example of a potential source is the Porsanger dolomite of Finnmark, Northern Norway (Tucker, 1977).

5.2 Element concentrations

5.2.1 Quality assurance

The sequential extraction of the certified reference material revealed low recoveries from the acid soluble and the easily reducible fractions. An explanation for this might be the minor deviations that was made from the standard protocol during the extraction process (Rauret et al., 1999). One of the deviations was the usage of an orbital shaker instead of the recommended end-over-end shaker. This can have limited the reaction between sediment and solution if the shaker failed to maintain the sediment in complete suspension.

The low recoveries from the acid soluble and easily reducible fractions might partly explain the high recoveries in the oxidizable and residual fractions. This is because a low recovery from the first two extraction steps leaves a higher concentration of the element in the sediment to be extracted at a later stage. This effect can be seen clearly in the determined concentrations of Cd and Pb, which are underestimated in the first two fractions. Yet, it is also in these two fractions they are most abundant. The consequence is >150% recovery of both elements in the oxidizable and residual fractions. The determination of Cd and Pb in the oxidizable fraction is also reported as the least accurate in the literature (Sutherland, 2010). The same logic can be applied to account for at least parts of the discrepancy in the determination of Cr, Cu and Zn. The different method used for the extraction of the residual fraction (UltraClave vs. *agua regia*) may also explain some of the inaccuracy.

The low recovery from the acid soluble and easily reducible fraction should be taken into account when considering the absolute concentrations determined from the sequential extraction. There is a risk that the concentrations are underestimated.

Spread in the concentration of an element can be observed between samples collected on the same day. Part of this can be attributed to the natural variability and heterogeneity of sediments, but some of the spread may relate to the setup used in the experiments. Because of the point inlet and outlet of water, the CO_2 was not uniformly distributed in the TiTank. The different sediment trays would therefore have experienced variable CO_2 exposure. The geochemical response recorded in the sediments is expected to vary accordingly. The effect would, however, be similar to the natural non-uniformity of CO_2 exposure anticipated in a leakage scenario (Blackford et al., 2014).

5.3 Distribution of major elements by fraction

5.3.1 The acid soluble fraction

5.3.1.1 Sodium

Sodium (Na) is the most abundant cation in the marine environment and a major contributor to the acid soluble fraction of the Trondheimsfjord and Barents Sea sediments (Millero, 2005). It adsorbs to negatively charged surfaces at pH 7.5-8 in solutions of high ionic strength, e.g. seawater (Stumm and Morgan, 1996). Contrary to seawater, the 0.11M acetic acid solution added during the first extraction step has a pH = 2.8 and a slightly lower ionic strength. At these conditions, H^+-ions has a higher affinity for the surface than Na, which leads to a cation exchange reaction where H^+-ions adsorb to the mineral surfaces and Na^+-ions get released into the solution. Cation-exchange of the interlayer cations of 2:1 clays like illite and smectite may likewise account for the Mg and K present in the acid soluble fraction (Liu et al., 2018).

5.3.1.2 Calcium

Even though some surface adsorption of calcium (Ca) can be expected, the Ca in the acid soluble fraction is more likely to represent the presence of calcium carbonate minerals ($CaCO_3$). This is supported by a significant correlation between the Ca-concentration and calcite content of both sediments. When CO_2 is added to natural waters, the concentration of dissolved inorganic carbon increases, while the pH is decreased and the carbonate equilibrium shifts towards lower concentrations of the carbonate ion (Emerson and Hedges, 2008). The net effect is a decrease in the ion activity product and hence saturation index of any calcium carbonate phases, e.g. aragonite and calcite. If the saturation index with respect to these mineral phases sinks below unity, the thermodynamic prediction is that they will start to dissolve. This would occur for aragonite first, due to its higher solubility product (Millero, 2005). The 10.5% decrease of Ca in the acid soluble fraction of the Trondheimsfjord sediment is therefore likely to reflect dissolution of $CaCO_3$ induced by the CO_2 exposure. Interestingly, no decrease in Ca-concentration is observed in the Barents Sea sediment. One possible explanation is that the higher calcite concentration of the Barents Sea sediment can have buffered the pH decrease in the pore-water during the exposure phase of the experiment. This effect would have been augmented by the presence of smectite, as it decreases the permeability of sediment when it swells and thereby reduces the pore-water exchange rate (Stumm and Morgan, 1996). Increased pore-water concentrations of Ca, B, Sr and Li as a result of CO_2 exposure was observed by Blackford et al. (2014) and Lichtschlag et al. (2015) who ascribed it to $CaCO_3$ dissolution. Their measured pH-decrease was from pH = 7.7 to pH = 7.5. It is puzzling why our pH-decrease from pH = 8.2 to pH = 6.9 did not cause a similar dissolution of $CaCO_3$ in the Barents Sea sediment. In addition, no discernible decrease in B, Sr and Li is observed during the experiments in this study. Steinsund and Hald (1994) found the bottom-waters of the

Barents Sea to be undersaturated with respect to calcite and aragonite. It is therefore possible that the most labile $CaCO_3$-particles were dissolved before the sediment was collected for the experiments. The dissolution of the residual biogenic $CaCO_3$ can have been inhibited by the presence of microbial biofilms on the crystal surfaces as described by Lüttge and Conrad (2004).

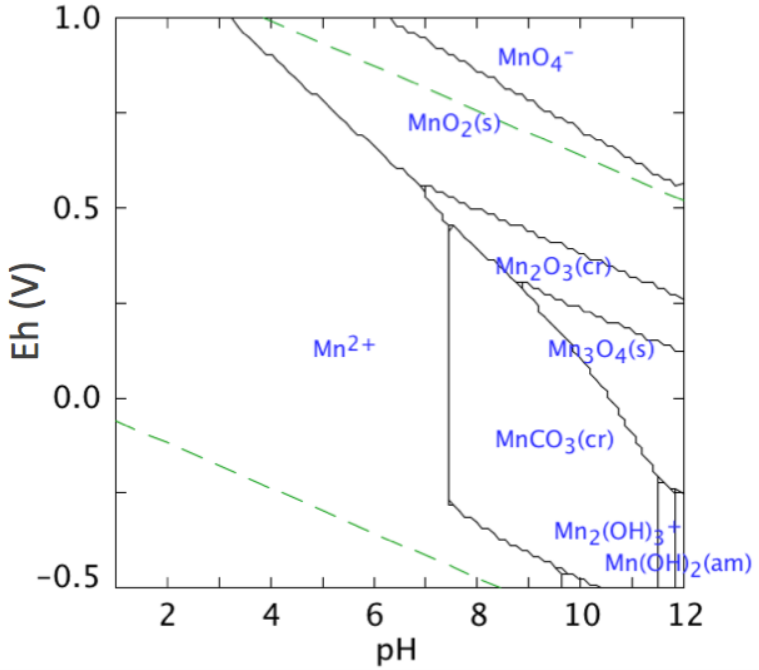

Fig. 26. Stability diagram of Eh versus pH for the Mn-CO_2-H_2O system. The solid phases considered are MnO_2, Mn_2O_3, Mn_3O_4, rhodochrosite $MnCO_3$ and $Mn(OH)_2$. $Mn(II)_{TOT}$ = 10µM and C_{TOT} =1mM. Modified from Stumm and Morgan (1996).

5.3.1.3 Iron and manganese

The minor contribution of Fe to the acid soluble fraction of both sediments suggests that only the adsorbed or surface-bound Fe-species and not any major Fe-bearing mineral phases were dissolved during the first extraction step. Contrary to Fe, a larger portion of the total Mn is partitioned into the acid soluble fraction than the easily reducible fraction, a pattern which can be recognized in both the Trondheimsfjord and Barents Sea sediments. Soluble Mn^{2+} can form from the dissolution of Mn(III)- and Mn(IV)-(hydr)oxides, as a response to a reduction in pH and/or pE (Stumm and Morgan, 1996) (Fig. 26). Mn(II)-phases (e.g. $MnCO_3$) are exceptions to this, since these only dissolve as a result of a decrease in pH (Fig. 26). Co is closely linked to the geochemical cycle of Mn, as it is incorporated into freshly precipitated Mn-(oxyhydr)oxides (Ardelan and Steinnes, 2010). Mn and Co are poorly correlated in the acid soluble fraction (Trondheimsfjord: R^2 = 0.19, Fig. 27a. Barents Sea: R^2 = 0.04, Fig. 27b), but well-correlated in the easily reducible fraction (Trondheimsfjord: R^2 = 0.65, Fig. 27c. Barents Sea: R^2 = 0.64, Fig. 27d). This suggests that despite the fact that Mn is more abundant in the acid soluble fraction, Mn-(oxyhydr)oxides are hosted in the easily reducible fraction. This interpretation is supported by the higher concentration of Co in the easily reducible fraction, especially in the Tronheimsfjord sediment. It indicates that it is primarily Mn(II)-species and adsorbed Mn that are solubilized during the first extraction step.

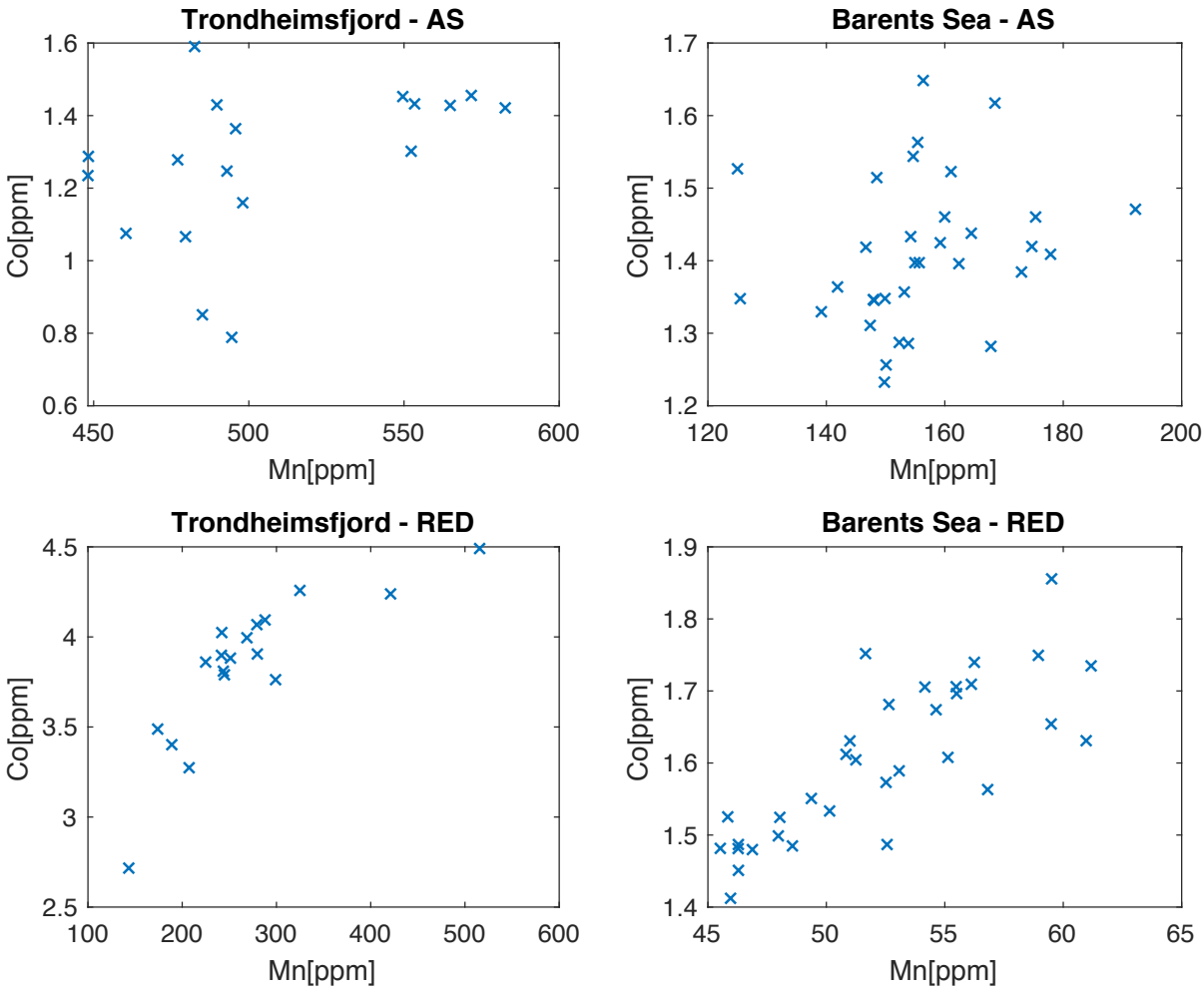

Fig. 27. Comparison of Co versus Mn in the acid soluble and easily reducible fraction. A. Trondheimsfjord sediment, acid soluble fraction. B. Barents Sea sediment, acid soluble fraction. C. Trondheimsfjord, easily reducible fraction. D. Barents Sea sediment, easily reducible fraction. Co and Mn are poorly correlated in the acid soluble fraction of both sediment where Mn is most abundant, but well-correllated in the easily reducible fraction.

5.3.2 The easily reducible fraction

The second extraction step aim to target poorly crystallized metal oxides such as Al-, Fe- and Mn-oxides (Ure et al., 1993). This is evident from the large contributions of Fe and Al to the easily reducible fraction. The higher concentration of especially Fe in the Trondheimsfjord sediment explains why the easily reducible fraction contributes to a larger portion of its total sediment mass compared to in the Barents Sea sediment (1.6% and 0.9%, respectively).

5.3.2.1 Phosphorus

Phosphorus (P), present in the marine environment as orthophosphate (PO_4^{3-}), is known to be adsorbed onto sinking Fe-(oxyhydr)oxides particles (Slomp et al., 1996). P and Fe show a strong positive correlation within the easily reducible fraction of both the Trondheimsfjord (R^2 = 0.70) and the Barents Sea (R^2 = 0.68) sediments (Fig. 28). This implies that a noticeable amount of the P within the sediment is bound to Fe-(oxyhydr)oxides (Hensen et al., 2006).

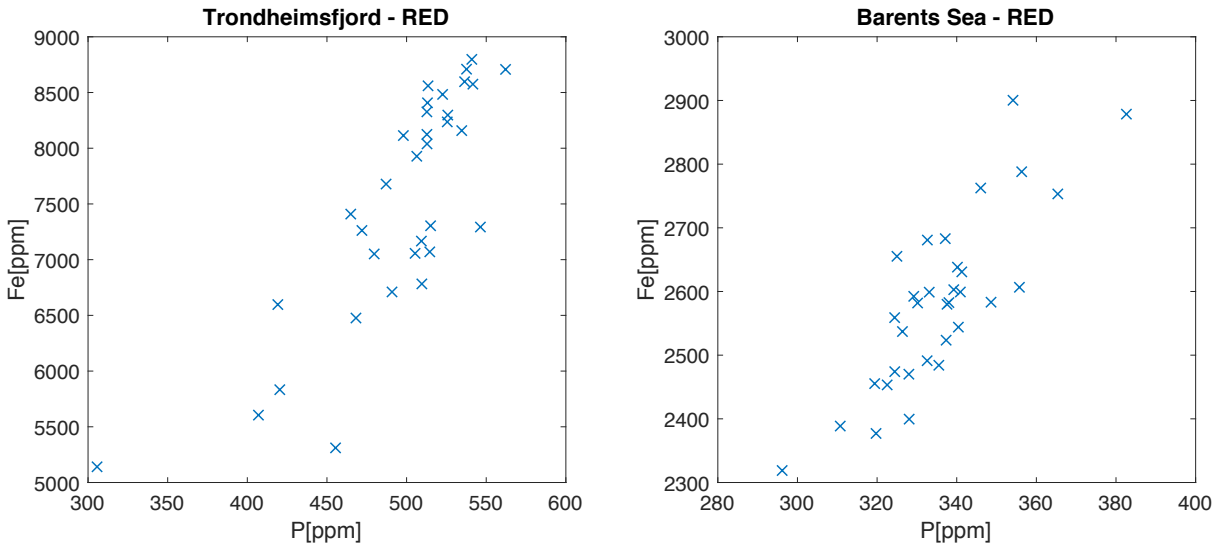

Fig. 28. Comparison of Fe versus P in the easily reducible fraction. A. Trondheimsfjord sediment B. Barents Sea sediment. The two elements are well-correlated in both sediments.

5.3.3 The oxidizable fraction

The oxidizable fraction targets reduced species, e.g. sulfide-compounds and organic material (Ure et al., 1993). It is the smallest of the four extracted fraction of both sediments (0.6% in both cases), but can potentially account for a substantially larger portion of the total sediment mass, as the major elements of organic material (C, O, N and H) have not been quantified by ICP-MS. S accounts for a small proportion of the oxidizable fraction, suggesting that reduced S-species like metal-sulfides are not abundant in either sediment. The elements present in the oxidizable fraction are therefore expected to be bound to or complexed with organic matter.

5.3.4 The residual fraction

The common cations of silicate minerals (Al, Fe, Mg, K and Ca) are abundant within the residual fraction except for Si, which is remarkably low. A possible explanation is that UltraClave digestion with 50 vol% HNO_3 disintegrates silicate minerals less effectively than an *agua regia* solution. It follows that the Fe that was dissolved by the UltraClave must reside within non-silicate mineral phases like the Fe-oxides hematite and magnetite. If true, it is unclear why neither of the Fe-oxides was detected by the XRD analysis, since the Fe of the residual fraction accounts for approximately 4% of the total sediment mass of the Trondheimsfjord sediment and 3% of the Barents Sea sediment. An alternative approach to explain the paradoxically low Si is to investigate the solubility of amorphous silica. Gorrepati et al. (2010) found that amorphous silica precipitates from strongly acidic solutions, hence the released Si from the dissolved silicate minerals can simply have reprecipitated as nanoparticles during the UltraClave digestion and thereby not have been detected in the ICP-MS analysis. Using this interpretation, the elements within the residual fraction can still represent detrital grains of silicate minerals like quartz, feldspars, pyroxenes, amphiboles and possibly also refractory organic material and clay minerals.

5.4 Changes in element concentrations

5.4.1 Unintended experimental effects during the control phase

The main target of this study is to investigate the element mobilization which occurs as a consequence of CO_2 exposure. However, for the elements Fe, P, V, Ni, Cr, Co, Cu and Zn in the acid soluble fraction and Hg in the oxidizable fraction, large changes take place already in the control phase of the Barents Sea experiment. This unintended experimental effect reflects a response to differences between the conditions of the acclimatization phase and those of experimental phase. Potential mechanisms capable of producing such a signal will now be discussed. The low number of Trondheimsfjord samples not affected by bivalves inhibits an assessment of whether the same development took place during the Trondheimsfjord experiment.

The elements Fe, V, Ni, Cr, Co, Cu and Zn are all transition metals and exist at trace concentrations in the marine environment due to scavenging by adsorption onto the surfaces of metal-hydroxides (Tribovillard et al., 2006). It is therefore likely that these elements are associated with the solid phase by surface complexation. If the elements are listed in order of percentage decrease from the first to the last day of the control phase, the following sequence is found: Fe > V > P > Zn > Co ≥ Ni ≥ Cd. Jeon et al. (2003) studied metal adsorption on hematite and found a selectivity sequence of Fe ≥ Zn > Co ≥ Ni > Cd. The two trends are identical, except for V and P, which were not studied by (Jeon et al., 2003). This strongly implies that the mobilization happened through desorption from an Fe-oxide or hydroxide surface.

Different mechanisms are able to induce desorption. It can be either a chemical perturbation of surface equilibria, a change in pressure, flow processes or a combination. In the following sections, these will be discussed in turn.

Surface complexation equilibria are controlled by three main factors: 1) pH, 2) solution variables and 3) surface characteristics (Stumm and Morgan, 1996). It is safe to assume that the surface characteristics do not change, since the overall sediment composition is the same. The same inlet water was also used during the acclimatization and experimental phase. Therefore, a change in the solution variables would have to stem from interactions between the sediment and the solution itself, which is considered unlikely to cause major changes to surface complexation equilibria. A pH effect can be produced by biological processes taking place within the sediment. An example is the remineralization of organic matter, which releases CO_2 and H^+-ions causing the pore-water to become more acidic (Jørgensen, 2006). This pH-decrease would occur locally within the sediment and is therefore not detectable in pH-measurements of the outlet water. Surface complexation is competitive, which means that H^+-ions may compete with metal ions for the available surface sites. Since a reduction in pH inherently increases the concentration of H^+-ions in the solution, this could cause a release of metal ions to the solution. A gradual remineralization of organic matter would progressively reduce pore-water pH and promote metal desorption in a pattern similar to what is observed in the control phase. Still, this explanation fails to resolve why the desorption process comes to a halt by the onset of the exposure phase as the addition of CO_2 would be expected to accelerate this process. An indication to why mobilization stops by the onset of the exposure phase can be found in the oxidizable fraction and by studying the sediment hosted bacteria. The vast majority of Hg found within marine waters is complexed with organic matter (Han and Gill, 2005). The mobilization of Hg during the control phase therefore implies that remineralization of labile organic matter could also be the cause. Bacterial cultures were analyzed as part of the

experiments. An analysis of rates of extracellular release of adenosine triphosphate (ATP) by the sediment hosted bacteria reveals a decrease in microbial activity by the onset of the exposure phase (Ana R. Borrero-Santiago, personal communication, 2018). If a viable mechanism can be invoked to explain the reduction in organic matter remineralization rate, it provides a way to interpret the cessation of trace metal release as CO_2 exposure commences.

Pressure can have a pronounced influence on thermodynamic equilibria including those of surface complexation reactions (Byrne and Laurie, 1999). The direct influence of a change in pressure (P) on the equilibrium constant (K) can be described by the following equation:

$$RT(\frac{\partial lnK}{\partial P})_T = -\Delta V$$

Where R and T are constants, and ΔV represents the difference between the partial molar volume of reactants and products. Based on Le Chatelier's principle, a change in pressure would cause the thermodynamic equilibrium to shift in direction of minimizing the molar volume (Stumm and Morgan, 1996). Estimates of ΔV for complexation reactions, and especially surface complexation reactions, are sparse and considered questionable by many, but most evidence points towards positive values (Byrne and Laurie, 1999). This means that an increase in pressure would tend to decrease the degree of complexation, and thereby cause a release of surface complexed species to the solution. Due to its relatively small magnitude, the pressure change from 1 to 30 bar is therefore unlikely to have caused the large changes in element concentrations observed. An attempt to calculate the ΔV's for the mobilized elements could not confirm that the mobilization would affect the elements in the observed order. Furthermore, because of the fast kinetics of surface complexation reactions, a new equilibrium is expected to established within a shorter time span than the observed 21 days (Hayes and Leckie, 1987).

A physical process that may affect surface adsorption is advection, or flow, of the aqueous phase. As stated in the section above, surface complexation reactions are rapid, hence the transport of solutes to the surface by advection can sometimes be the rate limiting factor (Stumm and Morgan, 1996). The change from the acclimatization phase (static aqueous phase) to the experimental phase (flowing aqueous phase) represents an increase in water exchange rate. Logically, this will affect outer-sphere complexes more than inner-sphere complexes, due to the lower strength of electrostatic bonds compared to covalent bonds. The diffusive layer of the Stern model would also constantly be replaced causing further destabilization of outer-sphere complexes. However, the affected elements Fe, Ni, Co and Zn have been shown to form inner-sphere complexes on Fe-(hydr)oxides (Stumm and Morgan, 1996; Jeon et al., 2003). The same is true for P and V, which are primarily present as anionic species in seawater (Krauskopf and Bird, 1995; Peacock and Sherman, 2004).

In order to confidently determine a signal which has its origin in the CO_2 exposure, a clear difference between the direction of change in element concentration during the control phase and the exposure phase is required. A shift in the rate of change or the cessation of change by the onset of the exposure phase is not sufficient, because the same trend could also indicate that the system is approaching or have reached a new equilibrium. Therefore, the direction of change within the exposure phase must occur in another direction than within the control phase for it to be validated as an effect of the CO_2 exposure.

5.4.2 The effect of CO_2 exposure on trace element distribution

Each part of the following section will begin with an introduction to the marine geochemistry of the element, followed by a discussion of its distribution between the four fractions and its response to CO_2 exposure.

5.4.2.1 Iron and manganese

The biogeochemical cycle of iron and manganese plays an important role in the diagenesis of marine sediments (Canfield et al., 1993; Calvert and Pedersen, 1996). Oxides and hydroxides of both elements may act as terminal electron acceptors in the remineralization of organic matter under sub-oxic conditions (Froelich et al., 1979; Thomson et al., 1993). Upon reduction, the Fe and Mn-(hydr)oxides are dissolved, whereby soluble Fe^{2+} and Mn^{2+} are released into the pore-water and become available for new reactions. This can lead to the formation of solid sulfide (e.g. FeS_2 - pyrite) or carbonate (e.g. $MnCO_3$ - rhodochrosite) phases. The dissolved Fe- and Mn-cations may also diffuse to the oxic-anoxic boundary, become oxidized and reprecipitate as oxide or hydroxide species. This redox-cycling of iron and manganese also affects the distribution of trace metals within marine sediments. Fe- and Mn-(hydr)oxides contain amphoteric surface sites, which trace metals can bind to through surface complexation reactions. If the Fe- and Mn-(hydr)oxides are reduced and hence dissolved, the adsorbed trace metals will be released into the pore-water alongside Fe^{2+} and Mn^{2+}. This phenomenon is sometimes referred to as the Fe and Mn redox-shuttle (Ardelan and Steinnes, 2010).

Significant differences exist between the geochemical behavior of manganese and iron. The Gibb's free energy yield from Mn-(hydr)oxide reduction is higher than that of Fe-(hydr)oxide, which is why the former will tend to be reduced first. In addition, the kinetics of the oxidation reaction of Mn(II) are slower than those of Fe(II) (Tribovillard et al., 2006). The sum of these two observations can cause Mn-oxides to be reduced and Mn^{2+} transported to the water column, while Fe is retained within the sediment.

In the easily reducible fraction of the Barents Sea sediment, no distinct trend in the Fe-concentration is discernible within the control phase, while an increase is both detectable and statistically significant by the onset of the exposure phase. This represents an increase in the concentration of Fe-(hydr)oxides in the surface sediment. The elevated, but steady, concentration of Fe suggests that it represents a new equilibrium rather than a transient phase. Such a new equilibrium can be reached by increasing the flux of dissolved Fe(II) from the subsurface sediment to the surface sediment. The lower the pH, the smaller the drop in pE is required to dissolve Fe-(hydr)oxides (compare the vertical distance to the predominance area of Fe^{2+} from the red point (exposure phase) and the green point (control phase) in Fig. 29). For this reason, the decrease in pH induced by CO_2 exposure can potentially advance the reductive dissolution of Fe-(hydr)oxides in the subsurface sediment. In order to test this hypothesis, the subsurface sediment should be extracted and analyzed by the same procedure as the surface sediment. A decrease in the Fe-concentration of the easily reducible fraction by the onset of the exposure phase would provide support for this hypothesis. However, this is beyond the scope of this thesis. Ardelan and Steinnes (2010) also detected a disruption of the Fe- and Mn-cycle in their CO_2 exposure experiment, albeit of a much larger magnitude. The discrepancy can be a result of a lower oxygen replenishment rate in their batch-type experiment compared to the flow-through conditions used in this study.

5.4.2.2 Pb, Ni, Cu, CO, Zn, Cr, V and Hg

The distribution of the trace elements Pb, Ni, Cu, Co, Zn, Cr, V and Hg within the marine environment is strongly governed by their association with particulate and organic matter. In oxygenated seawater, the inorganic fraction of Pb, Ni, Cu, Co and Zn is present as soluble divalent cations or as monovalent chloride complexes, which readily adsorbs onto Fe- and Mn-(hydr)oxide surfaces (Tribovillard et al., 2006). In comparison, the dominant inorganic forms of Cr and V are the anionic species vanadate oxyanions (HVO_4^{2-} and $H_2VO_4^-$) and chromate anions (CrO_4^{2-}), respectively (Wehrli and Stumm, 1989). These may also adsorb onto Fe- and Mn-(hydr)oxides, but, contrary to the cationic species, they have strongest surface affinity at low pH (Stumm and Morgan, 1996). This explains why V and Cr are not released in appreciable amounts during the first extraction step and hence their small contribution to the acid soluble fraction. Despite its primary association with Fe- and Mn-(hydr)oxides, the build-up of V within the pore-water of surface sediments can also be related to complexation with dissolved organic matter (Morford et al., 2005). Similarly, the immobilization of Ni, Cu, Zn and Hg is partly linked to the formation of organometallic complexes, which explains their presence within the oxidizable fraction (Tribovillard et al., 2006). As an example, a study on the estuarine and coastal waters near Galveston, Texas, found >99% of the total dissolved Hg(II) to be complexed by organic ligands (Han and Gill, 2005).

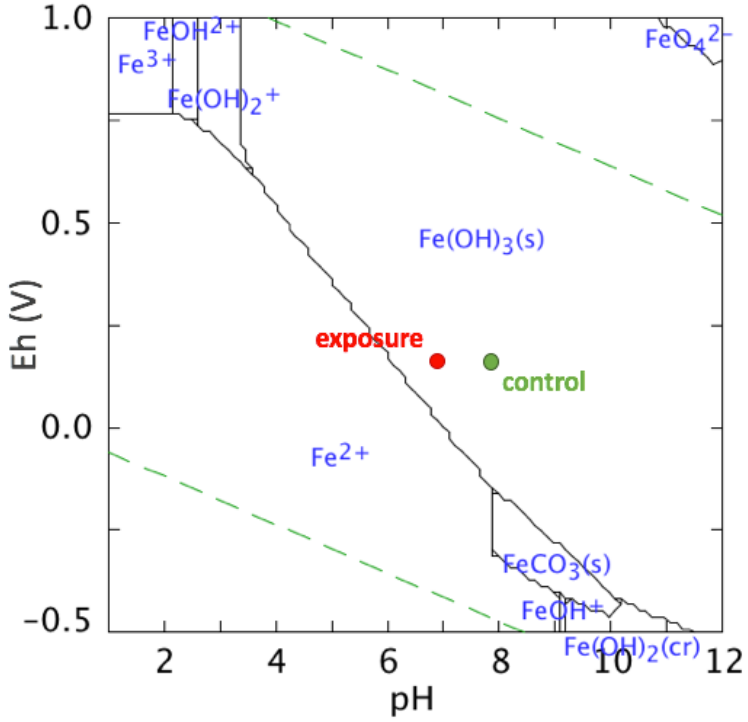

Fig. 29. Stability diagram of pE versus pH for the Fe-CO_2-H_2O system. The solid phases considered are amorphous $Fe(OH)_3$, siderite $FeCO_3$ and $Fe(OH)_2$. $Fe(III)_{TOT}$ = 10μM and C_{TOT} =1mM. Notice how the solution conditions of the exposure phase (red point) are closer to the stability field of Fe^{2+} than those of the control phase (green point). Modified from Stumm and Morgan (1996).

The trace elements Pb, V, Cr, Co, Ni, Cu and Zn are heavily present in the easily reducible fraction and, interestingly, more so in the Trondheimsfjord sediment compared to the Barents Sea sediment. When keeping pH and pE constant, theory predicts that the

concentration of the adsorbed species is controlled by the concentration of the adsorbate in the solution and the site density and characteristics of the adsorbent (Stumm and Morgan, 1996). A potential link can therefore be established to the higher concentration of Fe in the Trondheimsfjord sediment. More Fe in the easily reducible fraction corresponds to more Fe-(hydr)oxides and hence more adsorption sites for the trace elements to bond to. This is true, provided that the adsorbate concentrations in the solution is identical. It should be noted that Pb, V, Cr, Co, Ni, Cu, Zn and As are enriched in ultramafic rocks like those present in the Trondheimsfjord area (McLennan et al., 1993), which can have caused a corresponding enrichment in their weathering products (Faust et al., 2014).

5.4.2.3 Uranium

The dominant U-species at seawater conditions is $UO_2(CO_3)_2^{2-}$. The primary removal pathway of U is by diffusion into the sediment column, where it is reduced at conditions similar to Fe(III) (Andersen et al., 2017). In the sediment column, it forms insoluble U-species, e.g. uraninite (UO_2), possibly via some intermediate species (Chaillou et al., 2002; McManus et al., 2005). Importantly, U-enrichment is considered to occur independently of the Fe- and Mn-redox-shuttle across the sediment-water interface (Klinkhammer and Palmer, 1991). The distribution of U is therefore considered to reflect the redox-conditions within the sediment, rather than the state of a dynamical redox-cycle.

The increase of the U-concentration in the acid soluble and easily reducible fraction during the exposure phase indicates that solid U-species are formed as a consequence of the CO_2 exposure. Importantly, the magnitude of the U-enrichment is on the order of 5-50 ppb, compared to the several ppm increase commonly observed in anoxic sediments (Klinkhammer and Palmer, 1991). As previously stated, uranium is primarily present in seawater as $UO_2(CO_3)_2^{2-}$. The properties of this uranium carbonate complex are similar to CO_3^{2-}, which is why it is able to form solid phases with Ca^{2+} (Swart and Chung, 1990). Swart and Chung (1990) argue that the draw-down of the carbonate ion concentration that follows an increase in pCO_2, increases the $UO_2(CO_3)_2^{2-}$/ CO_3^{2-}-ratio of the pore-fluid. As a consequence, the proportion of $UO_2(CO_3)_2^{2-}$ which gets incorporated into cements and recrystallized carbonate minerals during diagenesis will increase relative to CO_3^{2-}. This represents a possible mechanism capable of producing the observed increase of U during the exposure phase. Alternatively, U-reducing conditions can have developed within the pore-water (Klinkhammer and Palmer, 1991). Yet, this fails to explain why Mn-(hydr)oxides are not simultaneously reduced and released from the surface sediment to the water-column.

5.4.2.4 Arsenic

Arsenic occur in two oxidation states, As(III) and As(V), the latter being the dominant species in oxygenated water bodies where it is present as the oxyanion arsenate (AsO_4^{3-}) (Bowell et al., 2014). Arsenate may adsorb onto or co-precipitate with Fe-(hydr)oxides, clay minerals and organic matter (Bowell et al., 2014). In its reduced form, As(III), arsenic has a conservative behavior in the water column, except in the presence of free H_2S, where it may get incorporated into Fe-sulfides or form its own As-sulfide species (Oremland et al., 2000).

Because no anoxic conditions were detected in the surface sediment, the acid soluble arsenic is likely to represent surface adsorbed arsenate. Thus, the decrease in As-concentration observed within the acid soluble fraction of the Trondheimsfjord sediment is interpreted to represent desorption of arsenate bound to Fe-(hydr)oxide surfaces (Bowell et al., 2014). In contrast, the arsenic hosted within the easily reducible fraction is

unaffected by the CO_2 exposure. de Orte et al. (2014) made similar observations and ascribed it to incorporation of As into Fe-(hydr)oxides. As-mobilization is therefore only expected occur from the easily reducible fraction upon dissolution of its host Fe-phases.

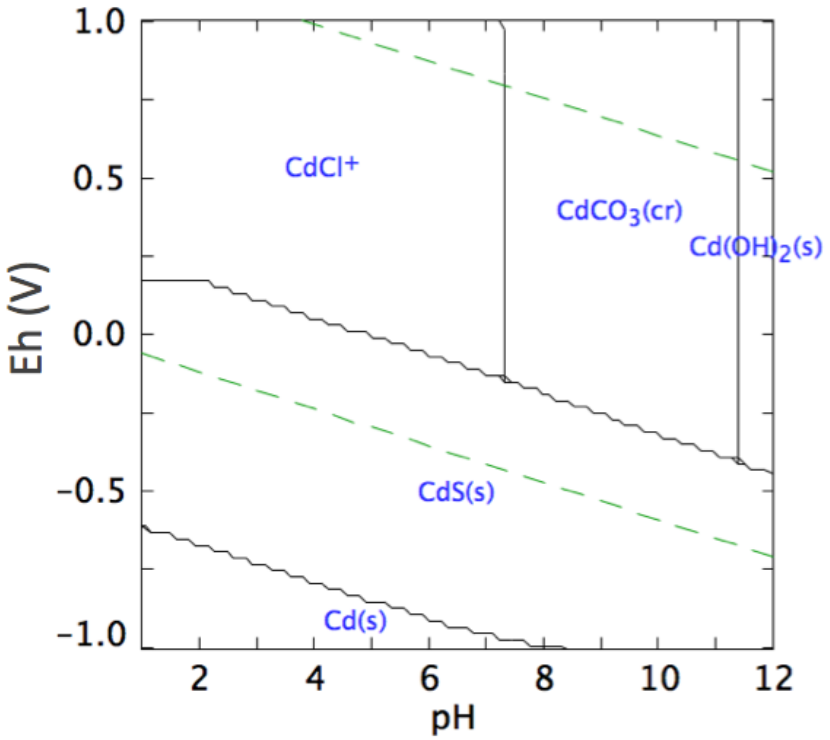

Fig. 30. Stability diagram of pE versus pH for the Cd-Cl-HS-CO_2-H_2O system. The solid phases considered are $Cd(OH)_2$, $CdCO_3$, CdS and Cd. $Cd(II)_{TOT}$ = 10µM, $[HS^-]$ =10mM, $[Cl^-]_{TOT}$ =100mM and C_{TOT} =1mM. The green lines frame the stability field of water.

5.4.2.5 Cadmium

The incorporation of Cd into marine sediments is complex, and may follow several pathways (Tribovillard et al., 2006). . It has only one coordination state, Cd(II), and its predominant inorganic species in seawater is $CdCl^+$ (Fig. 30). Under reducing conditions in the presence of dissolved H_2S, it may form insoluble CdS (Calvert and Pedersen, 1993). In the absence of H_2S, Cd forms complexes with organic matter, binds through chemisorption onto the surface of calcium carbonate particles or adsorbs onto Fe-(hydr)oxides and clay minerals (Calvert and Pedersen, 1993; Thakur et al., 2006; Liu et al., 2018). Through chemisorption, Cd reacts with $CaCO_3$-minerals and forms $CdCO_3$ on the surfaces (Thakur et al., 2006). This is an effective retention mechanism for Cd, especially at elevated pH and low solution Cd-concentration. A scatterplot of Ca vs. Cd reveals good correlation between the two elements in both the acid soluble and easily reducible fraction of the Trondheimsfjord sediment (AS: R^2 = 0.63, RED: R^2 = 0.67, Fig. 31). The slopes are equivalent to an average Cd/Ca molar ratio of 1.4-1.7 $\frac{\mu mol}{mol}$. In comparison, the Cd/Ca-ratio in benthic foraminifera tests from the North Atlantic and Pacific ocean are 0.8 $\frac{\mu mol}{mol}$ and 2.2 $\frac{\mu mol}{mol}$, respectively (Emerson and Hedges, 2008). The data is therefore well within the expected range for Cd incorporated into biogenic $CaCO_3$. A similar correlation is not observed in the Barents Sea sediment, where the two elements are poorly correlated (AS: R^2 = 0.26, RED: R^2 = 0.03, Fig. 31). This indicates that Cd is not associated with Ca-

bearing minerals in the Barents Sea sediment. Cd^{2+} complexed to Fe-(hydr)oxides has been shown to be more susceptible to desorption than Zn^{2+}, Cu^{2+} and Ni^{2+} (Stumm and Morgan, 1996; Lumsdon and Evans, 2002). This makes it interesting to note that Cd is not mobilized alongside Zn, Cu and Ni during the control phase of the Barents Sea experiment. It provides evidence that adsorption onto Fe-(hydr)oxides is not the primary mechanism by which Cd^{2+} is bound in the Barents Sea sediment. Cd-retention is also possible through sorption onto clay minerals like kaolinite and smectite. This aligns well with the observation that Cd is the only reactive element more abundant in the Barents Sea sediment, where kaolinite and smectite is present, than the Trondheimsfjord sediment, where kaolinite and smectite is absent. The mechanism for Cd-sorption onto clay minerals involves two different reaction pathways. The first is ion exchange at the permanently charged silanol faces, taking place when pH > 4, while the other revolves around inner-sphere complexation at pH > 7 (Angove et al., 1997).

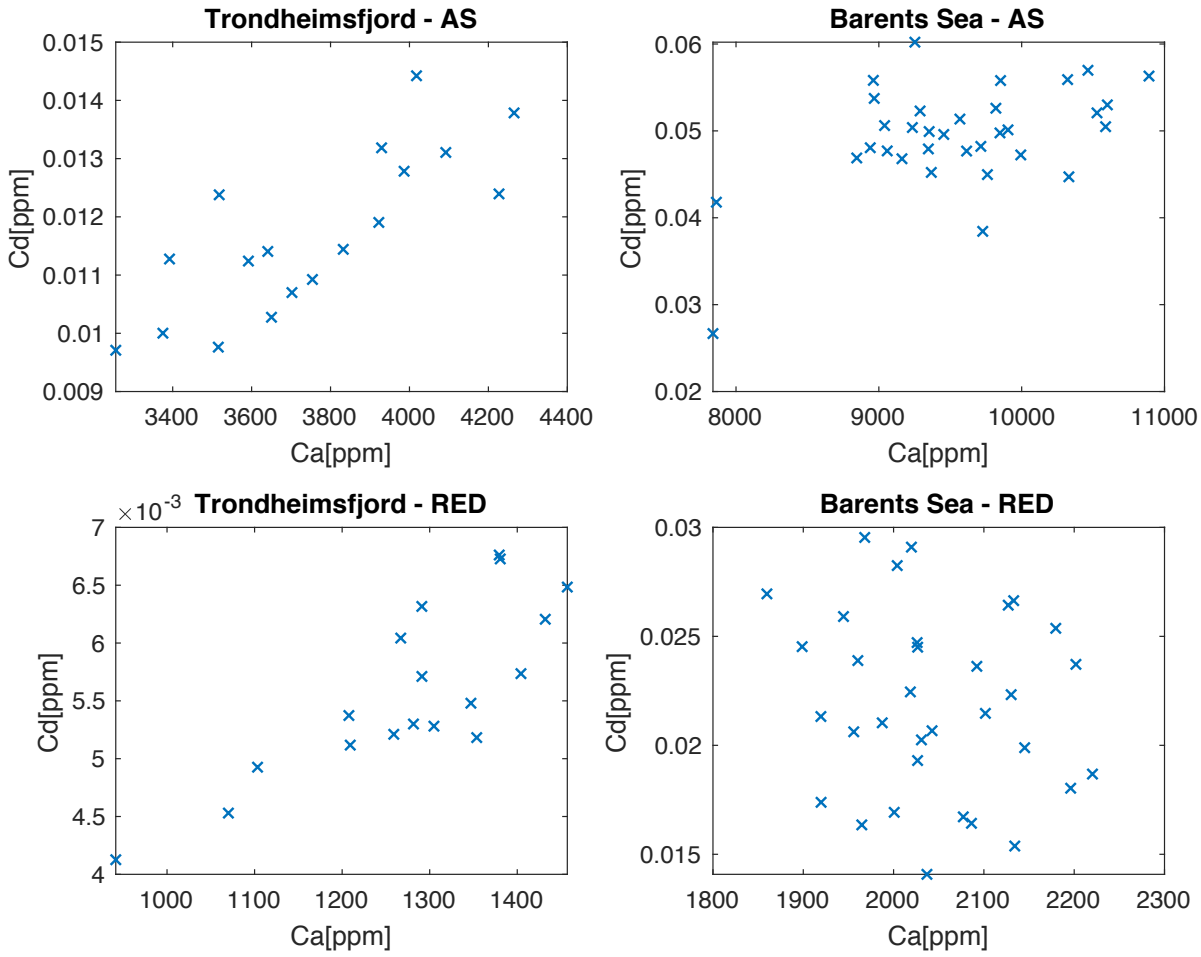

Fig. 31. Comparison of Cd versus Ca in the acid soluble and easily reducible fraction of the Trondheimsfjord and Barents Sea sediment. The two elements show good correlation in Trondheimsfjord sediment, but are poorly corelated in the Barents Sea sediment.

A large proportion of the total Cd is found within the acid soluble fraction and easily reducible fraction of both the Trondheimsfjord sediment and the Barents Sea sediment. The sediments show a consistent pattern of decrease in Cd-concentration during the exposure phase. This indicates that CO_2 exposure is capable of mobilizing cadmium from the sediment. If the released Cd is bound as CdS, it would be stable under strongly reducing

conditions, but dissolve and release its components into the solution under oxic conditions. Rosenthal et al. (1995) found the kinetics of the oxidation reaction of CdS to be quite rapid. A recharge of oxidants is therefore expected to mobilize Cd within a short period of time. Contradictory to this, the release from both the Trondheimsfjord and Barents Sea sediments is slow and gradual, speaking against such an interpretation. Additionally, if the mobilization of Cd occurs by oxidation of CdS, the effect is expected to be observed in the oxidizable fraction. However, Kersten (2002) discusses how oxygen-exposure during sample handling results in a redistribution of Cd from its primary sulfide phase (CdS) to the acid soluble and easily reducible fraction of anoxic sediments. Based on the unclear results from the Barents Sea sediment with respect to $CaCO_3$-dissolution, one can question whether the decrease in Cd can originate from release of chemisorbed $CdCO_3$. Albeit, since chemisorption is a surface-phenomenon, a release of Cd from the surface is possible without a quantitative dissolution of the bulk $CaCO_3$-component of the sediment (Thakur et al., 2006). Alternatively, the adsorption of Cd onto kaolinite and smectite by inner-sphere complexation can account for 50-80% of the total surface-bound Cd (Angove et al., 1997). The inner-sphere complexation model of Angove et al. (1997) has been scrutinized by Srivastava et al. (2005), who argue for an outer-sphere complexation model on the permanently charged surface sites on kaolinite. Either way, desorption from clay minerals provide means by which substantial release of Cd can occur from the Barents Sea sediment as a consequence of the CO_2 exposure.

Interestingly, the Cd-mobilization takes place within different fractions of the two sediments. It occurs in the acid soluble fraction of the Trondheimsfjord and the easily reducible fraction of the Barents Sea sediment. This disparity is best explained by readsorption onto the permanently charged faces of clay minerals, like smectite and kaolinite, through ion exchange reactions during the extraction of the Barents Sea sediment (Liu et al., 2018). These clay minerals have a high surface site density onto which adsorption of Cd may occur, and are only present in detectable amounts in the Barents Sea sediment. In addition, the total Cd concentration of the Barents Sea sediment is more than twice that of the Trondheimsfjord sediment (90ppb vs. 40ppb), which promote the need to invoke additional binding mechanisms for Cd in the Barents Sea sediment. Studies of Cd-contaminated soils have shown that up to 30% of the Cd in the acid soluble fraction can readsorb onto Fe- and Mn-oxides during the extraction and hence appear as if it is part of the easily reducible fraction (Ho and Evans, 2000). A similar signal would develop if Cd diffuses into cracks and irregularities on the Fe-(hydr)oxide surface or is incorporated into its crystal structure (Mustafa et al., 2006). In this study, Cd shows a poor negative correlation with Fe in the easily reducible fraction of the Barents Sea sediment ($\alpha = -1.56 * 10^{-5}$, $R^2 = 0.25$), which weighs against an association with Fe-(hydr)oxide phases. For this reason, readsorption onto permanently charged clay mineral surfaces appears to be the mechanism that satisfies the widest range of observations.

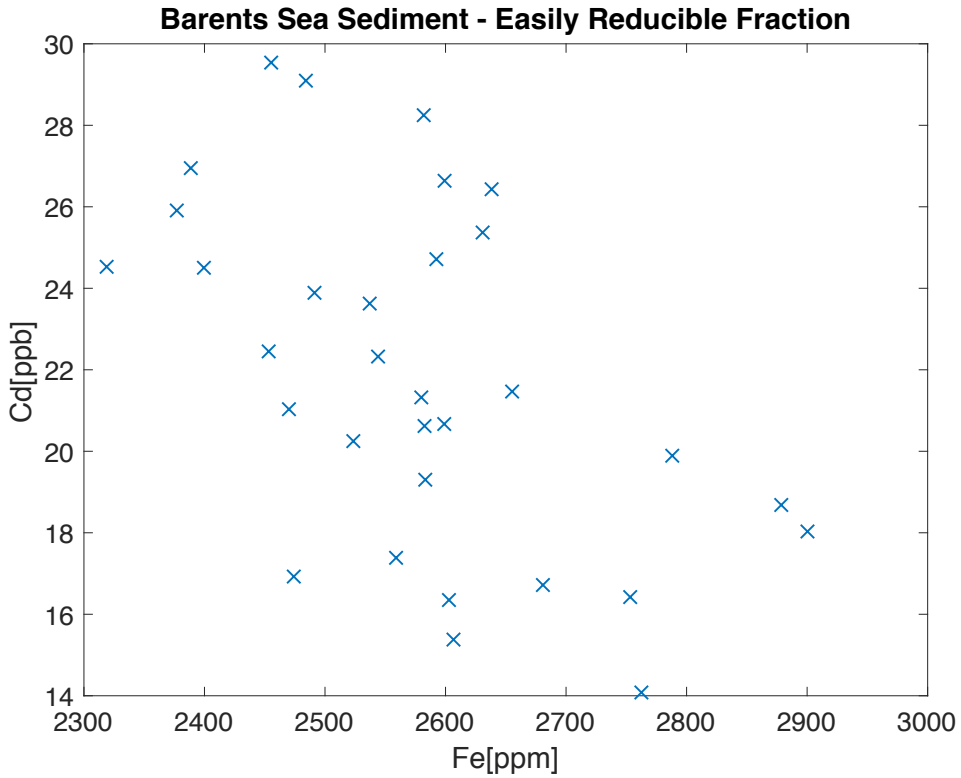

Fig. 32. Cd versus Fe in the easily reducible fraction of the Barents Sea sediment. The poor negative correlation indicates that the two elements are not associated in the easily reducible fraction.

Insufficient specificity and uncertainty regarding the targeted phases in the sequential extraction procedure inhibits any conclusive remarks to be made about the association of Cd with the sediment. To resolve this, future studies should include an investigation of the binding mechanism of Cd e.g. by extended X-ray absorption fine structure spectroscopy (EXAFS).

5.5 Environmental implications

Arsenic and cadmium are elements with well-characterized toxicological effects, even at low levels of exposure (Tchounwou et al., 2012). However, Lane and Morel (2000) found that Cd is also an important micronutrient for marine primary producers. It may replace Zn in the enzymes conducting carbonic anhydrase, i.e. acquiring inorganic carbon for photosynthesis. Human exposure to cadmium happens primarily via industrial sources, but also through smoking and consumption of cadmium-contaminated food including fish and shellfish (Davenport, 2015). Longtime exposure to food from cadmium-contaminated crops is known to have led to bone pain and kidney dysfunction in humans (Nordberg, 2003). Inorganic As(III) is the most toxic arsenic-species present in environment (Neff, 1997). Reduction of As(V) to As(III) can be mediated by marine phytoplankton and bacteria through dissimilatory As-reduction (Oremland et al., 2000). As contamination of drinking water in Bangladesh has been described by the WHO as the largest mass-poisoning in human history, giving rise to a range of medical conditions including cardiovascular disease and lung, bladder and skin cancer (Nickson et al., 1998; Smith et al., 2000). Importantly, these examples of Cd- and As-intoxication are cases where the exposure originated from the terrestrial environment. The environmental risk associated with elevated levels of Cd and As in the marine environment, on the other hand, is less studied. Experiments

conducted on rainbow trout reveal toxic and bioaccumulation effects in juvenile specimens as a consequence of exposure to inorganic As(III) species (Erickson et al., 2019). Cadmium exposure in a similar experimental setup exhibits no effect on trout growth and survival rate (Erickson et al., 2010). Shellfish consume Cd directly from the dissolved Cd-pool, and as benthic biota they are expected to be especially vulnerable to release of Cd from the sediment (Bendell, 2010).

5.5.1 Modelling the environmental effect of trace metal mobilization

There are multiple approaches to assess the impact of arsenic and cadmium mobilization. A commonly applied method is to determine the partitioning of an element between the aqueous and solid phase (e.g. de Orte et al., 2014). This is done by measuring the concentration within both the sediment and the pore-water water, and applying this information to calculate its distribution coefficient. Unfortunately, pore-water samples were not collected during the experiments. An alternative approach is therefore to use a box model to describe the effect of Cd and As mobilization. The possible outcome is a quantification of the increase in water column concentrations of Cd and As that would follow a CO_2 leakage occurring at a rate similar to our experimental dosing. This "back-of-the-envelope" approach is of course an oversimplification of the natural system and the results should be interpreted with this in mind. This exercise is done solely to provide a first impression of the expected environmental impact of a potential CO_2 leakage. A better approximation to the natural system would be attained using a dynamical model that incorporates a proper characterization of element mobilization and speciation, molecular diffusion and seawater advection, e.g. using two-step models for combined complex transport and reaction processes (Schulz, 2006a).

5.5.1.1 Model description

The water column is described as a cube of unit width and depth, where *a* is the vertical thickness of the water column and *b* is the thickness of the surface sediment affected by the CO_2 exposure (Fig. 33). Trace elements are mobilized from this part of the sediment column. The parameter τ describes the ratio between *a* and *b*, i.e. $\tau = \frac{b}{a}$.

The following assumptions are made:

- The trace elements are mobilized from the surface sediment down to a depth of *b.*
- The trace elements are mobilized instantaneously and subsequently distributed homogeneously within a water body of thickness *a*.
- No exchange of trace elements occurs between the water masses inside and outside the box model.
- The amount of trace elements that gets mobilized is equal to the difference between the mean concentration of the control and recovery phase samples.

As part of the model parametrization, appropriate values must be selected for surface sediment porosity (θ) and dry bulk density (ρ). Values for θ were obtained during the sequential extraction procedure for both sediments (Trondheimsfjord: $\theta = 0.55$, Barents Sea: $\theta = 0.4$). A dry bulk density of $\rho = 2700 \frac{kg}{m^3}$, representative for marine sediments, was selected from the literature (Allen, 1985).

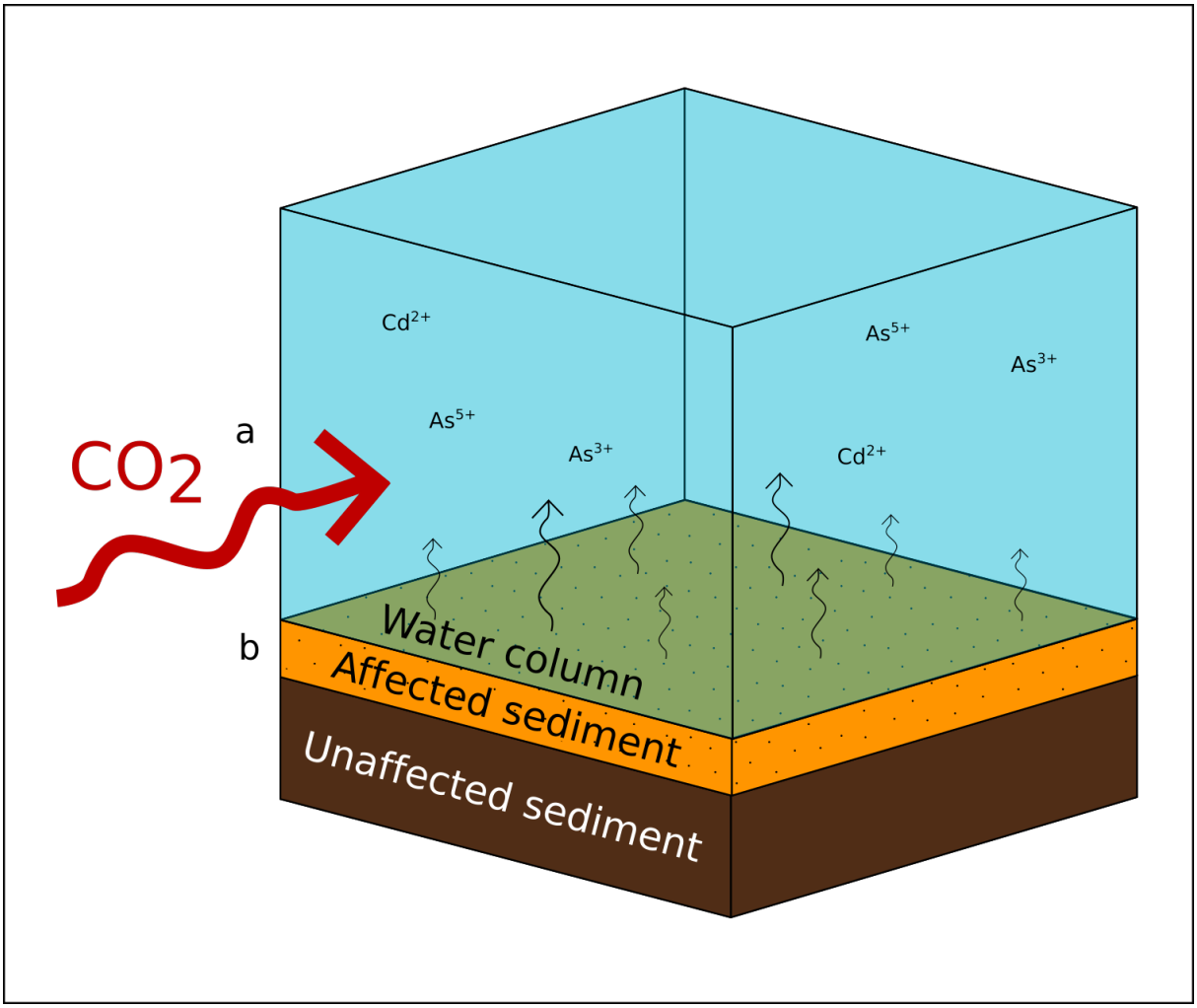

Fig. 33. Sketch of box model used to quantify As and Cd mobilization. *a* is the vertical thickness of the water column and *b* is the thickness of the sediment column affected by CO_2 exposure. The red arrow depicts a diffuse flux of CO_2 from a nearby CO_2 leakage point.

Two different values for τ are used in the model, $\tau_1 = 10^{-3}$ and $\tau_2 = \frac{1}{3} * 10^{-5}$, representing two different cases of trace metal distribution, and hence dilution. This is done in order to assess the sensitivity of the model to how far the trace metals spread within the water column. $\tau = \tau_1$ can be viewed as a scenario where the trace metals diffuse up into the bottom-waters and are distributed there, but not beyond. Using $\tau = \tau_2$ represents a situation where the mobilized trace metals are transported and mixed into the water column by a combination of molecular diffusion and advection. The increase in trace metal concentration of the seawater within the box model, ΔMe_{sw}, can be calculated using:

$$\Delta Me_{sw} = \frac{\Delta Me_{sed} * \rho * (1 - \theta) * \tau}{M}$$

where ΔMe_{sed} is the amount of the trace metal mobilized from the sediment determined in the experiments, M is the molecular mass of the trace metal, and ρ, θ and τ are the constants described previously.

5.5.1.2 Model results

The results are shown in Table 8 alongside a comparison to the mean ocean concentration (MOC) of the same trace elements as compiled by Sarmiento and Gruber (2006).

Element	sediment/ fraction	ΔMe_{sed} [ppb]	MOC [nmol m^{-3}]	ΔMe_{sw} [nmol m^{-3}]		% of MOC	
				τ_1	τ_2	τ_1	τ_2
Cd	TF / AS	1.3	600	14	0.5	2.3	0.08
Cd	BS / RED	7.7	600	111	3.7	18.5	0.6
As	TF / AS	48.5	30000	786	26	2.6	0.09

Table 8. Model results. TF = Trondheimsfjord. BS = Barents Sea. AS = acid soluble fraction. RED = easily reducible fraction. MOC = mean ocean concentration, from Sarmiento and Gruber (2006). ΔMe_{sed} equals the amount of trace metals mobilized by CO_2 exposure. Values are retrieved from the experimental results. ΔMe_{sw} is the change in seawater trace metal concentrations resulting from the mobilization. "% of MOC" is the size of the mobilization relative to the MOC.

In the case of τ_2, ΔMe_{sw} is indistinguishable from the MOC for both Cd in the Barents Sea sediment, and Cd and As in the Trondheimsfjord sediment. In the case of τ_1, the model results imply that the Cd and As mobilization from the Trondheimsfjord sediment would only cause a minor increase in seawater concentration above the MOC. With regards to the Cd-mobilization from the Barents Sea sediment, an 18.5% increase is noteworthy and could potentially affect bottom-dwelling fish and shellfish (Bendell, 2010). However, Cd-mobilization from marine sediments is known to occur naturally during diagenesis above the zone of sulphate reduction (Morford and Emerson, 1999). It is unclear whether the CO_2-induced mobilization would exceed this background flux. It is important to note that the model does not incorporate adsorption or precipitation mechanisms as well as flow processes, which would act to immobilize and dilute the trace element concentration in the water column, respectively. For this reason, the model overestimates the concentration of As and Cd that would follow a low flux CO_2 leakage. The results should therefore be treated as an upper limit for the potential impact.

Importantly, the Trondheimsfjord sediment contains about 80% less cadmium and roughly 50% less arsenic than the average shale, while the Barents Sea sediment contains about 60% less cadmium and 70% less arsenic (Turekian and Wedepohl, 1961). This implies that As and Cd are depleted in the two sediments. If a CCS-project is considered in an area where the overlying sediments are contaminated with As and Cd, one may speculate whether the picture might be completely different and the environmental impact of CO_2 leakage much larger (de Orte et al., 2014).

6 Conclusion

This study shows that low-flux CO_2 exposure, corresponding to a decrease in pH from 8.0 to 6.9, is able to cause detectable changes in the composition of surface sediments.

The two experiments demonstrate that CO_2 exposure leads to dissolution of calcium carbonate ($CaCO_3$) in the Trondheimsfjord sediment but not in the Barents Sea sediment, even though they were subject to equal CO_2 dosing. The absence of $CaCO_3$ dissolution in the Barents Sea sediment is a consequence of either buffering of the pH in the pore-water or low sediment permeability due to a significant presence of the swelling clay mineral smectite. Alternatively, the history of $CaCO_3$ dissolution by corrosive bottom-waters in the Barents Sea might already have resulted in dissolution of the most labile $CaCO_3$ particles. Organic biofilms could have inhibited dissolution of the residual biogenic $CaCO_3$ during the exposure phase of the experiment.

The CO_2 exposure in the experiments caused a disruption of the Fe redox-cycle. This is evident from an increase in the concentration of Fe-(hydr)oxides in the surface sediment. Because of the nature of the disruption, no mobilization of trace elements from the easily reducible fraction was detected. Investigating the concurrent response of the subsurface sediments in future studies may contribute to validating these findings.

Arsenic and cadmium are mobilized as a result of CO_2 exposure. The mobilization of As takes place in the acid soluble fraction, while As in the easily reducible fraction is unaffected. This implies that Fe-(hydr)oxide phases in the surface sediment escape dissolution, in line with previous studies, but that inorganic As(V)-species were mobilized by desorption from Fe-(hydr)oxides surfaces. It is necessary to invoke multiple mechanisms to explain the mobilization of Cd. In the Trondheimsfjord sediment, evidence points towards mobilization of Cd by dissolution of $CaCO_3$-minerals onto which cadmium is chemisorbed. In contrast, the Cd mobilization from the Barents Sea sediment is best explained by desorption from kaolinite or smectite.

As and Cd are known environmental toxicants. It is therefore of utmost interest to study and quantify the mobilization of these elements. Preliminary results from a simple box model indicates that the amount of As and Cd released to the water column is small compared to the mean ocean concentration. The mobilization of As and Cd is therefore not likely to have significant adverse effects on marine biota.

An objective of this study was to investigate whether compositional differences between sediments would result in dissimilar element mobilization patterns. The results have revealed disparate behavior with respect to adsorption of As and Cd and $CaCO_3$-dissolution between the two sediments. This demonstrates that the state of the Fe and Mn redox-cycle, the $CaCO_3$-content and the clay mineral composition play dominant roles in determining how sediments respond to CO_2 exposure. The origin of the contrasting mineralogical composition of the sediments can be linked to the geological setting of the Trondheimsfjord and the Barents Sea. The mineralogical composition of the two sediment types correlates well with the bedrock composition and an inferred dominance of physical over chemical weathering in the provenance of the two areas. This highlights the value of obtaining a general understanding of the geology and geological history of the area when conducting environmental studies.

6.1 Implications for future research

Desorption of Fe, P, V, Co, Ni, Zn and liberation of Hg from organic matter were observed during the control phase. It has proven difficult to determine the reason why it occurred and several mechanisms may be invoked to account for the observations. These include changes in pressure, secondary effects related to oxidation of organic matter, changes in pH or changes in flow conditions in the aqueous phase. To reduce the risk of producing such a signal when conducting experiments using flow-through chambers at elevated pressure, future studies should ensure that the sediment acclimatization phase is carried out at the same conditions as the control phase of the experiments. Furthermore, since the distribution of transition metals appears to have been disturbed by bioturbation, it is not recommended to conduct studies on biological effects and elements mobilization simultaneously.

Future studies should make attempts to falsify binding mechanisms that have been proposed for arsenic and cadmium in this thesis. This could be done by analyzing the sediments by extended X-ray absorption fine structure spectroscopy (EXAFS), as previous studies have demonstrated that EXAFS is a valuable method for obtaining precise information about surface binding mechanisms (e.g. Peacock and Sherman, 2004).

It is well-established facts that marine sediments are redox-stratified and that the Fe and Mn redox-cycle is the main driver of trace element transport across the redox-zones (Calvert and Pedersen, 1993; Thomson et al., 1993; Calvert and Pedersen, 1996; Tribovillard et al., 2006). Therefore, an objective for future research could be to extract and analyze the subsurface sediment collected during the two experiments. This would enable an investigation of concurrent trends in the two sediment fractions.

7 References

Alcalde, J. et al., 2018. Estimating geological CO2 storage security to deliver on climate mitigation. Nature Communications, 9: 1-13.

Allen, J.R.L., 1985. Principles of Physical Sedimentology. Chapman & Hall, London, 272 pp.

Andersen, M.B., Stirling, C.H., Weyer, S., 2017. Uranium isotope fractionation. Reviews in Mineralogy and Geochemistry, 82(1): 799-850.

Angove, M.J., Johnson, B.B., Wells, J.D., 1997. Adsorption of cadmium(II) on kaolinite. Colloids and Surfaces A: Physicochemical and Engineering Aspects, 126(2): 137-147.

Ardelan, M.V., Steinnes, E., 2010. Changes in mobility and solubility of the redox sensitive metals Fe, Mn and Co at the seawater-sediment interface following CO2 seepage. Biogeosciences, 7: 569-583.

Ardelan, M.V., Steinnes, E., Lierhagen, S., Linde, S.O., 2009. Effects of experimental CO2 leakage on solubility and transport of seven trace metals in seawater and sediment. Science of The Total Environment, 407(24): 6255-6266.

Arrhenius, S.A., 1896. On the influence of carbonic acid in the air upon the temperature of the ground. Philosophical Magazine and Journal of Science, 41: 237-276.

Bakken, T., Holthe, T., Sneli, J.-A., 2000. Strøm, Vannutveksling og Tidevand. In: Sakshaug, E., Sneli, J.-A. (Eds.), Trondheimsfjorden. Tapir forlag, Trondheim, pp. 336.

Basallote, M.D., Rodríguez-Romero, A., De Orte, M.R., Del Valls, T.Á., Riba, I., 2015. Evaluation of the threat of marine CO2 leakage-associated acidification on the toxicity of sediment metals to juvenile bivalves. Aquatic Toxicology, 166: 63-71.

Bendell, L.I., 2010. Cadmium in shellfish: The British Columbia, Canada experience—A mini-review. Toxicology Letters, 198(1): 7-12.

Bickle, M., Chadwick, A., Huppert, H.E., Hallworth, M., Lyle, S., 2007. Modelling carbon dioxide accumulation at Sleipner: Implications for underground carbon storage. Earth and Planetary Science Letters, 255(1): 164-176.

Blackford, J. et al., 2015. Marine baseline and monitoring strategies for carbon dioxide capture and storage (CCS). International Journal of Greenhouse Gas Control, 38(Supplement C): 221-229.

Blackford, J. et al., 2014. Detection and impacts of leakage from sub-seafloor deep geological carbon dioxide storage. Nature Climate Change, 4(11): 1011-1016.

Bowell, R., Alpers, C., Jamieson, H., Nordstrom, D., Majzlan, J., 2014. The environmental geochemistry of arsenic - an overview. Reviews in Mineralogy & Geochemistry, 79: 1-16.

Byrne, R.H., Laurie, S.H., 1999. Influence of pressure on chemical equilibria in aqueous systems - With particular reference to seawater (Technical Report).

Bøe, R., Rise, L., Blikra, L.H., Longva, O., Eide, A., 2003. Holocene mass-movement processes in Trondheimsfjorden, Central Norway. Norwegian Journal of Geology, 83(1): 3-22.

Calvert, S.E., Pedersen, T.F., 1993. Geochemistry of recent oxic and anoxic marine sediments: Implications for the geological record. Marine Geology, 113: 67-88.

Calvert, S.E., Pedersen, T.F., 1996. Sedimentary geochemistry of manganese; implications for the environment of formation of manganiferous black shales. Economic Geology, 91(1): 36-47.

Canfield, D.E., Thamdrup, B., Hansen, J.W., 1993. The anaerobic degradation of organic matter in Danish coastal sediments: Iron reduction, manganese reduction, and sulfate reduction. Geochimica et Cosmochimica Acta, 57(16): 3867-3883.

Chaillou, G., Anschutz, P., Lavaux, G., Schäfer, J., Blanc, G., 2002. The distribution of Mo, U, and Cd in relation to major redox species in muddy sediments of the Bay of Biscay. Marine Chemistry, 80(1): 41-59.

Cooper, C. et al., 2009. A Technical Basis For Carbon Dioxide Storage. In: Project, T.C.C. (Editor), CPL Press, United Kingdom, pp. 86.
Cuong, D.T., Obbard, J.P., 2006. Metal speciation in coastal marine sediments from Singapore using a modified BCR-sequential extraction procedure. Applied Geochemistry, 21(8): 1335-1346.
Davenport, A., 2015. Trace Elements in Patients with Chronic Kidney Disease. In: Kimmel, P.L., Rosenberg, M.E. (Eds.), Chronic Renal Disease. Academic Press, San Diego, pp. 429-439.
de Orte, M.R., Sarmiento, A.M., DelValls, T.Á., Riba, I., 2014. Simulation of the potential effects of CO2 leakage from carbon capture and storage activities on the mobilization and speciation of metals. Marine Pollution Bulletin, 86(1): 59-67.
Dzombak, D.A., Morel, F., 1990. Surface complexation modeling: hydrous ferric oxide. John Wiley & Sons.
EC, 2003. Technical Guidance Document on Risk Assessment in support of commission directive 93/67 on risk assessment for new notified substances, commission regulation (EC) no 1488/94 on risk assessment for existing substances and Directive 98/8/EC of the Parliament and of the Council concerning the placing of biocidal products on the market.
Emerson, S.R., Hedges, J.I., 2008. Chemical Oceanography and the Marine Carbon Cycle. Cambridge University Press, Cambridge, 453 pp.
Erickson, R.J. et al., 2019. The effects of arsenic speciation on accumulation and toxicity of dietborne arsenic exposures to rainbow trout. Aquatic Toxicology, 210: 227-241.
Erickson, R.J. et al., 2010. Effects of copper, cadmium, lead, and arsenic in a live diet on juvenile fish growth. Canadian Journal of Fisheries and Aquatic Sciences, 67(11): 1816-1826.
Eriksson, G., 1979. An algorithm for the computation of aqueous multi-component, multiphase equilibria. Analytica Chimica Acta, 112(4): 375-383.
Faust, J.C. et al., 2014. Geochemical composition of Trondheimsfjord surface sediments: Sources and spatial variability of marine and terrigenous components. Continental Shelf Research, 88: 61-71.
Fordham, A.W., 1990. Weathering of biotite into dioctahedral clay minerals. Clay Minerals, 25(1): 51-63.
Froelich, P.N. et al., 1979. Early oxidation of organic matter in pelagic sediments of the eastern equatorial Atlantic: suboxic diagenesis. Geochimica et Cosmochimica Acta, 43(7): 1075-1090.
Gardiner, W.P., 1997. Statistical analysis methods for chemists: A software-based approach. Royal Society of Chemistry, Cambridge, 367 pp.
Gorrepati, E.A., Wongthahan, P., Raha, S., Fogler, H.S., 2010. Silica precipitation in acidic solutions: Mechanism, pH effect, and salt effect. Langmuir, 26(13): 10467-10474.
Han, S., Gill, G.A., 2005. Determination of mercury complexation in coastal and estuarine waters using competitive ligand exchange method. Environmental Science & Technology, 39(17): 6607-6615.
Hansen, O. et al., 2013. Snøhvit: The history of injecting and storing 1 Mt CO2 in the fluvial Tubåen Fm. Energy Procedia, 37: 3565-3573.
Harvey, O.R. et al., 2013. Geochemical implications of gas leakage associated with geologic CO2 storage—A qualitative review. Environmental Science & Technology, 47(1): 23-36.
Haszeldine, R.S. et al., 2014. Sleipner CO2 securely stored deep beneath seabed, in spite of unexpected Hugin fracture discovery.
Hayes, K.F., Leckie, J.O., 1987. Modeling ionic strength effects on cation adsorption at hydrous oxide/solution interfaces. Journal of Colloid and Interface Science, 115(2): 564-572.
Hensen, C., Zabel, M., Schulz, H.N., 2006. Benthic Cycling of Oxygen, Nitrogen and Phosphorous. In: Schulz, H.D., Zabel, M. (Eds.), Marine Geochemistry. Springer, Berlin, pp. 207-240.
Hiemenz, P.C., Rajagopalan, R., 1997. Principles of Colloid and Surface Chemistry. CRC Press, Florida, 672 pp.

Ho, M.D., Evans, G.J., 2000. Sequential extraction of metal contaminated soils with radiochemical assessment of readsorption effects. Environmental Science and Technology, 34(6): 1030-1035.
IEA, 2017. World Energy Outlook 2017.
Ingri, N., Kakolowicz, W., Sillén, L.G., Warnqvist, B., 1967. High-speed computers as a supplement to graphical methods: Haltafall, a general program for calculating the composition of equilibrium mixtures. Talanta, 14(11): 1261-1286.
IPCC, 2005. IPCC Special Report on Carbon Capture and Storage, UK.
IPCC, 2013. Climate Change 2013: The Physical Science Basis. Contribution of Working Group I to the Fifth Assessment Report of the Intergovernmental Panel on Climate Change, Cambridge, United Kingdom and New York, NY, USA.
IPCC, 2014. Climate Change 2014: Impacts, Adaptation, and Vulnerability. Summaries, Frequently Asked Questions, and Cross-Chapter Boxes. A
Contribution of Working Group II to the Fifth Assessment Report of the Intergovernmental Panel on Climate Change, World Meteorological Organization, Geneva, Switzerland.
Jeon, B.-H., Dempsey, B.A., Burgos, W.D., Royer, R.A., 2003. Sorption kinetics of Fe(II), Zn(II), Co(II), Ni(II), Cd(II), and Fe(II)/Me(II) onto hematite. Water Research, 37(17): 4135-4142.
Jørgensen, B.B., 2006. Bacteria and Marine Biogeochemistry. In: Schulz, H.D., Zabel, M. (Eds.), Marine Geochemistry. Springer, Berlin, pp. 169-206.
Keeling, C.D. et al., 2001. Exchanges of atmospheric CO2 and 13CO2 with the terrestrial biosphere and oceans from 1978 to 2000, I. Global aspects, SIO Reference Series. Scripps Institution of Oceanography, San Diego, California, USA, pp. 88.
Kersten, M., 2002. Speciation of trace metals in sediments. In: Ure, A.M., Davidson, C.M. (Eds.), Chemical Speciation in the Environment. Blackwell Science, Oxford, pp. 452.
Kersten, M., Förstner, U., 1986. Chemical fractionation of heavy metals in anoxic estuarine and coastal sediments. Water Science and Technology, 18(4-5): 121-130.
Kirsch, K., Navarre-Sitchler, A.K., Wunsch, A., McCray, J.E., 2014. Metal release from sandstones under experimentally and numerically simulated CO2 leakage conditions. Environmental Science & Technology, 48(3): 1436-1442.
Klinkhammer, G.P., Palmer, M.R., 1991. Uranium in the oceans: Where it goes and why. Geochimica et Cosmochimica Acta, 55(7): 1799-1806.
Krauskopf, K.B., Bird, D.K., 1995. Introduction to Geochemistry. McGraw-Hill, New York, 647 pp.
Lane, T.W., Morel, F.M.M., 2000. A biological function for cadmium in marine diatoms. Proceedings of the National Academy of Sciences, 97(9): 4627-4631.
Langseth, E., Landrø, M., 2012. Time-lapse 2D interpretation of gas migration in shallow sand layers – Compared to reservoir simulation. International Journal of Greenhouse Gas Control, 10: 389-396.
Leeder, M.R., 2011. Sedimentology and Sedimentary Basins: From Turbulence to Tectonics. Wiley-Blackwell, Chichester, 768 pp.
Lichtschlag, A., James, R.H., Stahl, H., Connelly, D., 2015. Effect of a controlled sub-seabed release of CO2 on the biogeochemistry of shallow marine sediments, their pore waters, and the overlying water column. International Journal of Greenhouse Gas Control, 38: 80-92.
Lidmar-Bergström, K., 1995. Relief and saprolites through time on the Baltic Shield. Geomorphology, 12(1): 45-61.
Liu, Y. et al., 2018. Acid-base properties of kaolinite, montmorillonite and illite at marine ionic strength. Chemical Geology, 483: 191-200.
Lumsdon, D.G., Evans, L.J., 2002. Predicting Chemical Speciation and Computer Simulation. In: Ure, A.M., Davidson, C.M. (Eds.), Chemical Speciation in the Environment. Blackwell Science Ltd, Oxford, pp. 89-131.
Lüttge, A., Conrad, P.G., 2004. Direct observation of microbial inhibition of calcite dissolution. Applied and Environmental Microbiology, 70(3): 1627.
Manahan, S.E., 2017. Environmental Chemistry. CRC Press LLC, Boca Raton, 784 pp.
McLennan, S.M., Hemming, S., McDaniel, D.K., Hanson, G.N., 1993. Geochemical approaches to sedimentation, provenance, and tectonics. 284: 21-40.

McManus, J., Berelson, W.M., Klinkhammer, G.P., Hammond, D.E., Holm, C., 2005. Authigenic uranium: Relationship to oxygen penetration depth and organic carbon rain. Geochimica et Cosmochimica Acta, 69(1): 95-108.
Millero, F.J., 1983. Influence of pressure on chemical processes in the sea, Chemical oceanography. Elsevier, pp. 1-88.
Millero, F.J., 2005. Chemical Oceanography. CRC Press, Bosa Roca, 530 pp.
Monastersky, 2013. Seabed scars raise questions over carbon-storage plan. Nature, 504: 339-340.
Morel, F.M.M., Price, N.M., 2003. The biogeochemical cycles of trace metals in the oceans. Science, 300(5621): 944-947.
Morford, J.L., Emerson, S., 1999. The geochemistry of redox sensitive trace metals in sediments. Geochimica Et Cosmochimica Acta, 63(11-12): 1735-1750.
Morford, J.L., Emerson, S.R., Breckel, E.J., Kim, S.H., 2005. Diagenesis of oxyanions (V, U, Re, and Mo) in pore waters and sediments from a continental margin. Geochimica Et Cosmochimica Acta, 69(21): 5021-5032.
Morillo, J., Usero, J., Gracia, I., 2004. Heavy metal distribution in marine sediments from the southwest coast of Spain. Chemosphere, 55(3): 431-442.
Mucci, A., 1983. The solubility of calcite and aragonite in seawater at various salinities, temperatures, and one atmosphere total pressure. American Journal of Science, 283(7): 780-799.
Mustafa, G., Kookana, R.S., Singh, B., 2006. Desorption of cadmium from goethite: Effects of pH, temperature and aging. Chemosphere, 64(5): 856-865.
Neff, J.M., 1997. Ecotoxicology of arsenic in the marine environment. Environmental Toxicology and Chemistry, 16(5): 917-927.
Nesbitt, H.W., Young, G.M., 1982. Early Proterozoic climates and plate motions inferred from major element chemistry of lulites. Nature, 299(5885): 715-717.
Nesbitt, H.W., Young, G.M., McLennan, S.M., Keays, R.R., 1996. Effects of chemical weathering and sorting on the petrogenesis of siliciclastic sediments, with implications for provenance studies. The Journal of Geology, 104(5): 525-542.
Nichols, G., 2009. Sedimentology and Stratigraphy. Wiley-Blackwell, West Sussex, UK, 456 pp.
Nickson, R. et al., 1998. Arsenic poisoning of Bangladesh groundwater. Nature, 395(6700): 338.
Nordberg, M., 2003. Cadmium toxicology. In: Caballero, B. (Ed.), Encyclopedia of Food Sciences and Nutrition (Second Edition). Academic Press, Oxford, pp. 739-745.
Nordgulen, Ø., Andresen, A., 2013. De eldste bergartene dannes. In: Ramberg, I.B., Bryhni, I., Nøttvedt, A. (Ed.), Landet Blir Til. Norsk Geologisk Forening, Trondheim, Norge, pp. 62-119.
Oremland, R.S. et al., 2000. Bacterial dissimilatory reduction of arsenate and sulfate in meromictic Mono Lake, California. Geochimica et Cosmochimica Acta, 64(18): 3073-3084.
OSPAR, 2005. Agreement on background concentrations for contaminants in seawater, biota and sediment (OSPAR Agreement 2005-6).
Ottesen, D., Frengstad, B., Rokoengen, K., 1995. Deglaciation of the outermost Trondheimsfjord area, mid-Norway. Norwegian Geological Survey Bulletin, 427: 59-63.
Peacock, C.L., Sherman, D.M., 2004. Vanadium(V) adsorption onto goethite (α-FeOOH) at pH 1.5 to 12: a surface complexation model based on ab initio molecular geometries and EXAFS spectroscopy. Geochimica et Cosmochimica Acta, 68(8): 1723-1733.
Pueyo, M. et al., 2001. Certification of the extractable contents of Cd, Cr, Cu, Ni, Pb and Zn in a freshwater sediment following a collaboratively tested and optimised three-step sequential extraction procedure. Journal of Environmental Monitoring, 3(2): 243-250.
Rauret, G. et al., 1999. Improvement of the BCR three step sequential extraction procedure prior to the certification of new sediment and soil reference materials. Journal of Environmental Monitoring(1): 57-61.

Rosenthal, Y., Lam, P., Boyle, E.A., Thomson, J., 1995. Authigenic cadmium enrichments in suboxic sediments: Precipitation and postdepositional mobility. Earth and Planetary Science Letters, 132(1): 99-111.
Rullkötter, J., 2006. Organic Matter: The Driving Force for Early Diagenesis. In: Schulz, H.D., Zabel, M. (Eds.), Marine Geochemistry. Springer, Berlin, pp. 125-168.
Sarmiento, A.M., Nieto, J.M., Olías, M., Cánovas, C.R., 2009. Hydrochemical characteristics and seasonal influence on the pollution by acid mine drainage in the Odiel river Basin (SW Spain). Applied Geochemistry, 24(4): 697-714.
Sarmiento, J.L., Gruber, N., 2006. Ocean Biogeochemical Dynamics. Princeton University Press, Princeton, Woodstock, 503 pp.
Schindler, P.W., Stumm, W., 1987. The surface chemistry of oxides, hydroxides, and oxide minerals. IN: Aquatic Surface Chemistry: Chemical Processes at the Particle-Water Interface. John Wiley and Sons, New York. 1987. p 83-110, 13 fig, 7 tab, 49 ref.
Schulz, H.D., 2006a. Conceptual Models and Computer Models. In: Schulz, H.D., Zabel, M. (Eds.), Marine Geochemistry. Springer, Berlin, pp. 513-545.
Schulz, H.D., 2006b. Quantification of Early Diagenesis: Dissolved Constituents in Pore Water and Signals in the Solid Phase. In: Schulz, H.D., Zabel, M. (Eds.), Marine Geochemistry. Springer, Berlin, pp. 73-124.
Sellwood, B.W., Price, G.D., Shackleton, N.J., Francis, J., 1993. sedimentary facies as indicators of Mesozoic palaeoclimate [and discussion]. Philosophical Transactions: Biological Sciences, 341(1297): 225-233.
Skoog, D.A., West, D.M., Holler, F.J., Crouch, S.R., 2013. Fundamentals of analytical chemistry. Nelson Education.
Slomp, C.P., Epping, E.H.G., Helder, W., Raaphorst, W.V., 1996. A key role for iron-bound phosphorus in authigenic apatite formation in North Atlantic continental platform sediments. Journal of Marine Research, 54(6): 1179-1205.
Smith, A.H., Lingas, E.O., Rahman, M., 2000. Contamination of drinking-water by arsenic in Bangladesh: A public health emergency. Bulletin of the World Health Organization, 78(9): 1093-1103.
Srivastava, P., Singh, B., Angove, M., 2005. Competitive adsorption behavior of heavy metals on kaolinite. Journal of Colloid and Interface Science, 290(1): 28-38.
Steinsund, P.I., Hald, M., 1994. Recent calcium carbonate dissolution in the Barents Sea: Paleoceanographic applications. Marine Geology, 117(1): 303-316.
Stumm, W., Morgan, J.J., 1996. Aquatic Chemistry - Chemical Equilibria and Rates in Natural Waters. John Wiley & Sons, Inc., Canada, 1022 pp.
Sutherland, R.A., 2010. BCR®-701: A review of 10-years of sequential extraction analyses. Analytica Chimica Acta, 680(1): 10-20.
Swart, P.K., Chung, G.S., 1990. The concentration of uranium in freshwater vadose and phreatic cements in a Holocene ooid cay; a method of identifying ancient water tables. Journal of Sedimentary Research, 60(5): 735-746.
Tchounwou, P.B., Yedjou, C.G., Patlolla, A.K., Sutton, D.J., 2012. Heavy metal toxicity and the environment. EXS, 101: 133-164.
Tessier, A., Campbell, P.G.C., Bisson, M., 1979. Sequential extraction procedure for the speciation of particulate trace metals. Analytical Chemistry, 51(7): 844-851.
Thakur, S.K., Tomar, N.K., Pandeya, S.B., 2006. Influence of phosphate on cadmium sorption by calcium carbonate. Geoderma, 130(3-4): 240-249.
Thomson, J., Higgs, N.C., Croudace, I.W., Colley, S., Hydes, D.J., 1993. Redox zonation of elements at an oxic/post-oxic boundary in deep-sea sediments. Geochimica et Cosmochimica Acta, 57(3): 579-595.
Tribovillard, N., Algeo, T.J., Lyons, T., Riboulleau, A., 2006. Trace metals as paleoredox and paleoproductivity proxies: An update. Chemical Geology, 232(1-2): 12-32.
Tucker, M.E., 1977. Stromatolite biostromes and associated facies in the late precambrian porsanger dolomite formation of Finnmark, Arctic Norway. Palaeogeography, Palaeoclimatology, Palaeoecology, 21(1): 55-83.
Turekian, K., Wedepohl, H., 1961. Distribution of the elements in some major units of the Earth's crust. Geological Society of America Bulletin, 72: 175-192.

Ure, A.M., Quevauviller, P., Muntau, H., Griepink, B., 1993. Speciation of heavy metals in soils and sediments. An account of the improvement and harmonization of extraction techniques undertaken under the auspices of the BCR of the Commission of the European Communities. International Journal of Environmental Analytical Chemistry, 51(1-4): 135-151.

Usero, J., Gamero, M., Morillo, J., Gracia, I., 1998. Comparative study of three sequential extraction procedures for metals in marine sediments. Environment International, 24(4): 487-496.

van Heuven, S., Pierrot, D., Rae, J.W.B., Lewis, E., Wallace, D.W.R., 2011. MATLAB program developed for CO2 system calculations. Carbon Dioxide Information Analysis Center, Oak Ridge National Laboratory, U.S. Department of Energy, Oak Ridge, Tennessee.

Vogt, C., Knies, J., 2009. Sediment pathways in the western Barents Sea inferred from clay mineral assemblages in surface sediments. Norwegian Journal of Geology, 89: 41-55.

Warren, J., 2000. Dolomite: occurrence, evolution and economically important associations. Earth-Science Reviews, 52(1-3): 1-81.

Wehrli, B., Stumm, W., 1989. Vanadyl in natural waters: Adsorption and hydrolysis promote oxygenation. Geochimica et Cosmochimica Acta, 53(1): 69-77.

Wunsch, A., Navarre-Sitchler, A.K., Moore, J., McCray, J.E., 2014. Metal release from limestones at high partial-pressures of CO2. Chemical Geology, 363: 40-55.

Young, R.A., 1993. The rietveld method, 5. International union of crystallography.

Appendices

Appendix 1: Calendar, Trondheimsfjord experiment

Appendix 2: Calendar, Barents Sea experiment

Appendix 3: UltraClave digestion profile

Appendix 4: XRD spectrum. Trondheimsfjord sediment, fine fraction

Appendix 5: XRD spectrum. Barents Sea sediment, fine fraction

Appendix 6: Solution master variables, Trondheimsfjord experiment

Appendix 7: Solution master variables, Barents Sea experiment

Appendix 1: Calendar, Trondheimsfjord experiment

Calendar for the Trondheimsfjord experiment conducted during the fall of 2017. Courtesy of Ana Borrero-Santiago.

Appendix 2: Calendar, Barents Sea experiment

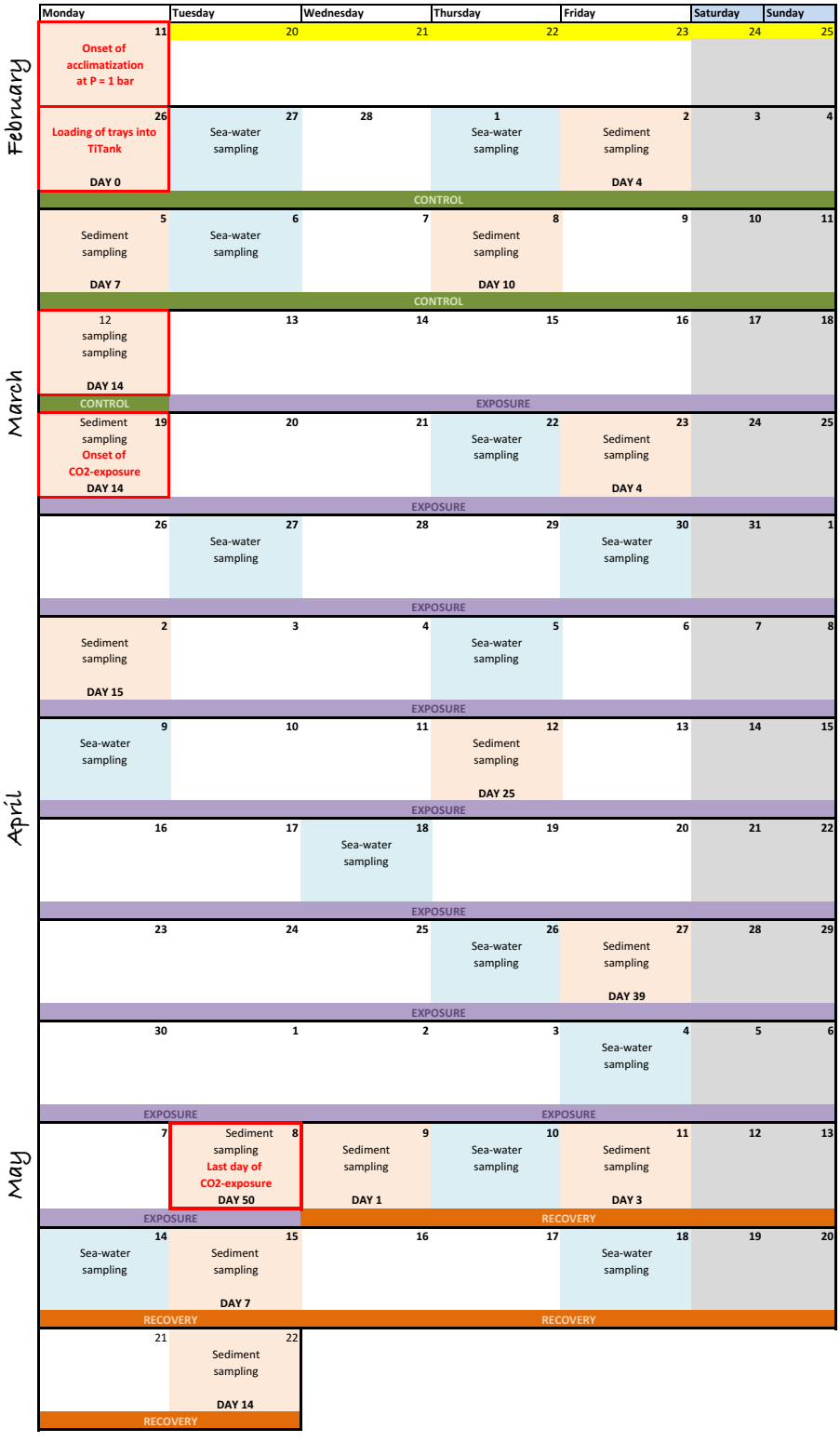

Calendar for the Barents Sea experiment conducted during the spring of 2018. Courtesy of Ana Borrero-Santiago.

Appendix 3: UltraClave digestion profile

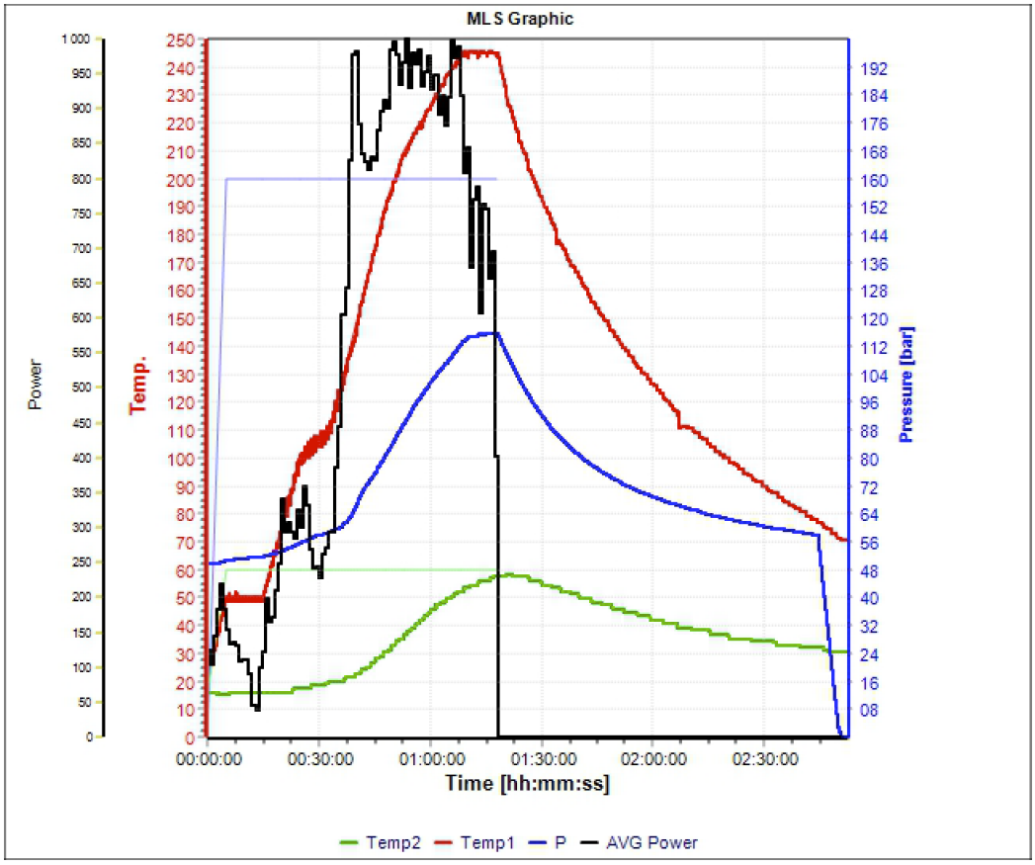

Pressure and temperature profile of UltraClave digestion. Temp2 is the external chamber temperature, temp1 is the internal chamber temperature, P is the chamber pressure, AVG power is the effect of the UltraClave heating unit.

Appendix 4: XRD spectrum. Trondheimfjord sediment, fine fraction

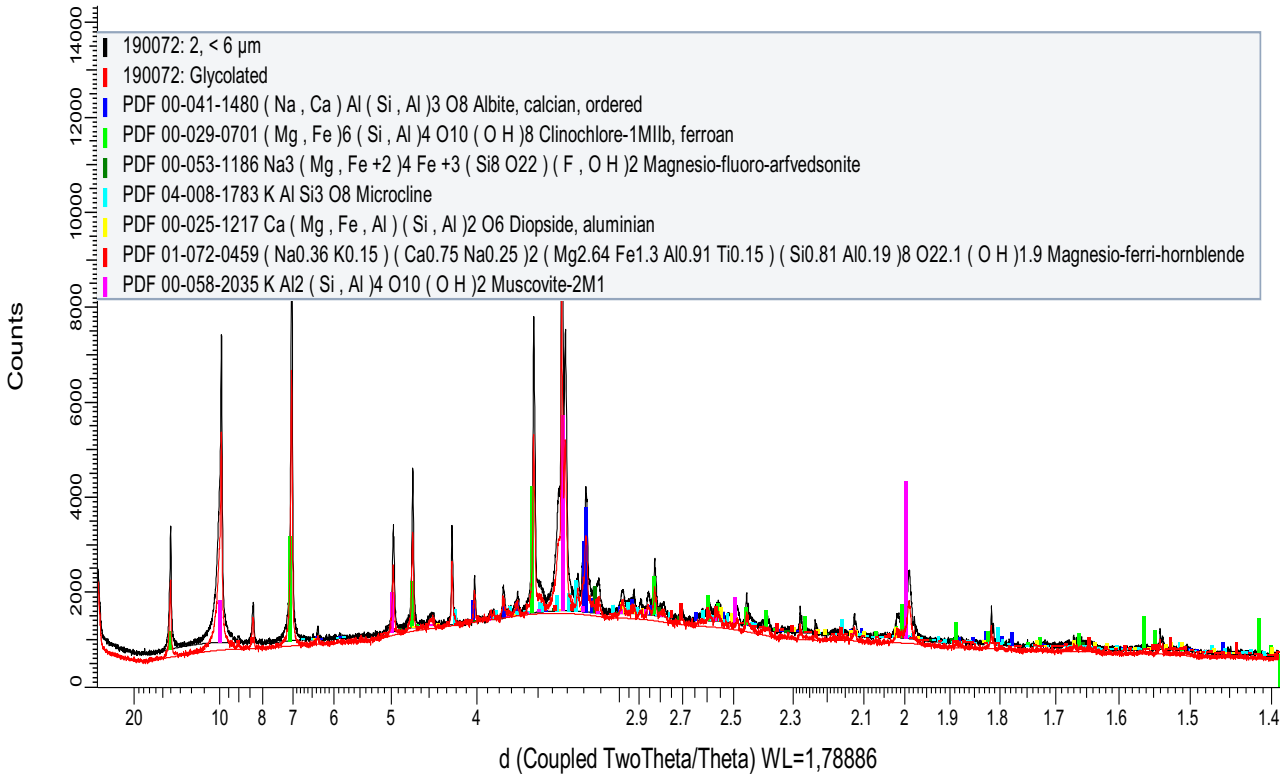

XRD spectrum of the fine-grained (here defined as grains smaller than 6μm) fraction of the Trondheimsfjord sediment. The red line represents the glycole-treated subsample. The black line represents the untreated subsample. No shift of the 14.5Å peak can be observed from the red line.

Appendix 5: XRD spectrum. Barents Sea sediment, fine fraction

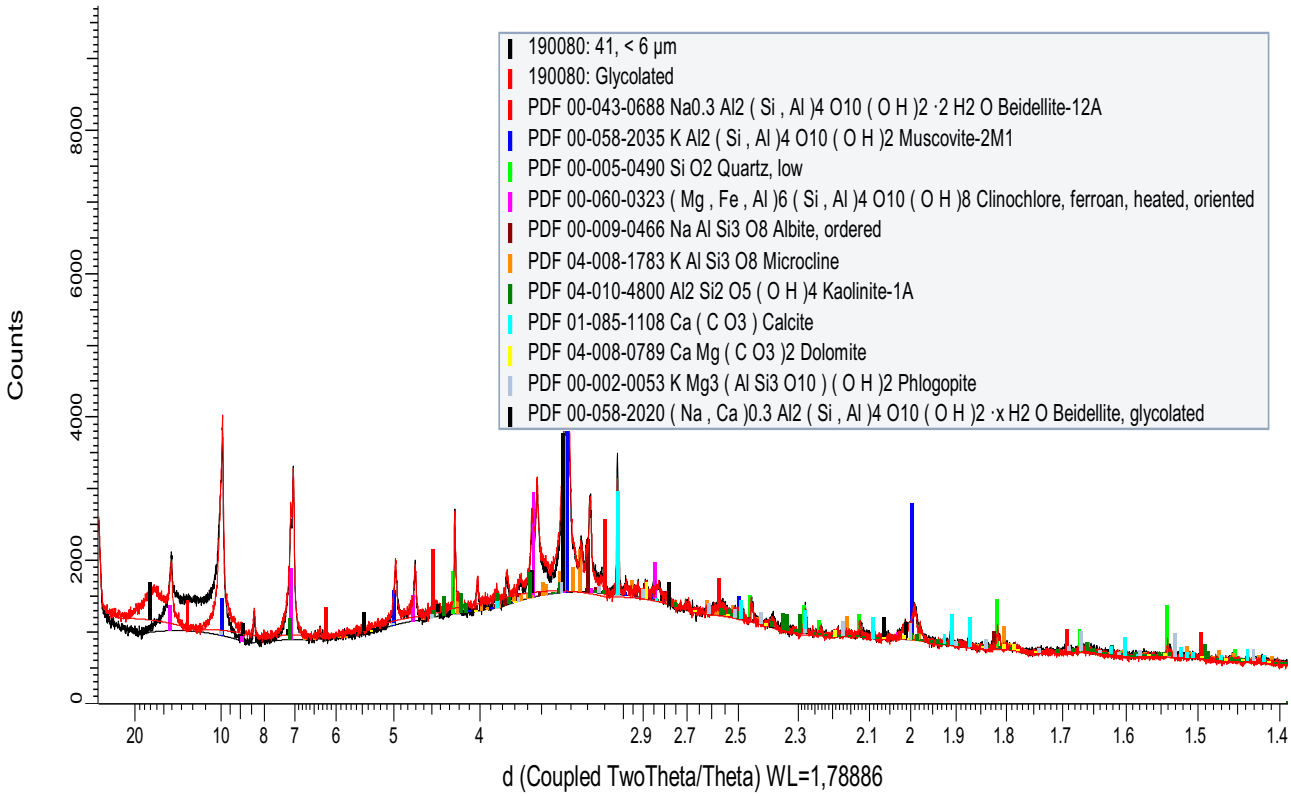

XRD spectrum of the fine-grained (here defined as grains smaller than 6μm) fraction of the Barents Sea sediment. The red line represents the glycole-treated subsample. The black line represents the untreated subsample. A shift of the 14.5Å peak to 16.5Å can be observed from the red line indicating that the sample contains a swelling clay mineral.

Appendix 6: Solution master variables, Trondheimsfjord experiment

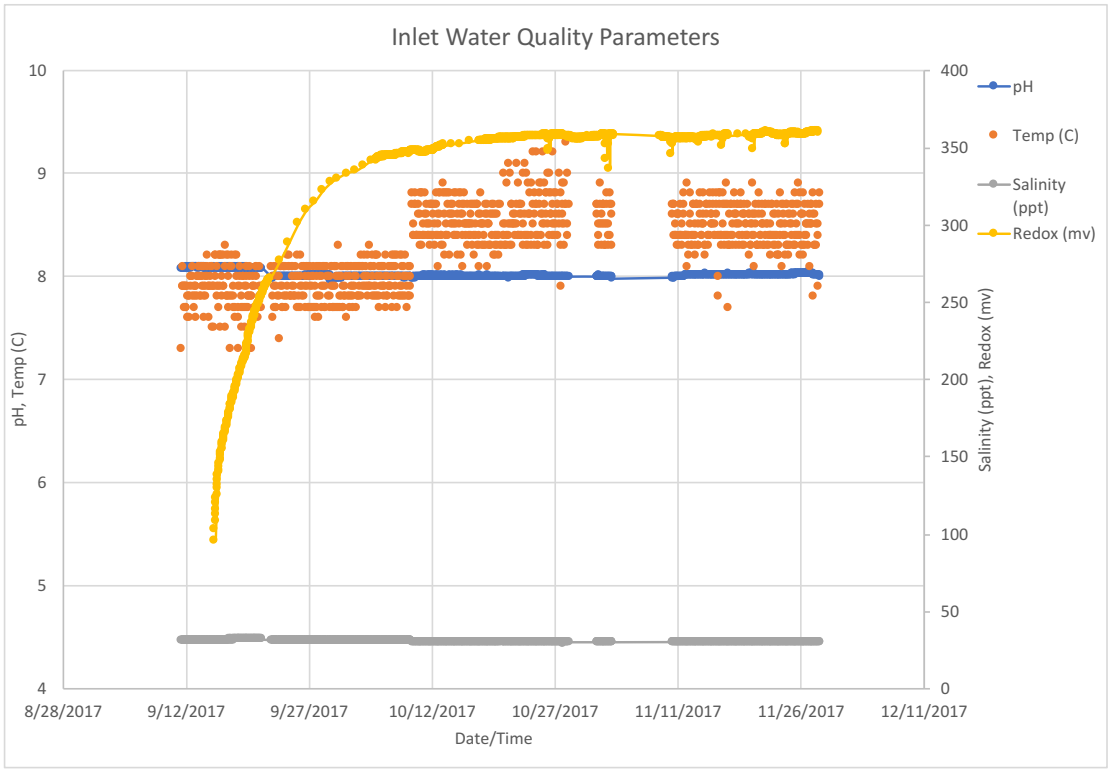

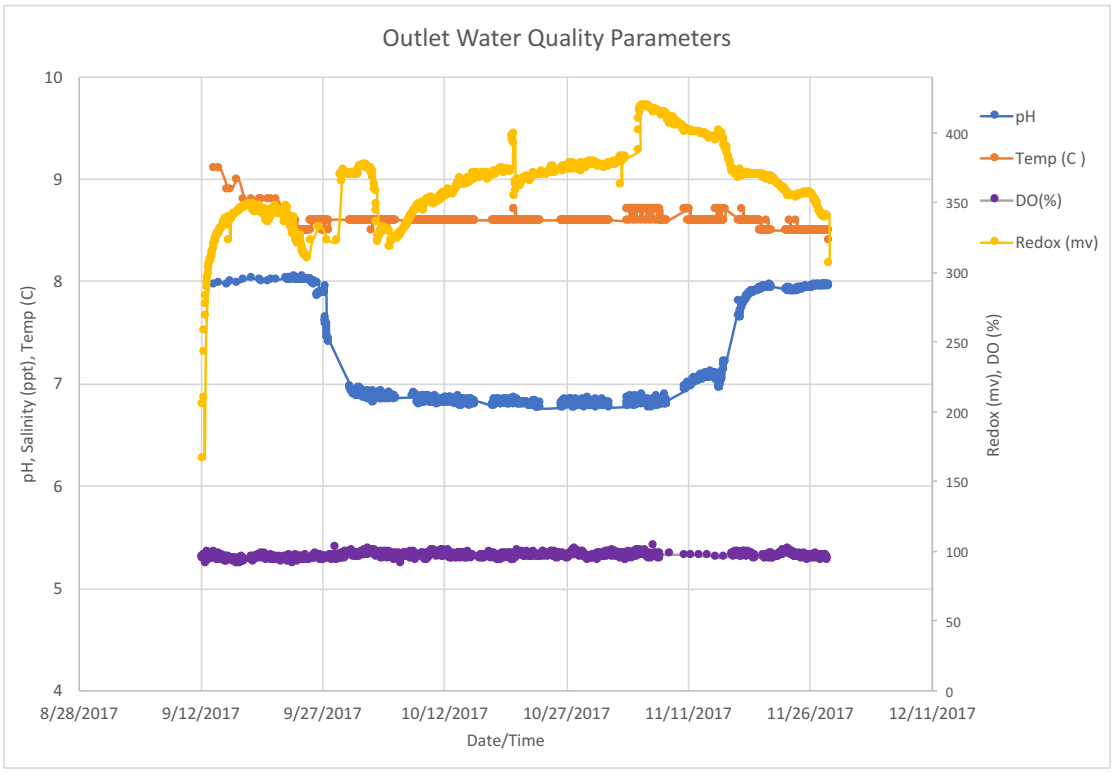

Inlet and outlet water quality parameters for the Trondheimsfjord experiment. Measurements of pH, T, dissolved oxygen (DO), salinity and redox.

Appendix 7: Solution master variables, Barents Sea experiment

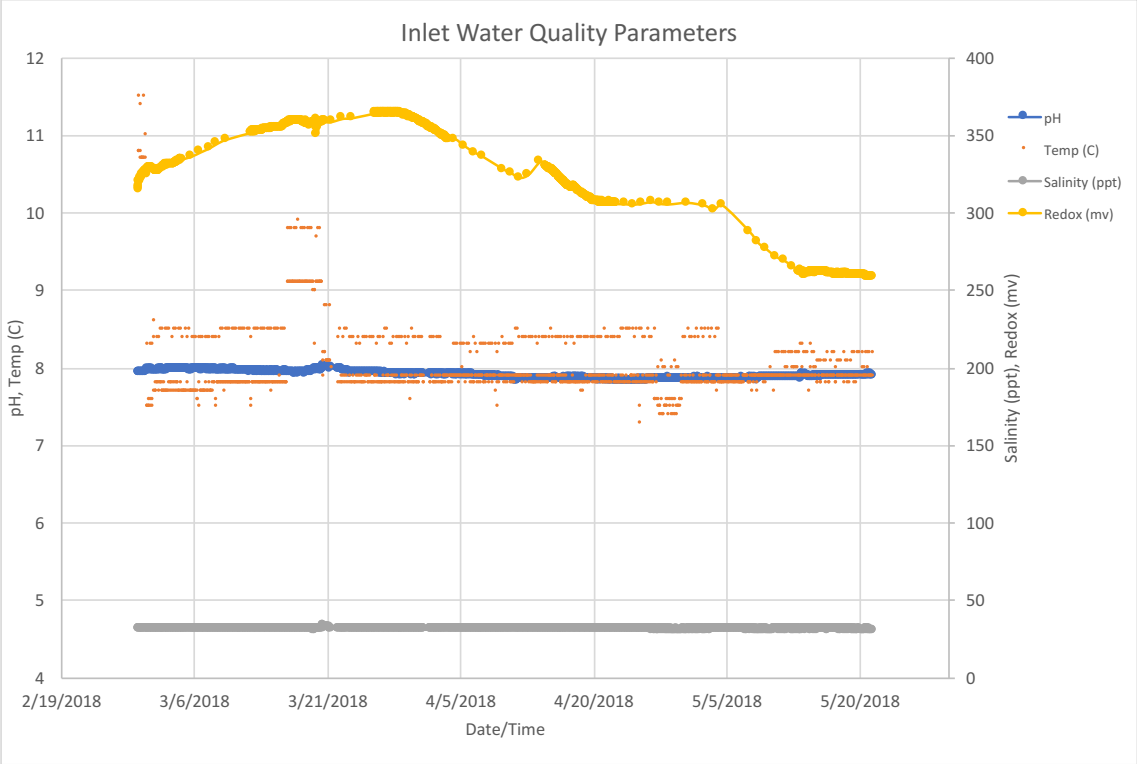

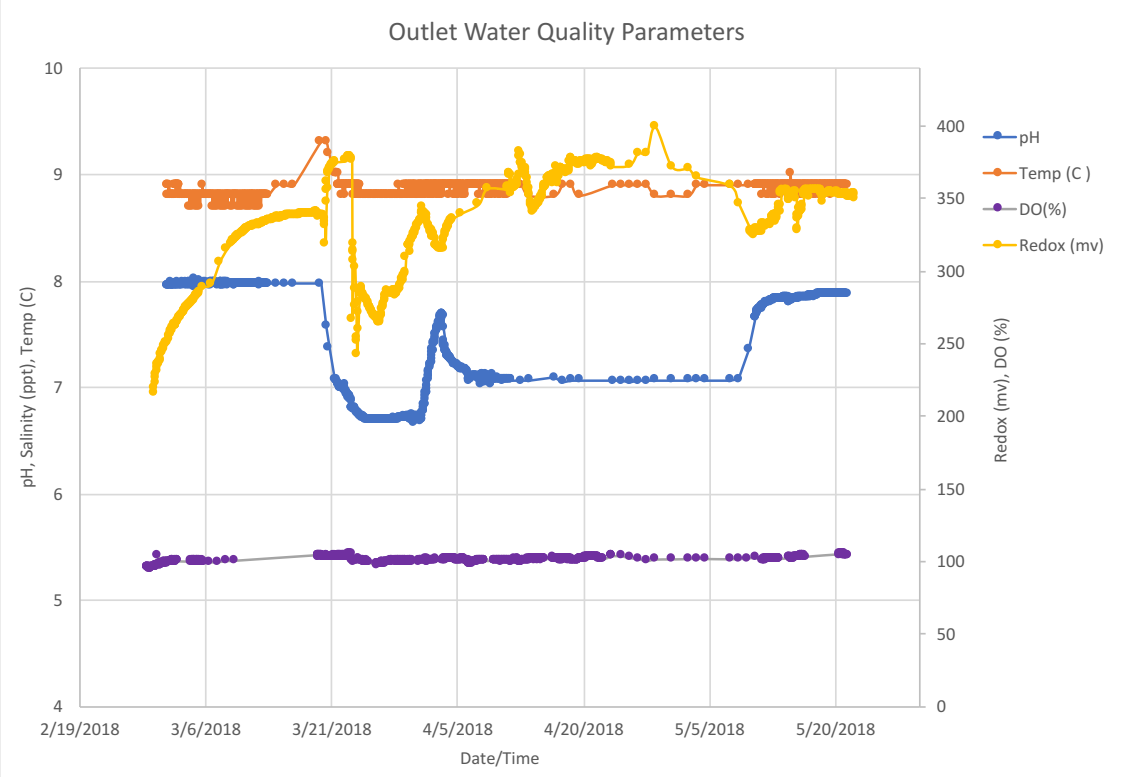

Inlet and outlet water quality parameters for the Barents Sea experiment. Measurements of pH, T, dissolved oxygen (DO), salinity and redox.